UNIVERSITY OF OKLAHOMA

GRADUATE COLLEGE

SYNTHESIS, PURIFICATION AND ASSEMBLY OF GOLD AND IRON OXIDE NANOPARTICLES

A DISSERTATION

SUBMITTED TO THE GRADUATE FACULTY

in partial fulfillment of the requirements for the

Degree of

DOCTOR OF PHILOSOPHY

By

PENGHE QIU
Norman, Oklahoma
2010

SYNTHESIS, PURIFICATION AND ASSEMBLY OF GOLD AND IRON OXIDE NANOPARTICLES

A DISSERTATION APPROVED FOR THE
DEPARTMENT OF CHEMISTRY AND BIOCHEMISTRY

BY

Dr. Chuanbin Mao, Chair

Dr. Paul F. Cook

Dr. Michael T. Ashby

Dr. Robert P. Houser

Dr. Matthew B. Johnson

Acknowledgements

The journey to a Ph.D. degree is a struggling process, accompanied with many occasions of frustration and sadness. Yet even a glimpse of success will be enough to energize one to leave behind the depressions and dig into the truth. If not for the support of numerous people, the finish of this dissertation would not be possible.

I would like to express my deepest appreciation to my Ph.D. advisor, Dr. Chuanbin Mao, for his guidance and support. The past few years have witnessed all the constructive guidance from an advisor to a Ph.D. candidate in all aspects toward a professional researcher. Dr. Mao has afforded me great academic freedom to explore my research interests. Under his guidance, I have learned how to convert a sudden inspiration or a chance discovery into a rationally designed and systematically fulfilled research project. The research experience and skills I gained from Dr. Mao's group will for sure benefit my future career.

A large portion of my experimental data was obtained from the Samuel Roberts Noble Electron Microscopy Laboratory (SRNEML) at OU. Thus, I would like to give my deep-hearted appreciation to Gregory W. Strout, Dr. Preston Larson and Dr. Scott D. Russell in SRNEML. They have been very patient and warmhearted in providing me with training on different microscopes and help of sample preparation. Without these assistances, my research progress would have been much slower. My thanks also go to

those who have contributed to equip the SRNEML with many handy tools and other research related instruments, which all have greatly facilitated the acquiring of data.

I would like to thank Dr. Andrew S. Madden in the School of Geology and Geophysics at OU for his generosity in training me on his Atomic Force Microscope (AFM) and letting me and other members in our group use the AFM at no charge. He also helped me with the data processing and discussion. Our collaborator, Dr. Rheal A. Towner, in Oklahoma Medical Research Foundation (OMRF) offered insightful help with Magnetic Resonance Imaging (MRI) of our iron oxide nanoparticles and I look forward to further collaboration with him in the future on magnetic nanoparticles based MR imaging. Dr. Kenneth Dormer in the Department of Physiology at OUHSC has always urged us to use the Zeta Potential Analyzer accommodated in his lab. I also want to express my appreciation to his technician, Greg H. Matlock, for the great convenience he provided in making appointments for the instrument. My advisory committee members, Dr. Paul F. Cook, Dr. Michael T. Ashby, Dr. Robert P. Houser and Dr. Matthew B. Johnson, helped me improve in various ways through my Ph.D. study.

I have had benefited a lot from working with a brilliant group of both current and past labmates. Haibao Zhu, Zipeng Zhen, Ziwei Deng, Naveen Gandra, Kaiping Guo, Ananta L. Ayyagari, Dong Li, Gopal Abbineni, Hong Xu, Dongdong Wang, Xuewei Qu, Huaiwen Wang, Tao He, Aihua Liu all broadened my knowledge of research and life. My special thanks are given to Fuke Wang and Binrui Cao for many times of helpful discussion on experiments and for many tons of sweat we sprayed in the badminton

court.

My sincere appreciation is expressed to my girlfriend, Ye Guan, for her years-long support, love, tolerance and sacrifice. She is someone that can make me feel spiritually relaxed at the difficult times. I am grateful for having her with me through those sweet and bitter moments. My parents are always proud of me and they are my source of confidence. I thank them from my soul for giving me life, for teaching me to think, learn and be independent as well as for providing me with decent education in my early ages. I owe a lot of thanks to my two elder sisters for always being thoughtful for their young brother and for taking care of the family in my absence. Thank you all for the silent but strong love.

I dedicate this dissertation to my beloved grandma and grandma-in-law, who passed away during my stay in the United States. I had experienced great love and care from them all through the way I grew up. It is my greatest regret that I was not able to be with them for the last moment of their life journey.

Table of Contents

List of Figures

List of Abbreviations

NPs	nanoparticles
NRs	nanorods
AuNPs	gold nanoparticles
AuNDs	dendritic gold nanoparticles
BHFs	branched hollow fibers
TEM	Transmission Electron Microscopy
SEM	Scanning Electron Microscopy
AFM	Atomic Force Microscopy
MRI	Magnetic Resonance Imaging
ZFC	zero field cooled
FC	field cooled
PVP	polyvinylpyrrolidone
HDA	hexadecylamine
CTAB	cetyl trimethyl ammonium bromide
NPCs	nanoparticles clusters
SPR	surface plasmon resonance
1-D	one dimensional
2-D	two dimensional
3-D	three dimensional

Abstract

The aims of the current research include developing new synthetic strategies to prepare structurally complex gold nanoparticles and new size sorting methods to separate nanoparticles of larger size, as well as studying the assembly of nanoparticles into novel hierarchical structures through both template-assisted and template-free strategies.

In the synthesis section of this dissertation (Chapters 2 & 3), a size controllable synthesis of dendritic gold nanoparticles through a seed-mediated process in ethanol is described. The effect of seeds size and shape as well as the carbon chain length of alkylamines on the formation of dendritic structure was investigated. The synthetic strategy developed is capable of forming dendritic structure on various substrates, like flat or rod-like gold particles. In another work, the shape evolution of gold nanoparticles in a seed-mediated growth as well as the kinetics of reduction of $HAuCl_4$ in the presence of seeds was studied. The reduction of the gold precursor by sodium citrate could be greatly accelerated in the presence of seed nanoparticles. Along with the enhanced reaction kinetics, dramatic shape evolution of gold nanoparticles was observed by changing ratios of precursors.

In the purification section (Chapter 4), a novel method of separating nanoparticles of different sizes in a viscosity gradient was developed. The viscosity gradient was created with polyvinylpyrrolidone (PVP) aqueous solutions. Previously, such size separation was all achieved in the density gradient, while the hidden contribution of viscosity difference

inside the density gradient was not well recognized. Through this work, it is clarified that the viscosity can contribute as importantly as density in the size sorting of nanoparticles through rate zonal centrifuge. It was also demonstrated both experimentally and mathematically that the viscosity gradient is more effective in separation of larger sized nanoparticles.

In the assembly section (Chapter 5, 6 & 7), nanoparticles were assembled into three different hierachical structures through both template-assisted and template-free approaches. In the template-assisted assembly, gold nanorods were aligned into ordered 1D linear pattern by using soft biological filamentous, namely bacteria flagella, as templates. Two different ways of assembling nanorods onto flagella were investigated. In another study, a highly commercialized polymer, polyvinylpyrrolidone (PVP), was discovered for the first time to be able to self-assemble into branched hollow fibers. Based on this discovery, two approaches (one through direct deposition of silica onto the PVP aggregate and the other through co-assembly of PVP covered gold nanoparticles with free PVP molecules) by which the self-assembly behavior of PVP could be exploited to template the formation of branched hollow inorganic fibers were demonstrated. In the template-free assembly, a general method for assembling nanoparticle into clusters (NPCs) in an oil-in-water emulsion system was investigated. Detailed studies on the mechanism of formation of NPCs structure, optimized conditions, scalable production and surface chemistry manipulation were carried out. Besides, comparison of the properties of individual and clustered iron oxide nanoparticles was

conducted. It was discovered that due to their collective properties, NPCs are more responsive to an external magnetic field and can potentially serve as better contrast enhancement agents than individually dispersed magnetic NPs in Magnetic Resonance Imaging (MRI).

CHAPTER 1

Introduction

1.1 Historical Overview

Nanoparticles are particles having at least one dimension between one and a hundred nanometers.[1,2] They are composed of limited number of atoms, and thus exhibit strong quantum confinement effect. For this reason, nanoparticles have optical, magnetic and electronic properties that are dramatically different from those of bulk solids.[3] Owing to these novel physical properties, nanoparticles have been playing essential roles in various applications, including molecular detection and sensing,[4] biological imaging and diagnostics,[5-7] targeted drug delivery and medical therapy,[8-12] catalysis,[13] electronics,[14,15] energy storage[16] *et al.* Among all inorganic materials, nanoparticles of gold have been one of the most actively studied nanoparticles. This is probably because: (1) benefiting from the surface plasmon resonance (SPR), gold nanoparticles have the size and shape dependent tunable optical properties, which can be applied in many research fields; (2) gold is a chemically inert and biologically compatible element; (3) synthesis of gold nanoparticles is relatively simple and well developed; (4) surface chemistry of gold nanoparticles can be readily manipulated by mercapto-containing functional molecules.

1.2 Morphology Control of AuNPs through Solution Phase Synthesis

It is well known that the optical properties of gold nanoparticles are significantly dependent on their size and shape.[17-19] Many research efforts have been previously invested into controlling size and especially shape of gold nanoparticles in order to achieve fine tune of their optical properties. In all these attempts, solution phase synthesis has been exclusively successful in controlling the shape of gold nanoparticles. And various shapes, such as solid[20] and hollow spheres[21-23], rods,[24,25] triangular plates,[26-29] polyhedrons,[30-32] cubes[33,34] and flowers,[35] have been prepared (Fig. 1.1).

The chemical nature of solution phase synthesis of gold nanoparticles is a simple inorganic reaction in which ionic gold gets reduced into atomic gold. The atomic gold will accumulate to form clusters, and further grow into particles. The surface of resulting particles is capped by ligands. These ligands will induce electrostatic repulsion or steric force among nanoparticles, so that they can be effectively prevented from aggregation and precipitation. Thus, in solution phase synthesis of gold nanoparticles, at least four chemicals are needed: ionic gold precursor, reducing agent, surface capping agent (ligands) and solvent. Tetrachloroauric acid ($HAuCl_4$) has been almost exclusively used in synthesis of all types of gold nanoparticles as a precursor of gold. Typical examples of reducing agents includes sodium citrate,[20] ascorbic acid (and its sodium salt),[25] sodium borohydride,[36] ethylene glycol (EG),[30,31] amino acids[37] and proteins.[38,39] Small organic molecules (with and without charges), surfactants,[25] and polymers[1] have been

used actively as surface capping reagents to stabilize the nanoparticles. Water, ethylene glycol[1] and dimethylfuran (DMF)[40] are the common solvents employed for synthesis of hydrophilic gold nanoparticles. Generally, careful selection of these reagents can result in gold nanoparticles of different shapes. Besides, pH,[31] reaction temperature[31] and addition of trace amount of “shape-inducing” ions[1,41,42] are also important in the formation of desired shaped gold nanoparticles. The methods of manipulating the shapes of gold nanoparticles can be divided into four categories, which will be reviewed below.

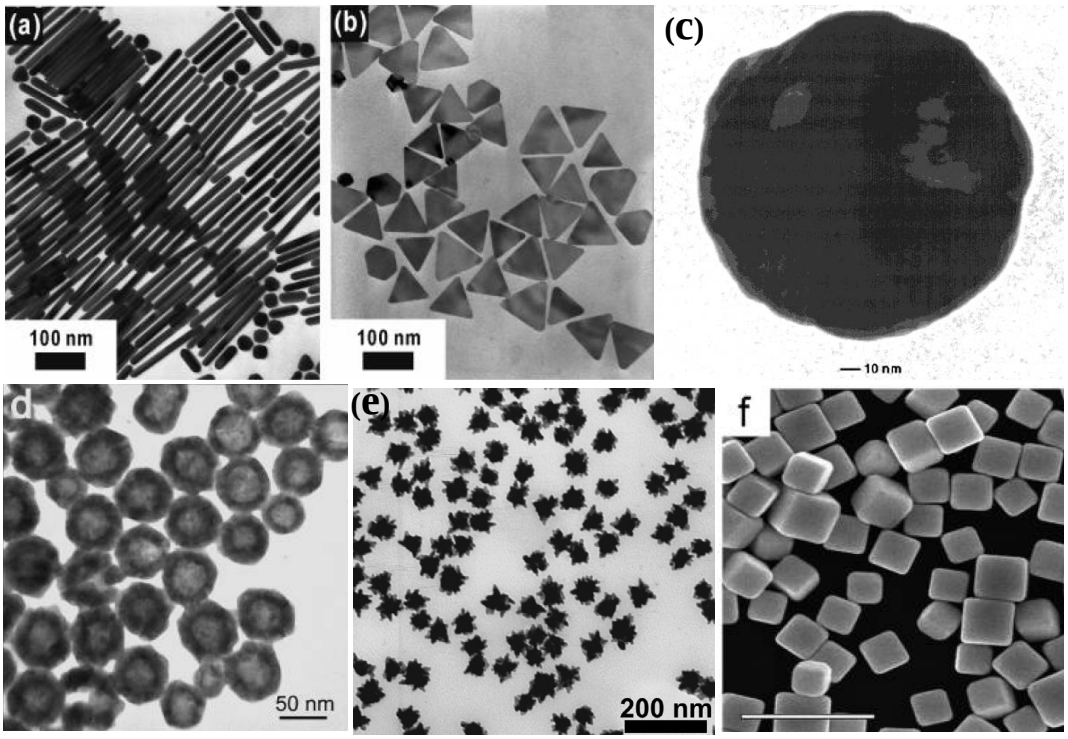

Figure 1.1, Electron microscope images of some typical gold nanoparticles: (a) nanorods[41]; (b) triangular nanoplates[41]; (c) nanoshells — a layer of gold coating on silica nanoparticles[64]; (d) hollow spheres[21]; (e) star-like nanoparticles[35] and (f) nanocubes[32]. Images reprinted with permission from the references as indicated: (a, b) Copyright 2007 American Chemical Society; (c) Copyright 2003 American Chemical Society; (d) Copyright 2005 American Chemical Society; (e) Copyright 2008 American Institute of Physics; (f) Copyright 2006 American Chemical Society.

1.2.1 One-Pot Direct Synthesis

One-pot synthesis is the most straightforward method in preparation of gold nanoparticles. It is widely adopted in making spherical nanoparticles. And the resulting nanospheres are very stable and uniform. The one-pot method has a long history. The

first documented preparation of colloidal gold nanoparticles, which dated back to 1851 by Michael Faraday, was done through a one-pot reaction of sodium tetrachloroaurate with phosphorous in carbon disulfide solvent.[43] The most popular reaction system used nowadays to make small, spherical gold nanoparticles was reported by Frens in 1973.[20] In that work, sodium citrate was used as both a reducing agent and a stabilizer of nanoparticles. The pioneer work of one-pot synthesis all featured fast nucleation and growth, which often preceded the anisotropic growth of different crystal planes and would inevitably result in spheres and undefined-shaped particles. It was not until the past decade did researchers start to turn their attention onto slow kinetic systems, where remarkable shape control of gold nanoparticles was discovered.[30-32,44] In these attempts, mild reducing agents, like EG and PVP were used. The formation of shape controlled gold nanoparticles was carried out under high temperature (150-200 ^{o}C) and relatively long reaction time. Gold nanoparticles of tetrahedrons,[30] octahedrons,[32] icosahedrons,[30] cubes[30,32] and triangular plates[27,39] have been reported. Polymeric surface capping reagents were proved to be crucial in controlling the shape of resulting gold nanoparticles, as they can specifically bind to a certain crystal plane and thus induce anisotropic growth during the enlargement of nanoparticles.[1] In addition, the introduction of foreign ions, like Ag^{+}, could also greatly affect the growth of nanoparticles along certain directions.[40] The combined effects of surface capping polymers and foreign ions have generated gold polyhedrons with different number of faces.

1.2.2 Seed-Mediated Synthesis

Unlike the one-pot synthesis, where gold nanoparticles can be obtained via a single step, seed-mediated synthesis could only be achieved through a two-step process. In the first step, tiny clusters of gold (2 – 4 nm) are prepared by reducing diluted $HAuCl_4$ with strong reductant (normally $NaBH_4$),[45] the small size of gold nanoparticles is the result of explosive formation of numerous gold nuclei upon addition of $NaBH_4$. In the second step, a small amount of tiny gold clusters will be added to a growth solution, which contains $HAuCl_4$, a different reductant and the capping reagent. The gold clusters will act as nuclei (or "seeds" as commonly mentioned) and newly reduced atomic gold in the growth solution will deposit directly on them. The second step is characterized by a slow reaction rate under mild reducing environment, which is favored for shape control of gold nanoparticles.

So far, the most excited shape of particles obtained from the seed-mediated synthesis is gold nanorods or rod-like nanoparticles.[25,45-47] Gold nanorods have sophisticated optical absorption and scattering properties that are very sensitive to their aspect ratio.[18,19] Many biological applications, such as cell imaging, controlled drug release and photothermal therapy of cancer, have been explored based on gold nanorods.[8,34] Cetyltrimethylammonium bromide (CTAB) is the key reagent to the successful formation of rod-like nanoparticles. It contributes in at least three aspects: firstly, CTAB can significantly reduce the rate of reaction between gold chloride and ascorbic acid, which favors anisotropic growth of gold nanoparticles; secondly, as a surface capping reagent,

CTAB stabilizes the resulting gold nanoparticles; thirdly and also most importantly, CTAB defines the rod-like shape of gold nanoparticles. Addition of foreign ions can significantly influence the yield and shape of synthesized gold nanoparticles, which is similar to that in slow-kinetic one-pot synthesis. The yield of gold nanorods could be increased to a maximum of 97% in the presence of trace amount of Ag^+,[48] and furthermore, their aspect ratios can be manipulated by the amount of Ag^+ added to the growth solution.[49] When I^- is added as foreign ions, triangular plates rather than nanorods can be obtained.[26] In addition, the concentration of CTAB and ascorbic acid,[28] the stirring during reaction[50] and the types of seeds[45] all impact greatly on the final shape of gold nanoparticles, although the underlying mechanism has not been uncovered clearly up to date.

Another seed-mediated synthetic system that has been intensively studied involves the reduction of $HAuCl_4$ by DMF in the presence of PVP stabilizer and seeds. Several different shapes of gold nanoparticles have been reported under different reaction conditions. When 2-3 nm spherical seeds are used, and the reaction takes place under sonication, uniform decahedral gold nanoparticles are obtained;[51] however, without sonication, larger spheres[52] and flower-like nanoparticles[35] are produced under low and high PVP concentration respectively. In another report, pre-synthesized gold nanorods, instead of 2-3 nm spherical nanoparticles, were used as seeds, and this lead to the formation of tip-sharpened nanorods as well as octahedral particles under different $HAuCl_4$ concentrations.[53]

1.2.3 Templating Synthesis

In both one-pot and seed-mediated synthesis, the shapes of gold nanoparticles are controlled by functional molecules and ions, which can induce anisotropic growth of nanoparticles. However, in templating synthesis, the shape of nanoparticles is determined by the shape of template particles. The fundamental principle lying in the templating synthesis is the galvanic replacement reaction between $HAuCl_4$ and another more chemically active metal in the form of nanoparticles. The resulting gold nanoparticles are featured with hollow interior and shapes similar to those of the templates.[21,22,54]

Although simple, the templating approach makes it possible to synthesize gold nanoparticles with shapes that are difficult to obtain through direct synthesis. Hollow gold nanospheres have optical absorption at near infrared (NIR) region, and thus they can be used in the photothermal therapy of cancer.[22,55] However, direct synthesis has so far only resulted in solid gold nanoparticles. Through templating synthesis, hollow spherical gold nanoparticles can be prepared by simply adding controlled amount of $HAuCl_4$ into colloidal solution of Ag or Co.[54,55] Besides hollow nanospheres, ultrathin gold nanorods, which could not be obtained through seed-mediated synthesis in CTAB, have also been made from the corresponding ultrathin Fe nanorods.[56]

The galvanic replacement reaction between Ag nanocubes and $HAuCl_4$ has resulted in different types of Au/Ag alloy nanoparticles that exhibit tunable optical properties.[34] The most interesting structure is the hollow-porous-cubic nanoparticle. The nanoparticles have not only the hollow interior but also pores on the surface, which provides a pathway

to load drug molecules into the hollow space. Even more importantly, these hollow-porous nanocubes can be tuned to absorb at NIR region, which has lead to the recent success of controlled drug release through on/off of laser irradiation.[57]

1.3 Optical Properties of Gold Nanoparticles

Gold has been used as a pigment for staining glass and ceramics ever since ancient Roman time. But it was not clear where the color of gold originates from. In 1857, Faraday first prepared the pure reddish gold colloidal, which had the same color as ruby glass, in solution phase. He recognized that the color was due to the minute size of the gold particles, which were so small that were not able to be seen by any of the microscopes developed at that time. In 1898, Richard Zsigmondy successfully observed the tiny colloidal gold with his ultramicroscope. In 1908, Mie first explained the physical origin of colors in gold colloidal solution by using the classical electromagnetic theory and his work is now known as “Mie theory”.

Mie theory can be used to calculate the absorption and scattering properties of spherical nanoparticles of various materials. For gold and other electron rich metallic nanoparticles, Mie theory describes the interaction of nanoparticles with light as induced oscillation of nanoparticles’ free surface electrons in the electromagnetic wave.[18,19] When nanoparticles are placed in the electric field of the incident light, their surface free electrons (also known as surface plasmon) will be dislocated relative to the core of nanoparticles. However, the Coulomb force between the ionic core and electrons will

generate a restoring force to pull back the electrons. Such interaction will result in the oscillation of surface plasmon in an alternative electric field of light. According to Mie theory, the oscillation frequency of surface plasmon is dependent on the size and shape of the metallic nanoparticles as well as the dielectric constant of the corresponding bulk solid metal and of the medium surrounding them. When the frequency of incident light is equal to that of surface plasmon oscillation, a strong absorption of light will be observed in the spectrum. And this is known as Surface Plasmon Resonance (SPR).[58]

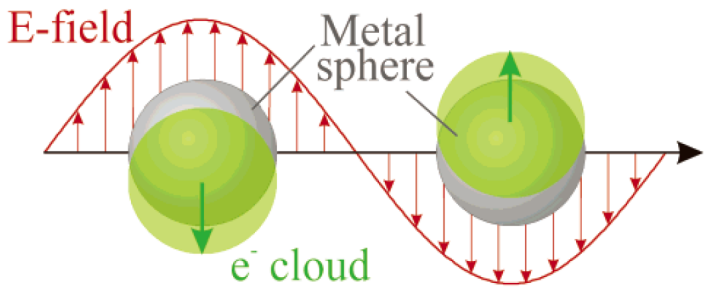

Figure 1.2, Schematic of surface plasmon oscillation in the electric field of incident light. Image reprinted with permission from ref. 18, Copyright 2003 American Chemical Society.

1.3.1 Nanospheres

Small spherical gold nanoparticles (< 20 nm) typically have a single narrow absorption peak in the visible range.[17] As the nanoparticles become larger, the absorption peak will be widened due to the inhomogeneous polarization of surface plasmon in the electric field of light. The extinction coefficient of gold nanoparticles is of

a few orders of magnitudes higher than that of conventional dyes.[59] Due to such a high extinction coefficient, spherical gold nanoparticles have been used extensively in detection and sensing applications with very high sensitivity. Nevertheless, the optical spectra of spherical gold nanoparticles are only limited in visible ranges, which makes them not suitable for many in vivo biological applications.

1.3.2 Nanorods

Rod-like gold nanoparticles demonstrate strong tunability in the optical spectrum. Gold nanorods have two absorption peaks, corresponding to the two directions of surface plasmon oscillation, one is along the transverse direction (at around 520 nm) and the other is along the longitudinal direction. The longitudinal SPR band is greatly dependent on the aspect ratio (R) of gold nanorods, which is the ratio of length along longitudinal direction over that of transverse direction.[18,60] For example, for nanorods of R=3.1, 3.9 and 4.6, their SPR bands are located at 730, 800 and 870 nm respectively.[19] Generally, by sophisticated control of the aspect ratio, the SPR bands of gold nanorods can be regulated from around 600 nm all the way to about 1500 nm. Such tunability in optical spectrum of gold nanorods has directly contributions in several important applications, like controlled release of multiple drugs[61] and polarization dependent multi-dimensional optical recording and image readout.[62] Besides, their absorption in the NIR region has attracted intensive research interest in the photothermal therapy of cancers.[6]

1.3.3 Nanoshells

Another way to achieve fine tune of optical properties of gold nanoparticles is to use the nanoshell structure. Similar to that of gold nanorods, the extinction spectrum of nanoshells can also tuned from visible to NIR regions.[63] The most common gold nanoshells have a solid spherical silica nanoparticular core coated by a gold shell. Both the inner diameter of silica core and the thickness of gold shell are tunable in the synthesis and the extinction spectrum of nanoshells will change correspondingly.[64] The SPR frequency of gold nanoshell increases almost exponentially with increasing ratio of shell thickness to core diameter.[65,66] For example, for a 40 nm silica core, when the gold shell thickness increase from 4 nm to 20 nm, the SPR band will shift from 860 nm to 520 nm.[19] Thus, for biological photothermal applications, a thin gold shell is always preferred.[67,68]

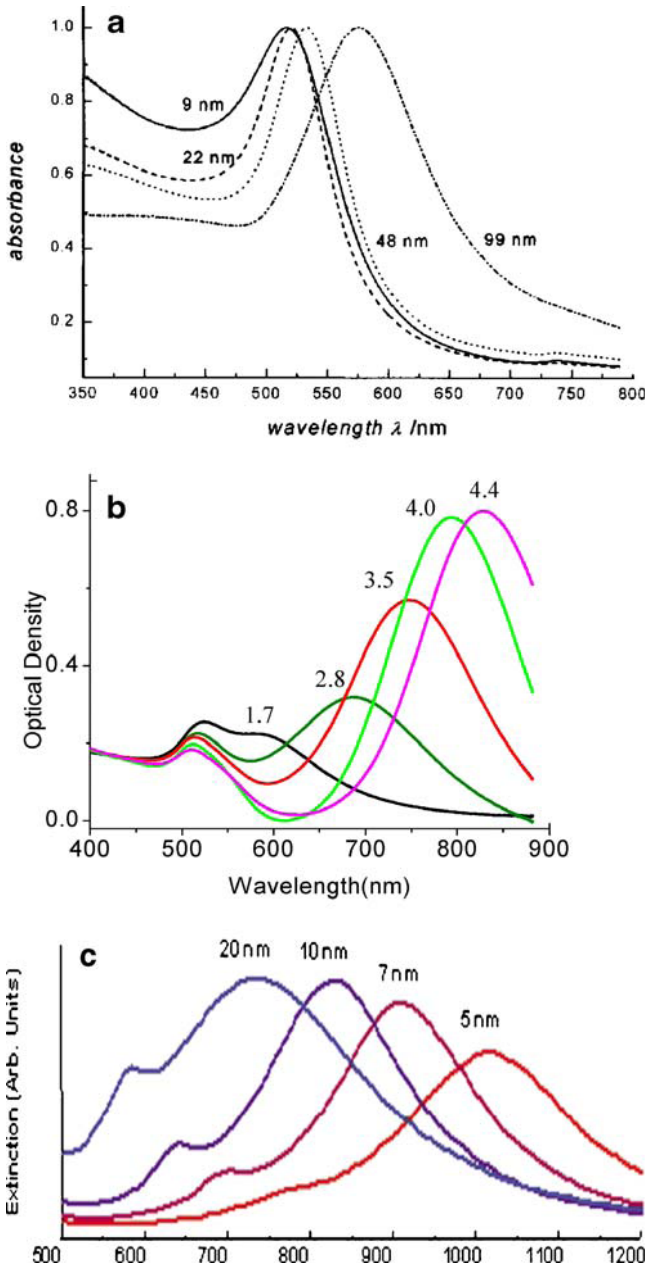

Figure 1.3, Optical tunability of gold nanoparticles of different size and shapes. (a) nanospheres of different sizes; (b) nanorods of different aspect ratios; (c) nanoshells of different shell thicknesses. Images reprinted with permission from ref. 17, Copyright 1999 American Chemical Society, ref. 49, Copyright 2003 American Chemical Society, and ref. 68, Copyright 2004 Adenine Press.

1.4 Biological Detection, Imaging and Therapy Based on Gold Nanoparticles

Due to their fascinating optical properties and good biocompatibility, gold nanoparticles have garnered plenty of research interest in exploring their biological applications. While the simple, well-developed synthesis protocols and the associating optical tunability as well as the uncomplicated surface modification has greatly facilitated such research attempts. Several different aspects relating to optical response of gold nanoparticles have been extensively studied for different applications, which will be reviewed below.

1.4.1 Surface Modification of Gold Nanoparticles

During the solution phase synthesis, the surface of gold nanoparticles is capped by some charged small molecules or polymers to achieve stabilization. Most of these capping molecules do not have biological functionality. However, in the biological applications, functional molecules or moieties, like site targeting peptides and antibodies, are often required to present on the surface of gold nanoparticles. For this reason, surface modification of as-prepared gold nanoparticles would be the first step before they can be readily applied for biological research.

Generally, two types of interactions can be employed to modify the surface of gold nanoparticles: electrostatic and covalent bonding. Electrostatic interaction first involves the layer-by-layer assembly of polyelectrolytes (ionic polymers) onto the nanoparticles,

and the functional molecules are electrostatically immobilized onto the surface that has the opposite charges.[69,70] Electrostatic approach is a simple, universal and highly efficient way to modify the surface chemistry of nanoparticles. However, the immobilized molecules can be easily detached from the surface in mediums of high ionic strength. Besides, since there is no selection in the sites of interaction, the configuration of some moieties may be destroyed upon immobilization onto the nanoparticles, which may further result in a loss of expected functionality. As an alternative to electrostatic interaction, conjugation through covalent bonding is considered as a more stable and selective method to manipulate the surface chemistry of nanoparticles. This method is normally done in two steps. In the first step, the nanoparticles surface is modified by molecules containing a thiol group on one end and a conjugatible group, typically –COOH and $–NH_2$, on the other end.[70,71] The thiol group will link firmly to gold nanoparticles by Au-S covalent bond. After the first modification, the desired functional moieties can be reacted with the conjugatible groups on the nanoparticle surface to form another covalent bond with the assistance of coupling reagents. Although giving stable conjugation products, this method could be very costly for functional moieties that do not initially have conjugatible groups, for it takes another step of tedious modification.

1.4.2 Optical Detection and Sensing

This application utilizes optical shift effect, caused by surface plasmon coupling, in aggregated or assembled gold colloidal particles. Spherical gold nanoparticles of 10-20

nm, which show intensive wind-red color in the solution phase, are often used. The surface of gold nanoparticles is first modified with molecules that can specifically recognize target molecules or ions. The interaction of surface modified nanoparticles with targets results in a close approach of several nanoparticles, which further causes an optical shift detectable either by naked eyes or a spectrometer.

A proof-of-concept research was first reported by Chad Mirkin in 1996 with DNA.[72] Single-strand DNA, which is complemental to the target DNA, is linked onto gold nanoparticles through Au-S chemistry. Since there is no interaction between the oligonucleotides after modification, gold nanoparticles can still exist as homogeneous, individual dispersion that shows a wine-red color. Upon addition of the target oligonucleotides to the colloidal solution, gold nanoparticles start to hybridize, under proper temperature, with the target sequence. Since there are multiple targeting oligonucleotides on one nanoparticle, the hybridization will result in an aggregation of a few nanoparticles, which will lead to a solution color change from red to purple or blue. Such targeting through hybridization of complemental oligonucleotides is very accurate, the optical shift of gold nanoparticles solution will not happen even there is only one base pair mismatched in the sequences.[73]

Following Mirkin's work, many research works were carried out based on the colorimetric detection of gold nanoparticles and various targets, including DNA,[74-76] amino acid[77] and metallic ions,[78,79] have been detected both qualitatively and quantitatively. Generally, gold nanoparticle based colorimetric detection has at least three

advantages that count for its long lasting attraction of research. First, the optical shift of the gold colloidal solution is highly sensitive. Within rationally designed system, as low as 1 pM target can be detected by naked eyes.[80] Second, the detection is very time-efficient. Normally, a color change in the gold nanoparticles solution can be observed a few minutes after addition of targets. Finally, unlike other detection methods, which depends heavily on the use of sophisticated instruments, colorimetric detection merely needs a UV-Vis spectrometer, and in most cases, naked eyes are quite enough to see the color change.

1.4.3 Biological Imaging

When the frequency of light is equal to the SPR frequency of gold nanoparticles, strong light scattering will take place. This optical property has greatly inspired the use of gold nanoparticles for biological imaging purposes. The degree of light scattering is significantly dependent on the size of gold nanoparticles. For small nanoparticles (<20 nm), the contribution of scattering is neglectable in the overall extinction of light. However, the light scattered is quite comparable to that absorbed for 80 nm gold nanoparticles.[19] For this reason, in biological imaging, larger gold nanoparticles are more commonly used. In comparison to the conventional dyes, the intensity of light scattered by a gold nanoparticle is about five orders of magnitude higher than that emitted by a dye molecule, making gold nanoparticles a potentially better option for biological imaging applications.[19]

Biological imaging with gold nanoparticles can be simply carried out under a regular optical microscope capable of doing dark-field imaging. The binding and internalization of nanoparticles to cells is achieved by culturing cells in the medium containing gold nanoparticles for a few hours. Unbound nanoparticles can then be washed away, leaving clean background for imaging. The incident white light is irradiated at a high angle to the vertical direction of cell culture plate in the dark field imaging, so that only light scattered by gold nanoparticles will be collected by the microscope objective. Each nanoparticle will appear as a colored bright spot under the microscope, and collection of spots from multiple nanoparticles inside each cell will result in the visualization of the whole cells.

When gold nanoparticles are incorporated with target specific molecules, dark field imaging can be used as a tool for diagnosis of diseases. Such targeting-enabled nanoparticles will bind densely onto the target cells generating a dark-field image with well-defined shape of cells. While for non-specific cells, gold nanoparticles will only randomly dispersed in a much lower density inside the cells and no clear cell images can be observed.[5,81,82]

1.4.4 Heat Based Therapy and Controlled Drug Release

The incident light will be absorbed strongly at the frequency equal to that of SPR of nanoparticles. The absorbed light will cause a heating effect to the nanoparticles lattice, from which the heat will further diffuse into the surrounding medium, resulting in a local

temperature increase around the nanoparticles.[83] Such property of gold nanoparticles has directly led to their application in the photothermal therapy of cancers and the controlled release of molecules.

Although heat generation is a universal phenomenon for gold nanoparticles having different SPR frequencies, biological applications, especially *in vivo* studies, prefer nanoparticles that can absorb at NIR region. The depth of penetration of light into skin is highly dependent on its wavelength, the longer the deeper. While most visible light can not penetrate through the skin, and light beyond the IR region is too low in energy, the desired wavelength range of light is from 650- 900 nm in the thermal application of gold nanoparticles.[83] Three different shaped gold nanoparticles, including nanorods,[6] nanoshells,[67] nanocages[84] and hollow spheres,[55] are often employed in the studies for their optical tunability in the NIR range.

Photothermal Therapy. The viability of cells is quite temperature sensitive. Exposure to temperature of a few degrees higher than 37 ^{o}C will cause death of cells. In the photothermal therapy of cancers, the nanoparticles are conjugated with cancer-targeting molecules, like anti-EGFR, so that they will specifically accumulate on the cancer cells.[5,81,82] Monochromatic laser that has the same wavelength as nanoparticles' absorption is used to destruct the cells as a result of localized heating effect from gold nanoparticles. The power of laser applied is so low that healthy cells, which have no affinity to the nanoparticles, will not be killed.

Controlled Drug Release. The heat energy produced by photo-irradiation of gold

nanoparticles is capable of breaking covalent bonds on their surface.[85] Thus, drug molecules conjugated through Au-S bond can be triggered to release.[86,87] Reminding that the photothermal effect only takes place when the frequency of incident laser is equal to that of the SPR of nanoparticles, in a mixture of several different types of nanoparticles, only one of them can be heated at one time. By conjugating each type of drug onto nanoparticles of a certain SPR frequency, selective release of drugs can be realized by using laser of corresponding frequencies.[61]

Photothermal effect of nanoparticles can also be used to induce phase transition of thermal sensitive polymer in a metal/polymer core/shell nanostructure. Gold nanoparticles employed in this kind of study are most often porous, like nanocages, so that their inner cavities can be used to accommodate drug molecules.[57] When the solution temperature is below the low critical solution temperature (LCST) of the selected polymer, its long chains are highly water compatible and fully extended. As a result, the pores on gold nanoparticles are covered by the polymer chains and drug molecules are confined inside the cavities. However, once the core/shell nanoparticles are irradiated by a proper laser, photothermal effect will cause an increase in the local temperature to above the LCST of the polymer.[57] A conformation change of the polymer from extended state to contracted state takes place immediately. And simultaneously pores on gold nanoparticles are exposed to the solution, resulting in the release of drug molecules. By switching on/off of the laser, drug release can be controlled to be on/off respectively.

1.5 Assembly of Nanoparticles into Hierarchical Structures

Approaches of fabricating microstructures based on nanomaterials generally fall into two categories: top-down etching and bottom-up assembly. The top-down etching involves selective sculpture of a bulk piece of material into nanostructured pattern. It is generally a multiple-step physical process. The top-down approach can be used to fabricate highly ordered nanostructures; however, it requires sophisticated equipments and suffers from high experimental cost and low productivity. The bottom-up assembly utilizes nano-sized particles as building blocks to make hierarchical structures. Chemical interaction is the major contributor in the assembly of nanoparticles. In rationally designed systems, nanoparticles can be assembled into highly ordered structures. And the desired nanostructures can be prepared in large quantity in both time- and cost- efficient manner. This part of introduction will focus on the bottom-up assembly approach of making hierarchical nanostructures.

During the assembly of nanoparticles, the chemical interaction mainly takes place through the molecules capping the surface of nanoparticles. Thus, proper manipulation of surface chemistry is critically important in the assembly of nanoparticles. And since the solid core of nanoparticles is not involved, strategies developed for assembling nanoparticles of one type of material should be readily applied to those of other materials as long as they have the same surface chemistry. The intensive study of bottom-up approach has resulted in various strategies to assemble nanoparticles into 1-D, 2-D and

3-D structures. Depending on whether templates are employed to assist assembly or not, these strategies can be divided into two groups: template-assisted assembly strategy and self-assembly strategy.

1.5.1 Template-Assisted Assembly

For many types of macromolecules, like block copolymers, DNA and proteins, they can self assemble to form highly organized structures under proper conditions. Because the nanoparticles are so small, when integrated with these functional macromolecules, they can be co-assembled into exactly the same ordered structures. These macromolecules are normally known as soft templates. In addition, due to the success in preparation of inorganic nanowires, 1-D assembly of nanoparticles has also been explored base on such linear structures. These inorganic nanowires are generally considered as hard templates.

1.5.1.1 Block Copolymers

Block copolymers are a type of polymer composed of two or more covalently linked homopolymers with various chain length. Each homopolymer can be considered as one segment. When a thin film (a few nm in thickness) is casted from the solution of a block copolymer that contains both hydrophilic and hydrophobic segments, micro-phase separation will take place under proper annealing conditions, resulting in an organized array (hexagonal or horizontally cylindrical) of microdomains.[88,89] Each microdomain is assembled from the same homopolymers, either hydrophilic or hydrophobic.[90] The

co-assembly of nanoparticles with block copolymers is normally carried out by mixing them into a homogeneous solution and being casted together into a film. Prior to mixing, the nanoparticles are surface modified with the same block copolymers or the corresponding homopolymers to improve the compatibility with the phase. Such modification will directly affect the location of nanoparticles in the microdomain after phase separation of block copolymers. If their surface is covered by hydrophobic homopolymers, the nanoparticles will be assembled into the microdomain composed of hydrophobic segment of the block copolymers, and *vice versa*.[91-94] More interestingly, when block copolymers, rather than homopolymers, are capping the surface of nanoparticles, the assembly will take place at the interface of hydrophobic and hydrophilic microdomains.[91,95] The modification of nanoparticles surface chemistry with different molecules provides more flexibility in manipulating the relative location of nanoparticles during the co-assembly process.

1.5.1.2 Protein Cages

Protein cages are self-assembled three-dimensional structures of proteins.[96] These spherical nanoparticles are characterized by having hollow cavities in the center. Benefiting from the naturally occurring self-assembly process, these supermacromolecules are quite uniform in both inner and outer diameters. When deposited onto a substrate, protein cages can organize themselves into ordered hexagonal 2-D arrays;[97] while induced crystallization in the solution phase will result in 3-D

ordered packing of protein cages.[98]

The self-organizing capability of protein cages can be applied to assemble other types of nanoparticles by incorporating them inside the cavities of the supermacromolecules.[99] The proteins, from which cage structure is assembled, can be modified and functionalized through genetic engineering to have specified interaction with a certain type of material. The pre-synthesized nanoparticles can then be directly intake into the hollow cavities of genetically modified protein cages.[97,100] Alternatively, ions of the corresponding nanoparticles can be adsorbed and reduced directly inside the cavities of the supermacromolecules.[101-103] Besides, without genetic modification, by mimicking the formation of virus, proteins can be induced to assemble onto pre-synthesized nanoparticles, the surface chemistry of which has been modified with the RNA sequence initiating the assembly of proteins during the formation of virus.[104] This mimicking approach also produces protein encapsulated nanoparticles that can self-assemble into ordered structures.

1.5.1.3 DNA

It has been reviewed in 1.3 that highly sensitive colorimetric detection of oligonucleotides can be achieved by linking gold nanoparticles with a complementary sequence to the target DNA. The high detection limit is a result of high selectivity in the hybridization of DNA oligonucleotides. Such self-recognition behavior of two complementary DNA oligonucleotides has also greatly facilitated the assembly of

nanoparticles. The thought of using DNA as building blocks to construct periodic structures had been raised ever since 1982.[105] Up to date, many types of periodic 1-D, 2-D and 3-D structures have been successfully fabricated based on DNA.[106-108] Generally, two fundamental components are involved to assemble DNA into patterned structures: tiles and overhung sticky ends.[109-111] Tiles are the smallest repeating units that compose the body of DNA patterns. Tiles are normally branched in structure and are self-assembled from several different ssDNA molecules. None of these ssDNA molecules are completely complementary, but one ssDNA can be divided into two or more segments that are complementary to part of the sequence on several ssDNA. The interlocking of these ssDNA oligonucleotides will result in tiles of many different shapes. At each end of the branches in a tile, there hangs a short piece of free ssDNA motif (sticky ends) that will link together the tiles to form the patterned structures.

In order to apply the patterned DNA structures as templates to achieve ordered assembly of nanoparticles, each tile is designed to have another free sticky end that will not be used as a structural linker but as an interaction site for nanoparticles.[112-115] The surface of nanoparticles, most often gold, will be modified with a corresponding complementary oligonucleotide so that the nanoparticles will only interact with the designated sites on the templates. Such approach of assembling nanoparticles through templating patterned DNA structures provides flexibility in controlling both the inter-particle distance and the pattern of nanoparticle arrays.[116]

1.5.1.4 Inorganic Nanowires

Nanowires of most inorganic materials are prepared under 50 nm in diameter and with length of a few micrometers. Their well-defined 1-D structures as well as the rigid mechanical property are considered to be good templates for linear assembly of nanoparticles. Unlike the assembly through soft templates, where nanoparticles are confined to a specific phase or site, interactions between nanoparticles and inorganic nanowires are non-specific. And thus, the assembled patterns are generally not as uniform as those based on the soft templates. The force inducing attachment of nanoparticles onto nanowire templates originates from electrostatic interaction or covalent bonding.[117-119] For either one, the templating nanowires are usually pre-treated with a multi-step surface modification to introduce necessary functional groups on their surface. The nanowire templates are structurally unique in oriented alignment of rod-like nanoparticles. When interacting with the templates, nanorods will selectively align their long axis with the longitudinal direction of the nanowires to achieve the strongest binding to the templates. And as a result of this selective interaction, rod-like nanoparticles can be unidirectionally aligned along the nanowire templates.[120]

1.5.2 Template-Free Assembly

The template-assisted assembly of nanoparticles emphasizes greatly the importance of templates in determining the final pattern of assembled structures. And the assembly of nanoparticles takes place through the interaction of their surface capping molecules with

the specific sites or spots on the templates. In the template-free approach, however, the assembly is through the externally stimulated interaction among the surface molecules on different nanoparticles. Thus, both the external stimulation and the surface capping molecules determine the arrangement of nanoparticles in the assembled structures. Most often, for a certain type of capping molecules, only a specific stimulation will induce the assembly. The typical stimulus involved in the template-free assembly of nanoparticles includes pH, temperature and solvents.

1.5.2.1 pH

When the surface of nanoparticles is capped by molecules that have functional groups, such as amine and carboxylic groups, capable of forming hydrogen bonds, pH values of the solution will significantly impact the nanoparticles' dispersion state.[121] For carboxylic groups, they are neutral under low pH and become charged at high hydroxide ions concentration. The charges on the nanoparticles surface will create a repulsive force to prevent their assembly. While in neutral state, strong hydrogen bonding effect among carboxylic groups on the surface of different nanoparticles will link them together. Such pH dependent assembly of nanoparticles is usually reversible. When the pH is adjusted back, nanoparticles aggregate can be disassembled to form a stable dispersion again.[122,123]

1.5.2.2 Temperature

It has been reviewed previously that free target DNA oligonucleotides can induce the aggregation of nanoparticles that have complementary sequence on the surface. The optical shift rising from the aggregation of gold nanoparticles can be used to detect the DNA sequence of interest. Similarly, when two types of nanoparticles that are coated by complementary DNA are mixed in the solution, assembly of nanoparticles will take place along with the hybridization of DNA.

It is well-known that the stability of DNA duplexes is highly temperature sensitive. Low temperature favors the formation of duplex structure; While if the temperature is above their melting point, the duplexes will be denatured and disassembled into two single strands. Thus, the complementary DNA coated nanoparticles will assemble at temperature below the melting point of DNA and disassemble at higher temperature.[124] Such temperature-induced assemble and disassemble of nanoparticles is highly reversible and is accurately correlated with the melting temperature of DNA.[125]

1.5.2.3 Solvent

Solvents have great effect on solubility of almost all chemicals. For macromolecules, like polymers, a change in solvent polarity usually causes a molecular conformation change. In a completely compatible solvent, polymer chains are fully extended and correspondingly, a homogeneous, transparent solution is observed. When an unfavored solvent is added gradually, the homogeneous solution will first become turbid and

eventually undergo a phase separation due to the contraction and anchoring of the polymer chains in unfavored surroundings. When the polymers are capping the nanoparticles surface, their behaviors in unfavored solvent will result in the assembly of nanoparticles. In well-designed systems, the structure of assembled nanoparticles can be tuned by the percentage of unfavored solvent added.[126]

1.6 Overview of Dissertation

Great accomplishments have been achieved in the synthesis and assembly of nanoparticles during the past decade. Nanoparticles with controlled size and well-defined shapes have been synthesized through careful selection of surface capping molecules and addition of trace amount of foreign ions in slow-kinetic reactions. The availability of shape-controlled nanoparticles has significantly facilitated the study of nanoparticles' optical properties both theoretically and experimentally. As a result, many optical-based biological applications have been explored successfully by using gold nanoparticles. In terms of bottom-up assembly of nanoparticles into hierarchical structures, a variety of research work that can be generalized into template-assisted and template-free approaches have been conducted.

However, synthesis of structurally complex gold nanoparticles, such as branched and dendritic nanoparticles, is still remaining a challenge. The structurally complex gold nanoparticles may possess both high surface area and interesting optical properties that could potentially be better suited for applications, such as highly-loaded drug delivery

and release, catalysis and optical-related biological treatments. Besides, not all nanoparticles can be synthesized uniformly, while current density gradient based size sorting of nanoparticles can only applied to separate small nanoparticles, a purification method that can be employed to achieve size selection of larger nanoparticles is in demand. Although many strategies have been reported to assemble nanoparticles into various hierarchical structures, developing new methodologies that can generate novel assembled structures or improve the assembly of a previously revealed structure is still necessary.

The current research aims at developing new synthetic strategy to prepare structurally complex gold nanoparticles and new size sorting method to separate nanoparticles of larger size, as well as studying the assembly of nanoparticles into novel hierarchical structures through both template-assisted and template-free strategies.

In Chapter 2, dendritic gold nanoparticles were prepared through a seed-mediated process in ethanol. Size control of the nanodendrites could be achieved by simply adjusting the ratio of $HAuCl_4$ to total number of seeds added. The surface of nanoparticles is capped by the hexadecylamine ($C_{16}H_{33}NH_2$). The carbon chain length of alkylamines ($C_nH_{2n+1}NH_2$) has great effect on the generation of gold nanodendrites. The dendritic structure can be observed only when $n \geq 12$. In the hexadecylamine-ethanol system, the dendritic structure could be produced on seeds of different shapes, including spherical, rod-like and flat triangular nanoparticles.

In Chapter 3, we studied the shape evolution of gold nanoparticles in a

seed-mediated growth as well as the kinetics of reduction of $HAuCl_4$ in the presence of seeds. The reduction of the gold precursor by sodium citrate was accelerated due to the addition of pre-synthesized seed nanoparticles. The investigation of shape evolution was carried out by manipulating the molar ratio (R) of sodium citrate to the gold precursor, $HAuCl_4$. Nearly single-crystalline gold nanowires were formed at a very low R value (R = 0.16) in the presence of the seeds as a result of the oriented attachment of the growing gold nanoparticles. At a higher R value (R = 0.33), gold nanochains were formed due to the non-oriented attachment of gold nanoparticles. At a much higher R value (R = 1.32), only larger spherical gold nanoparticles grown from the seeds were found. In the absence of gold seeds, no single-crystalline nanowires were formed at the same R value. Our results indicate that the formation of the 1D nanostructures (nanochains and nanowires) at low R values is due to the attachment of gold nanoparticles along one direction, which is driven by the surface energy reduction, nanoparticle attraction, and dipole–dipole interaction between adjacent nanoparticles.

In Chapter 4, we developed a novel method of separating nanoparticles of different sizes in a viscosity gradient. The viscosity gradient was created by stacking gradient concentration of polyvinylpyrrolidone (PVP) aqueous solutions. Previously, such size separation was all achieved in the density gradient, while the hidden contribution of viscosity difference inside the density gradient was not well recognized. Through this work, it is clarified that the viscosity can contribute as importantly as density in the size sorting of nanoparticles through rate zonal centrifuge. It was also demonstrated both

experimentally and mathematically that the viscosity gradient is more effective in separation of larger sized nanoparticles.

In Chapter 5, we investigated the oriented 1-D assembly of gold nanorods by using bacteria flagella as templates. This biological filamentous template was purified from the *Escherichia coli* bacteria. The assembly took place through electrostatic interaction between the positively charged gold nanorods and the negatively charged flagella. Two approaches were carried out to obtain the assembled structures. In one approach, nanorods and flagella were mixed directly in the solution phase; while in the other one, flagella were first immobilized onto a TEM grid, which was then floated on a drop of nanorods solution to allow adsorption. Both approaches generated well aligned gold nanorods structures. The optical shift of aligned gold nanorods was also studied. The flagella could potentially be a better template than the previously used carbon nanotubes, since carbon nanotubes involve tedious surface modification to get charges, while flagella are naturally charged and the charges could also be manipulated through genetic engineering.

In Chapter 6, novel branched hollow microfibers that were co-assembled from PVP stabilized gold nanoparticles and free PVP molecules in the solution were revealed. Initially, we discovered that PVP could self-assemble into branched hollow fibers in an aqueous solution after aging under room temperature for about two weeks. On the basis of this finding, we demonstrated two approaches (one is through direct deposition of silica onto the PVP aggregate and the other is through co-assembly of PVP covered gold

nanoparticles with free PVP molecules) by which the self-assembly behavior of PVP could be exploited to template the formation of branched hollow inorganic fibers. Our work suggests that the self-assembly of the PVP molecules in the solution can serve as a general method for directing the formation of branched hollow inorganic fibers.

In Chapter 7, a general method for template free assembly of nanoparticle into clusters (NPCs) in an oil-in-water emulsion system was investigated. The assembly was mediated by cetyl trimethylammonium bromide (CTAB) where previously, only individual nanoparticles were obtained. NPCs of magnetic, metallic and semiconductor nanoparticles have been prepared to demonstrate the generality of the method. The NPCs were spherical and composed of densely packed individual nanoparticles. The number density of nanoparticles in the oil phase was found to be critical for the formation, morphology and yield of NPCs. The method developed here is scalable and can produce NPCs in about 98% yield at a concentration of 5 mg/ml in water which is approximately 5 times higher than the highest value reported in literature. The surface chemistry of NPCs can also be controlled by replacing CTAB with polymers containing different functional groups via a similar procedure. The reproducible production of NPCs with well defined shapes has allowed us to compare the properties of individual and clustered iron oxide nanoparticles including magnetization, magnetic moments and contrast enhancement in magnetic resonance imaging (MRI). We found that due to their collective properties, NPCs are more responsive to an external magnetic field and can potentially serve as better contrast enhancement agents than individually dispersed magnetic NPs in MRI.

Chapter 8 is a summarization of all the research work conducted and outlooks of the future directions.

CHAPTER 2

A Facile Synthesis of Gold Nanodendrites via a Seed-Mediated Process

2.1 Introduction

Gold nanoparticles (AuNPs) have size- and shape-dependent surface plasmon resonance (SPR) spectra, which have been actively exploited in many research fields, including biological imaging and therapy,[127,128] signal enhancement,[129] detecting/sensing,[130] waveguides[131] and enhancement of light absorption in solar cells.[132] These applications require successful synthesis of AuNPs with controllable size and shape. Recent advances in the synthesis of structurally complex AuNPs allow for further tuning of the optical spectrum and endow more functionality on an individual particle.[35,133-136] As a typical example, star-shaped AuNPs (nanostars), which consist of a spherical core and several tips, exhibit multiple plasmon bands arising from the hybridization of individual tip and core plasmons.[50,136] And the gold nanostars have shown an extremely high Raman enhancement factor on the single-nanoparticle level due to the plasmon coupling effect.[137] However, the chemical synthesis of AuNPs complex is still challenging up to date and reported synthetic methods are suffering from low yield of interested structures. Here we developed a new strategy of preparing three dimensional (3D) gold nanodendrites (AuNDs), in 100% yield, through a seed-mediated overgrowth process.

Currently, only dendritic platinum nanoparticles (DPNs) have been successfully synthesized with controllable size. Song et al. reported the first synthesis of DPNs by using a photocatalytic seeding method in surfactant solution (SDS or Brij-35).[138] In their work, the tin-porphyrin photocatalyst can generate rapidly a huge number of small Pt nanoparticle seeds in the initial state of reaction. Following that, Pt complex was reduced through an autocatalytic growth approach on the seed surface.[138,139] Simpler synthetic strategies of DPNs and Pd-Pt bimetallic nanodendrites were revealed later in aqueous solutions of CTAB,[140] Pluronic F127 block copolymer[141] and PVP[142,143] either in the presence or absence of seeds. Though these synthetic approaches can produce finely-structured Pt nanodendrites, they are generally not suitable for making AuNDs. For example, in the aqueous solutions of PVP and CTAB, only spherical Au nanoparticles can be obtained under the same reaction condition.

2.2 Experimental Methods

2.2.1 Synthesis of PVP Covered Seed Nanoparticles

Gold nanoparticles of around 13 nm were synthesized by reduction of 5 ml 5.9 mM $HAuCl_4$ with 7 ml 38.8 mM sodium citrate in a total of 50 ml aqueous solution. The ligand exchange was done by adding 500 mg of PVP (10 K) into the cooled AuNPs solution and stirred for 24 h under the room temperature. The AuNPs were then concentrated by centrifuge and redispersed into 5 ml ethanol.

Gold nanoparticles of 2-3 nm were synthesized as follows: 600 μl 5.9 mM $HAuCl_4$

was mixed with 4 ml 2 wt. % PVP 10k aqueous solution, then 1 mg of solid $NaBH_4$ was added into the solution and mixed immediately by vigorous hand shaking for 10 s. The nanoparticles solution was placed for overnight and degassed by sonication before use.

2.2.2 Synthesis of Gold Nanodendrites

Typically, various volume of above seed solution was added to 4 ml 0.1 M hexadecylamine ethanol solution, followed by adding 20 μl 60 mM $HAuCl_4$. When the solution was thoroughly mixed, 20 μl 0.788 M ascorbic acid was injected and mixed by hand shaking. The vial was then placed on a rocking shaker for about 2 h. After that, the particles were centrifuged and redispersed into chloroform for further analyze. The amount of seeds (13 nm) added in Fig. 2.1 are 40, 20, 10, 5, 2, 0.5 μl from a to c. For control experiments, $HAuCl_4$ and ascorbic acid were used in the same amount as above. Octadecylamine, dodecylamine, octylamine and butylamine were all used in 0.1 M and in ethanol.

2.3 Results and Discussions

2.3.1 Characterization of Gold Nanodendrites

The size of AuNDs can be readily tuned by varying the ratio of $HAuCl_4$ to seeds (PVP stabilized). Fig. 2.1 shows a continuous increase in AuNDs size while fixing the amount of $HAuCl_4$ and decreasing the quantity of seeds. Here, we will describe the AuND as a core, which is a solid nanosphere, decorated by many nanohairs. The number

of nanohairs on an individual particle increases greatly with the enlargement of nanodendrites; however, the diameter of the core does not change significantly. Considering that the core only has surface area for a few hairs, the additional nanohairs observed on AuNDs should grow by forming branches on existing hairs, resulting in the formation of 3D dendritic structures. It should also be noted that although the particle sizes vary remarkably in Fig. 2.1 a-f, the diameter of nanohairs on each particle remains the same.

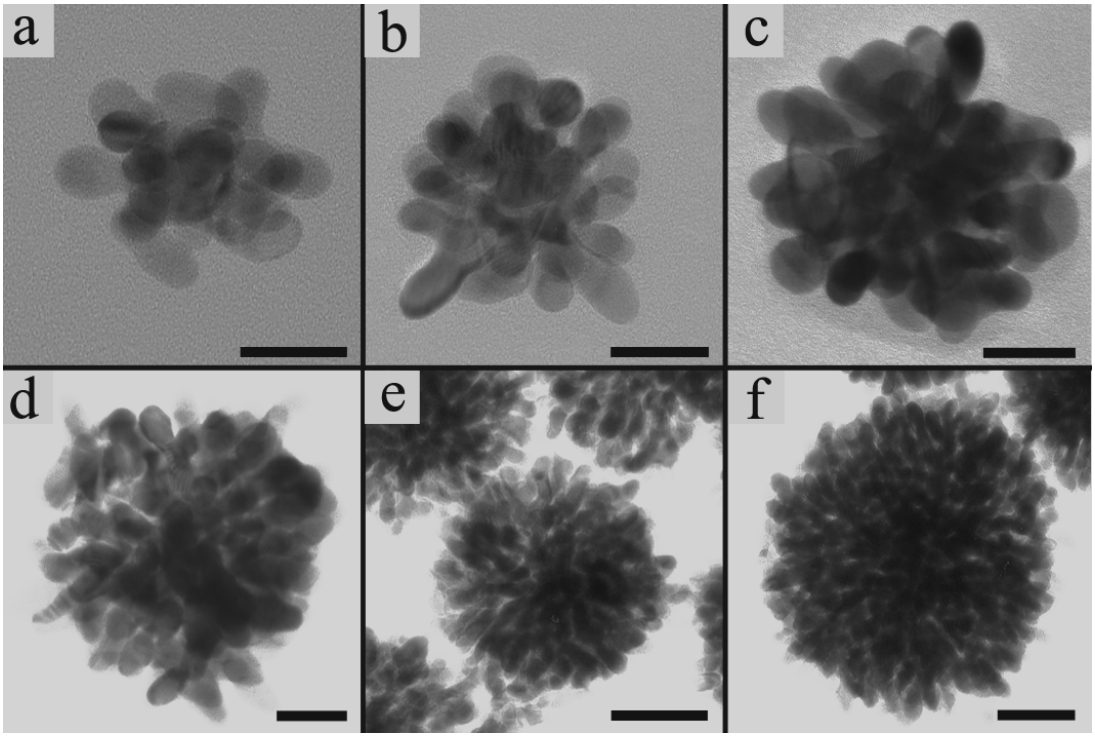

Figure 2.1, Gold nanodendrites of different size, prepared from a-f) 40, 20, 10, 5, 2, 0.5 μl 13 nm seeds respectively. Scale bars: a-d, 20 nm; e-f, 50 nm.

2.3.2 Effect of Seeds Size and Shapes on the Formation of Dendritic Structure

The effect of seed size on the formation of dendritic structure was studied. Instead of using 13 nm seeds, we prepared seeds of 2-3 nm (Fig. 2.2a). We found that when much smaller seeds were used, the dendritic structure could only be observed above a certain particle size. The 2-3 nm seeds can grow freely into larger nanospheres up to 8 nm (Fig. 2.2b); however, slightly beyond 8 nm, isotropic growth of spherical nanoparticles is prohibited and only elongated rod-like nanoparticles can be obtained (Fig. 2.2c). When the particles size was further increased, branches started to form onto the elongated nanoparticles, resulting in the formation of dendritic structure (Fig 2.2d). Further increasing nanoparticles size produced gold nanodendrites with much more complicated branched structures (Fig. 2.2d).

Besides the size of seeds nanoparticles, the effect of shape of seeds on the formation of dendritic structure was also investigated. The spherical 13 nm AuNPs seeds were replaced by rod-like (20 nm in diameter) and flat triangular shaped (250 nm in edge length) nanoparticles. Through a similar overgrowth process, many tiny nanohairs were generated onto the smooth surface of the seeds nanoparticles (Fig. 2.3). Thus, the formation of dendritic structure should be independent from the shape of seeds employed.

2.3.3 Effect of Alkylamines on the Formation of Dendritic Structure

The effect of carbon chain length of the alkylamines ($C_nH_{2n+1}NH_2$) on the formation

of dendritic structure was studied. The hexadecylamine (n=16) was replaced by alkylamines of varying carbon chain length, including octadecylamine (n=18), dodecylamine (n=12), octylamine (n=8) and butylamine (n=4). The concentration of these alkylamines remained as 0.1 M in ethanol. At n=18, gold nanodendrites with clearly identifiable branches were produced (Fig. 2.4). However, at decreasing carbon chain length, the resultant nanoparticles had much less characters of dendrites. At n=12, a number of branches could still be observed on the nanoparticles, but the solid cores had become much larger than those produced by hexadecylamines (Fig. 2.5). At n=8, there are only a few branches on large solid cores (Fig. 2.6), and at n=4, the seeded growth only resulted in large solid spherical nanoparticles (Fig. 2.7). Thus, it could be concluded that in the alkylamine-ethanol system, the formation of dendritic structure is favored by long carbon chain length ($n \geq 12$).

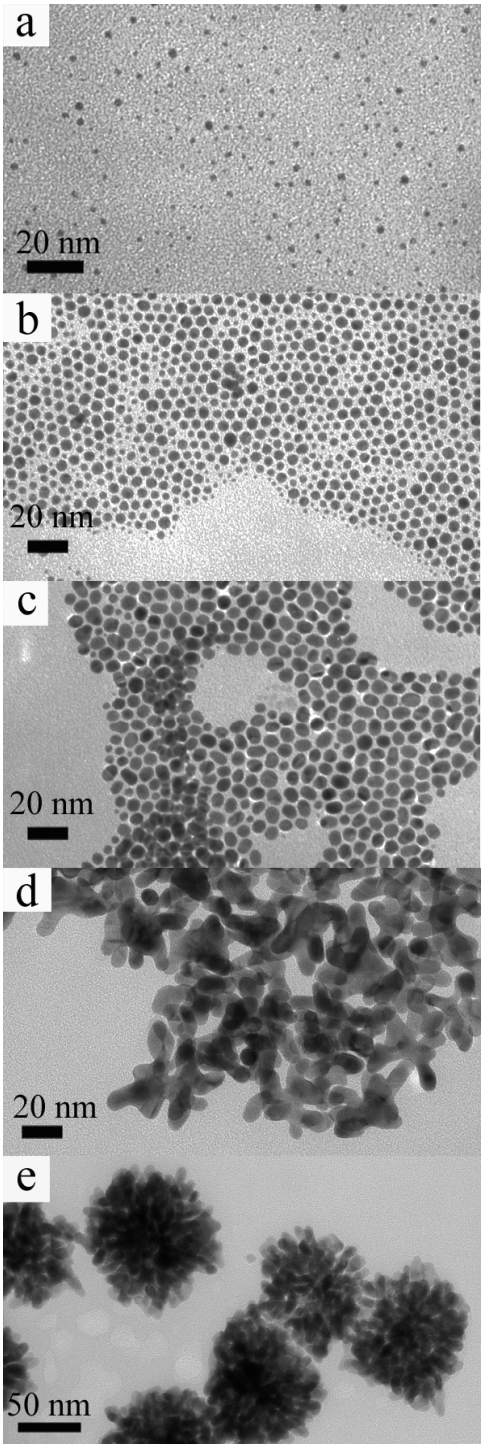

Figure 2.2, Morphology transition of gold nanoparticles from spherical to dendritic along with increase of size. a) As prepared 2-3 nm seeds; (b-e) Particles resulted from 200, 100, 20 and 2 μl tiny seeds, respectively.

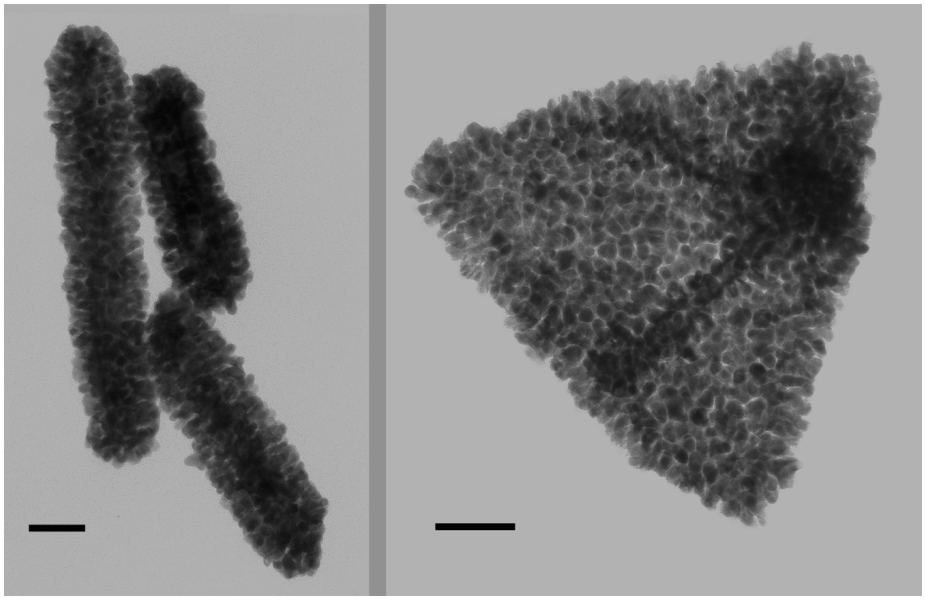

Figure 2.3, Overgrowth of nanohairs onto nanorods (left) and flat triangular nanoparticles (right). Scale bars: 50 nm for both.

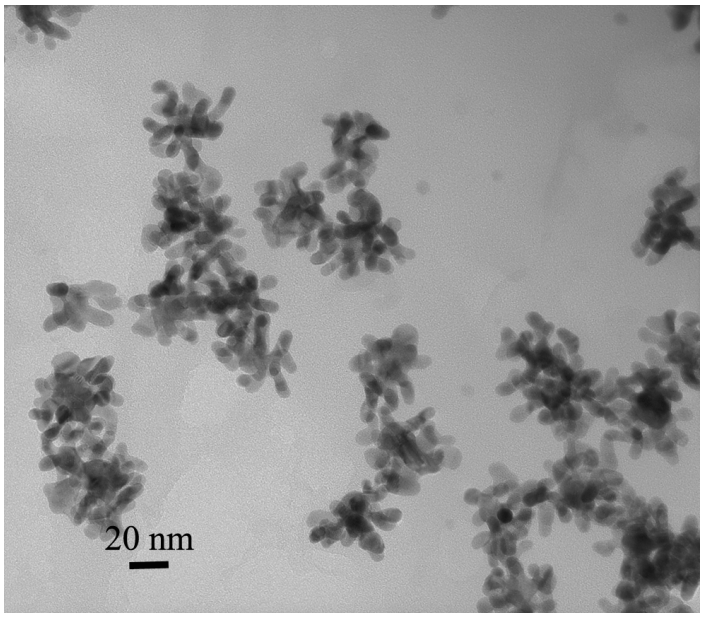

Figure 2.4, AuNDs obtained by using octadecylamine as capping reagent.

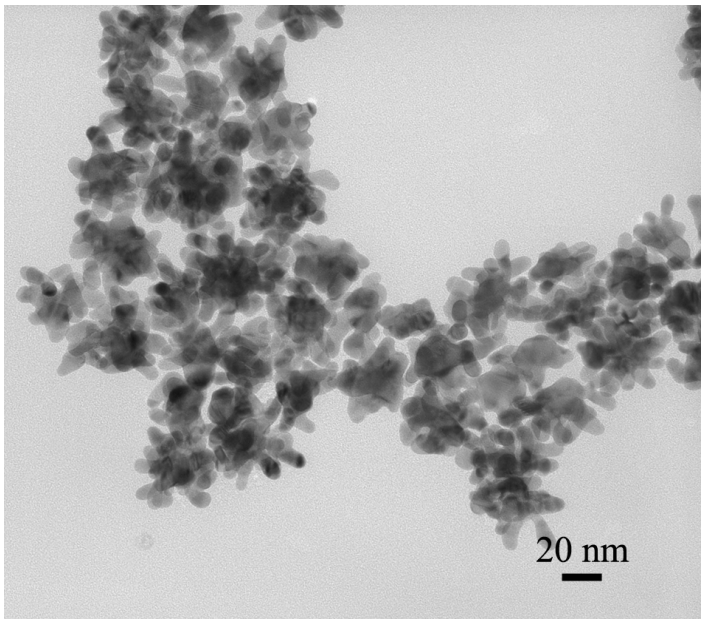

Figure 2.5, AuNDs obtained by using dodecylamine as capping reagent.

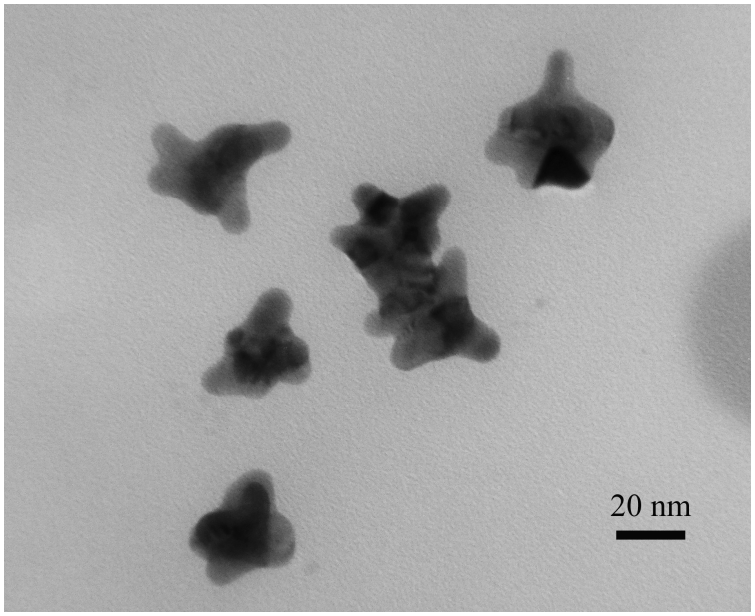

Figure 2.6, AuNDs obtained by using octylamine as capping reagent.

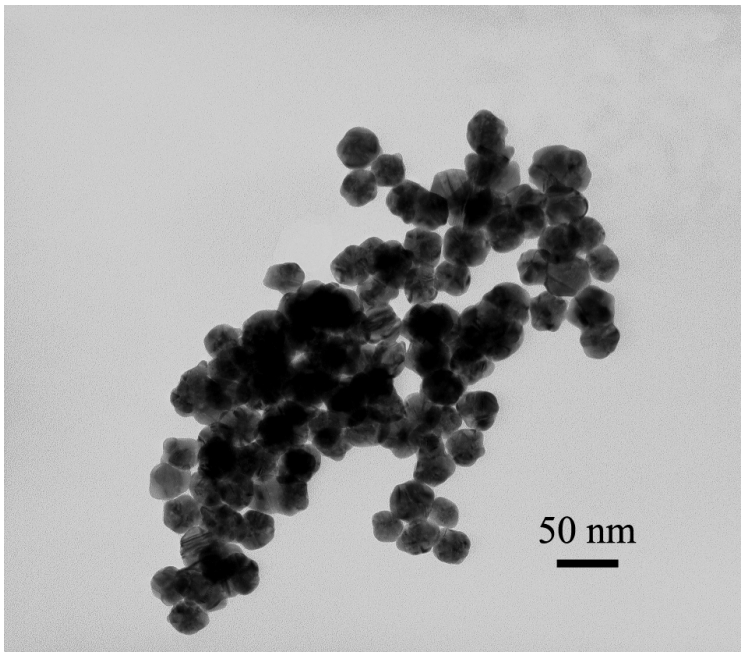

Figure 2.7, AuNDs obtained by using butylamine as capping reagent.

2.3.4 Optical Properties of Gold Dendritic Nanoparticles

The AuNDs exhibit broad extinction in the optical spectra (Fig. 2.8). There are two factors that contribute to such complicated spectra. First, the AuNDs are uniform in overall size but not in morphology. Since AuNDs are structurally complex, the number and symmetry of nanohairs, as well as the sites of branch growth are quite different from one particle to another. Due to the sensitive correlation between shape and optical property in AuNPs, even slight morphological difference will result in a significant variation in the spectrum.[150] The measurement was done in the solution phase with signals from billions of individual nanoparticles, so the sum puts together all the difference and gives a broad extinction. Second, the surface plasmon coupling of core/nanohairs and nanohair/nanohair further broadened the extinction spectrum. The

individual gold nanostars have multiple plasmon bands arising from the plasmon hybridization of the spherical core and each tip.[50] The AuNDs, complex of spherical core and nanohairs, are structurally similar to nanostars, so the individual nanodendrite should also possess multiple plasmon bands. However, the nanostars only have a few tips (typically less than 6),[136] while the AuNDs generally have numerous nanohairs. According to plasmon hybridization theory,[50,151] assuming that each of nanohairs on the same core is different, the individual AuNDs are expected to exhibit plasmon bands corresponding to the number of nanohairs. Besides, on one particle, especially large AuNDs (Figs. 2.1e and 2.1f), the neighboring nanohairs are sitting very close to each other, which will cause the extra plasmon coupling, adding more characters to the optical spectrum.

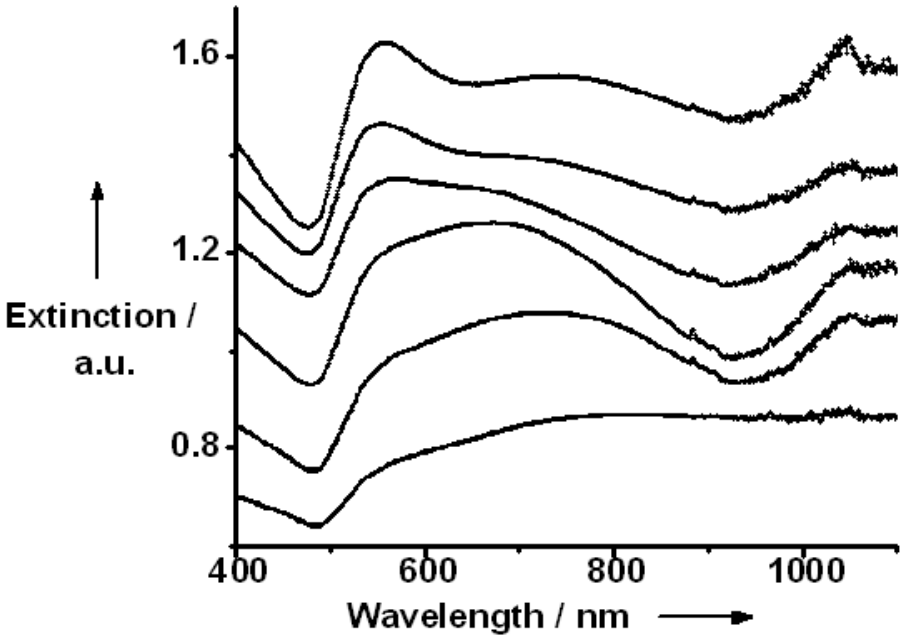

Figure 2.8, Extinction spectrum of as synthesized AuNDs with increasing particle size from top to bottom corresponding to Fig 2.1a-f.

2.4 Conclusion

To conclude, we have synthesized the dendritic AuNPs through a seed-mediated approach in the HDA-ethanol solution. The effect of seed size and shape, as well as the carbon chain length of the alkylamines on the formation of dendritic structure was studied. The broad extinction spectra of the AuNDs are attributed to both the structural nonuniformity of AuNDs and the plasmon coupling of core/nanohairs and nanohair/nanohair. Compared to solid nanoparticles, the dramatically increased surface area of AuNDs makes them better suited for a variety of applications, such as drug

delivery, catalysis, and electrochemisty. Also the individual AuNDs demonstrated here own the most complicated structure revealed on AuNPs up to date, which could act as a model for better understanding plasmon coupling/hybridization of complex nanostructures. Not only can the overgrowth of dendritic structure occur on the spherical seeds, but also on many other kinds of AuNPs surface, such as nanorods and nanoprisms, providing a general way of increasing nanoparticle surface area and tuning of optical properties.

CHAPTER 3

Seed-Mediated Shape Evolution of Gold Nanomaterials: from Spherical Nanoparticles to Polycrystalline Nanochains and Single-Crystalline Nanowires

3.1 Introduction

In the recent years, one-dimensional (1-D) metal nanostructures have stimulated fundamental and practical interests in nanotechnology.[152] For instance, due to the near-field coupling of the plasmons of adjacent metal nanoparticles, electromagnetic energy can be guided coherently along the 1-D nanostructures.[131,153-156] Apart from the optical and electronic properties, the 1-D nanostructures make them ideal choices as building blocks in fabricating nanoelectronic devices.[157-161] This interest has driven the development of new methods for the synthesis of 1-D metal nanomaterials, especially the 1-D gold nanostructures. Soft templates such as cetyltrimethylammonium bromide (CTAB) have been employed by Murphy and other groups in the synthesis of gold nanorods through a seed-mediated process.[41,149] In this approach, surfactant molecule CTAB formed rod-like micelles in the solution, which act as templates to direct the growth of gold nanorods and control of their aspect ratios. By an ultrasound irradiation in the presence of a biological directing agent, a simple and convenient approach to prepare

single-crystalline gold nanobelts has been recently reported.[162] Xia *et al.* reported the synthesis of silver nanobelts or triangular nanoplates by refluxing an aqueous dispersion of spherical colloids of silver with an average diameter of 3.5 nm.[163] Thermal treatment in their approach is assumed to facilitate the transport of atoms from the spherical colloids to the anisotropic plates in a process similar to the Ostwald ripening. Among these approaches, the solution-phase synthesis of nanostructures received much attention due to its potential to process metals into nanostructures with a range of well-defined morphologies and in bulk quantities. By simply adjusting the reaction conditions such as temperature,[164] capping reagent,[165] concentration,[166] or reaction time,[167] the morphologies of the final products can change from one to another. For instance, Pei *et al.* have demonstrated a simple method to prepare polycrystalline gold nanochains by directly reducing tetrachloroauric acid ($HAuCl_4$) with sodium citrate.[168] The formation of gold nanochains was attributed to the small amount of reducing agent used. The insufficient capping of citrate ions on the surface of gold nanoparticles makes them absorb $AuCl_4^-$ preferentially, which results in an attracting force between gold nanoparticles.[169,170] Recently, Kreiter *et al.* reported that polycrystalline gold nanowires were formed under very limited amount of 2-mercaptosuccinic acid (MSA), which, similar to sodium citrate, acted as both reductant and capping agent in the reaction.[171]

Seed-mediated process is extremely interesting and attractive in the synthesis of gold nanomaterials. It has been applied to synthesize various gold nanostructures such as nanorods,[172-174] nanoprisms,[29,175] and nanoparticles.[176,177] It was found that preformed

gold nanoparticles as seeds could increase the reducing ability of ascorbic acid, which was otherwise not able to reduce $AuCl_4^-$ at the room temperature.[172,173] Biggs *et al.* mentioned in their paper that gold particles might accelerate the reduction reaction rate of $HAuCl_4$ at the room temperature.[169] However, so far, no detail on seed-mediated reaction rates have been published.

It was reported that polycrystalline nanochains were transitional products, which would break into spherical gold nanoparticles, during the synthesis of spherical gold nanoparticles in the absence of gold seeds. We expect that in the presence of gold nanoparticles as nucleation seeds, when the amount of nanoparticle capping agent (e.g. citrate ions) is insufficient for fully capping nanoparticles, breakup of the aggregated nanoparticles will increase the surface energy and thus is not thermodynamically favorable, so they still adopt linear nanochain or nanowire morphology. Therefore, in this work, we study the kinetics of the reduction of the gold precursor ($HAuCl_4$) and the effect of the molar ratio (R) of the surface capping agent (i.e., citrate ions) and the gold precursor (i.e., $HAuCl_4$) on the shape evolution of gold nanomaterials in the presence of pre-formed 13 nm gold nanoparticles as nucleation seeds. For the first time, we found that at a particular low R value (R=0.16), nearly single-crystalline gold nanowires can be formed through the oriented attachment of growing gold nanoparticles.

3.2 Experimental Methods

3.2.1 Materials

Tetrachloroauric acid ($HAuCl_4$) solution (0.2 wt%, 5.9 mM), sodium citrate, sodium bromide and sodium borohydride were purchased from Sigma-Aldrich. All chemicals were used as received without further purification.

3.2.2 Preparation of Gold Nanoparticle Seeds

Gold nanoparticle seeds with 13 nm size were synthesized as follows. In a 10 ml vial, 600 μl 38.8 mM sodium citrate solution, 850 μl 5.9 mM $HAuCl_4$ solution and 3550 μl distilled water were mixed together. To this mixture 1 ml 2.2 mM freshly prepared $NaBH_4$ solution (placed less than two minutes after $NaBH_4$ dissolution) was added dropwise in the ice water bath under vigorous magnetic stirring. Under this low temperature condition, sodium citrate and $NaBH_4$ served as a nanoparticle surface capping agent and a reductant, respectively.[173,178] The stirring was continued for 15 min, and then the mixture was left standing at the room temperature for at least one week to allow the excess $NaBH_4$ to be hydrolyzed completely. For the sake of safety, the vial was loosened from time to time to release the hydrogen gas produced from the hydrolysis of $NaBH_4$. Average size of the obtained particles is 13 ± 2 nm by transmission electron microscopy (TEM) measurement (Fig. 3.1).

3.2.3 Seeded Growth of the Gold Nanomaterials

Different molar ratios ($R = N_{citrate}/N_{Au}$) of sodium citrate to $HAuCl_4$ were used in the seeded growth of gold nanomaterials. We chose three R values for the mixture of the seed solution and $HAuCl_4$ solution: 1.32, 0.33, and 0.16. The final gold nanomaterials corresponding to these different R values are termed **S1**, **S2** and **S3**, respectively. In a typical procedure for preparing sample **S1**, 5 ml of 0.059 mM $HAuCl_4$ solution (prepared by diluting 50 μl 5.9 mM $HAuCl_4$ stock solution to 5 ml with DI water) was added to a 10 ml sealed vial. The solution was then placed in a boiling water bath. During heating, 100 μl as-prepared gold nanoparticle seed (13 nm) solution was injected into the vial. At this time point, the concentration of sodium citrate that was introduced from the seed solution is 0.078 mM, resulting in a R value of 1.32 in the resulting reaction mixture. In the boiling water, citrate functioned both as a capping agent and a mild reductant.[20] After about one hour, the vial was placed into an ice water bath immediately. Similarly, two other initial concentrations of $HAuCl_4$ (0.236 and 0.472 mM) were used to prepare samples **S2** and **S3** to reach R values of 0.33 and 0.16, respectively. The amounts of gold seeds and sodium citrate are kept same for samples S1, S2 and S3.

3.2.4 Acceleration Effect of the Preformed Seeds

To study the seed acceleration effect on the formation of the gold nanomaterials, control experiments without preformed seeds were carried out with the same protocol except that instead of injecting 100 μl seed solution, 100 μl sodium citrate solution was injected to the vial. The injected sodium citrate solution had the same amount of sodium

citrate as in the seed solution, that is, R values in the control experiment were kept the same as the seeded growth experiment.

3.2.5 Measurement of the Remained $HAuCl_4$

The concentration of $HAuCl_4$ remained in the solution at different reaction times was measured by the colorimetric method.[179] During the measurement, 20 mg of NaBr was first added to the reaction solution, which was then subjected to centrifugation at 12000 rpm for 10 min to remove all Au^0 species. The concentration of $HAuCl_4$ in the supernatant was determined by measuring the absorption at 381 nm, which was assigned to the absorption of $AuBr_4^-$, formed by ion exchange of Br^- with $AuCl_4^-$.

3.2.6 Characterization

UV-visible spectra were acquired on a Shimadzu UV-2200 spectrometer, using the software supplied by the manufacturer. TEM samples were prepared by dropping 3 μl of a gold nanomaterial solution onto the carbon-coated copper grid, and let dry in the ambient air. TEM images were taken in a JEOL 2000 Transition Electron Microscope operated at 200 kV accelerating voltage.

3.3 Results

3.3.1 Shape Evolution of Gold Nanomaterials in the Presence of Gold Seeds

Gold nanoparticle seeds with an average diameter of 13 ± 2 nm were obtained after reduction of $HAuCl_4$ with $NaBH_4$ in the presence of citrate which serves as a surface

ligand for the nanoparticles (Fig. 3.1). We expect that at low R values (i.e., low citrate amount) and in the presence of seeds, gold nanoparticles will grow and tend to form aggregated nanostructures because gold nanoparticles are not fully capped by citrate ions and Au atoms can be directly added to the surface of the growing gold nanoparticles.[169] To examine the effect of the R values on the seed-mediated growth of gold nanoparticles, different R values have been used in the synthesis. Fig. 3.2 shows typical TEM images of the resulting gold nanomaterials prepared from the mixtures with different R values. It can be seen that the shapes of the final products depend significantly on the R values. When R = 1.32, separated gold nanoparticles larger than gold seeds were obtained (Fig. 3.2a). Decrease of the R values favored the formation of 1-D nanostructures (Figs. 2b-c). When the R value was decreased to 0.33, polycrystalline gold nanochains were formed (Fig. 3.2b) as a result of the attachment of gold nanoparticles grown from the seeds, which are crystallographically randomly oriented according to electron diffraction analysis (Fig. 3.2b inset). The obtained nanochains were similar to those reported by Pei *et al.* although they obtained the gold nanochains without the addition of seeds to the reaction mixture.[168] These results indicated that at a higher R value (R > 1) the seeds did not have a predominant effect on the morphology of the final products. After further decrease of the R value to 0.16, gold nanowires, which are fused from gold nanoparticles, were observed to be the main products as shown in Fig. 3.2c and d. Most importantly, the electron diffraction pattern (Fig. 3.2d inset) taken from a long section of the nanowires can be indexed by a gold single crystal structure. The electron diffraction pattern shown

in Fig. 3.2d inset is a [1$\underline{1}$1] zone axis spot pattern, that is, the incident electron beam is along the [1$\underline{1}$1] direction of a gold single crystal, which is perpendicular to the nanowire. Thus the nanowires have a single-crystalline structure, indicating that the gold nanoparticles have aggregated into nanowires through a recently discovered crystal growth mechanism called oriented attachment. It should be noted that several smaller nanoparticles are still attached to the end of the nanowires (Fig. 3.2d). This fact indicates that the nanowires were grown from the fusion of the smaller nanoparticles along the long axis of the nanowires. In addition, two neighboring nanowires tend to join together at the end, which is probably because the smaller nanoparticles originally present at the ends of the two nanowires are further fused when the ends of the two nanowires are close enough.

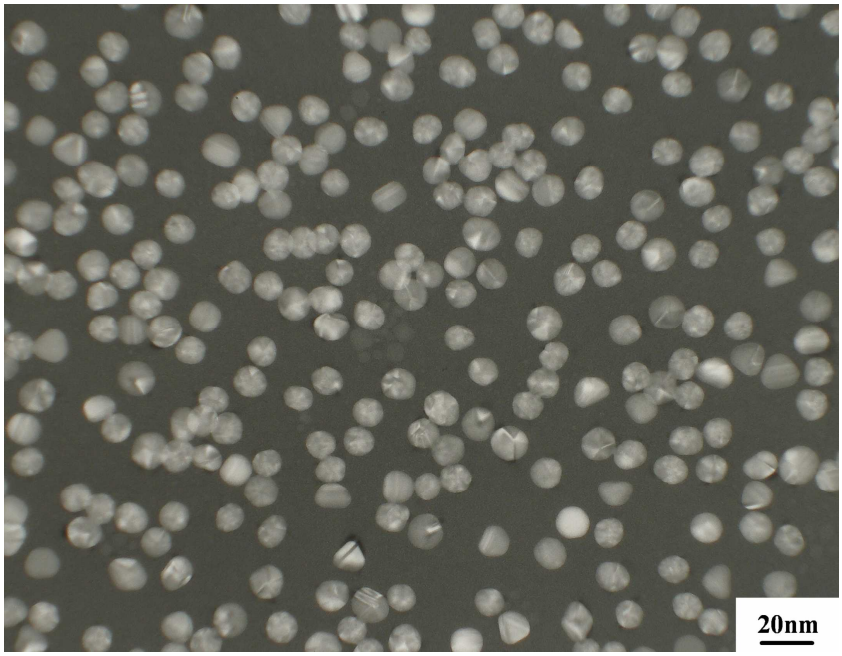

Figure 3.1, TEM image of 13 nm gold nanoparticle seeds. Image reprinted with permission from ref. 36, Copyright 2009 Springer Science + Business Media.

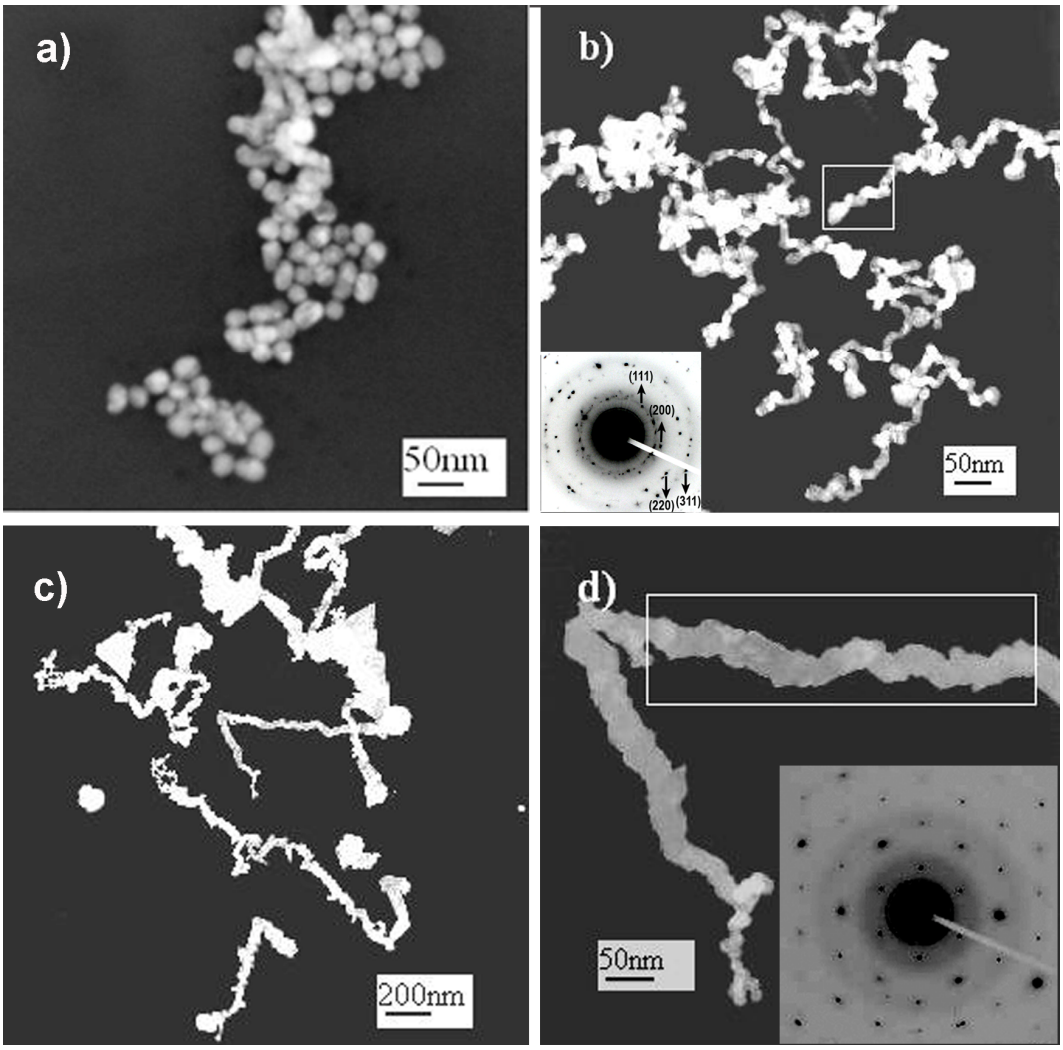

Figure 3.2, TEM images of gold nanomaterials prepared by addition of 13 nm seeds to the boiling solution with different ratio of sodium citrate and $HAuCl_4$ (R): (a) S1: R = 1.32, (b) S2: R = 0.33, (c) S3: R = 0.16, (d) one gold nanowire in (c) at a higher magnification. The insets in (b) and (d) are the electron diffraction patterns of the framed section of the nanochain (b) and nanowire (d), respectively. The diffraction pattern in (b) can be indexed by a polycrystalline gold crystal. The diffraction pattern in (d) can be indexed by a [1$\underline{1}$1] zone axis-oriented single crystalline gold crystal. All of the gold

nanomaterials were prepared after the solution was boiled for one hour. Image reprinted with permission from ref. 36, Copyright 2009 Springer Science + Business Media.

3.3.2 UV-visible Spectra of Seed-Mediated Gold Nanomaterials

Gold nanomaterials show unique optical properties as a result of surface plasmon resonance. In Fig. 3.3a, from left to right, the solution colors are pink, blue and sea green, which are corresponding to nanoparticles, nanochains and nanowires shown in Figs. 3.2a-c, respectively. This result is consistent with the well-known fact that the optical appearance of a gold nanomaterial solution is strongly dependent on the shape of its content. Spherical gold nanoparticles often exhibit a single size-dependent absorption band between 520 to 580 nm, while anisotropic gold particles show two surface plasmon resonance absorption peaks: transverse band and longitudinal bands.[180] The UV-Vis spectra of the gold nanomaterials shown in Fig. 3.2 (i.e., obtained under different R values) are shown in Fig. 3.3b. The gold nanomaterials prepared under a larger R value (R = 1.32) shows a relatively narrow band at 524 nm, which was attributed to the absorption of spherical gold nanoparticles (Fig. 3.2a). With the decrease of the R value, both transverse and longitudinal absorption band were expected due to the formation of anisotropic nanochains and nanowires. It is reported that when a 1D gold nanostructure reached a length of more than about 60 nm, a longitudinal absorption band would be expected at a wavelength above 1000 nm.[181] Since the nanochains and nanowires in Fig. 3.2 are much longer than 60 nm, the long axis surface plasmon absorption (i.e., the

longitudinal absorption band), will be above 1000 nm, and thus cannot be seen within our experimental range (300-900 nm), which is the capability of our UV-visible spectrophotometer. As shown in Fig. 3.3b, the absorption along the short axes of the nanowires (i.e., the transverse absorption band) appears within this range (300-900 nm) as expected. Fig. 3.3b also shows a general red shift of the plasmon absorbance in the range of the 520-600 nm with the decrease of the R values, which was attributed to the coupling of the plasmon absorbance of the aggregated nanoparticles.[182,183] Therefore, a tunable optical property can be realized by simply changing the molar ratio of citrate and $HAuCl_4$ in the reaction mixtures in the presence of gold nanoparticle seeds.

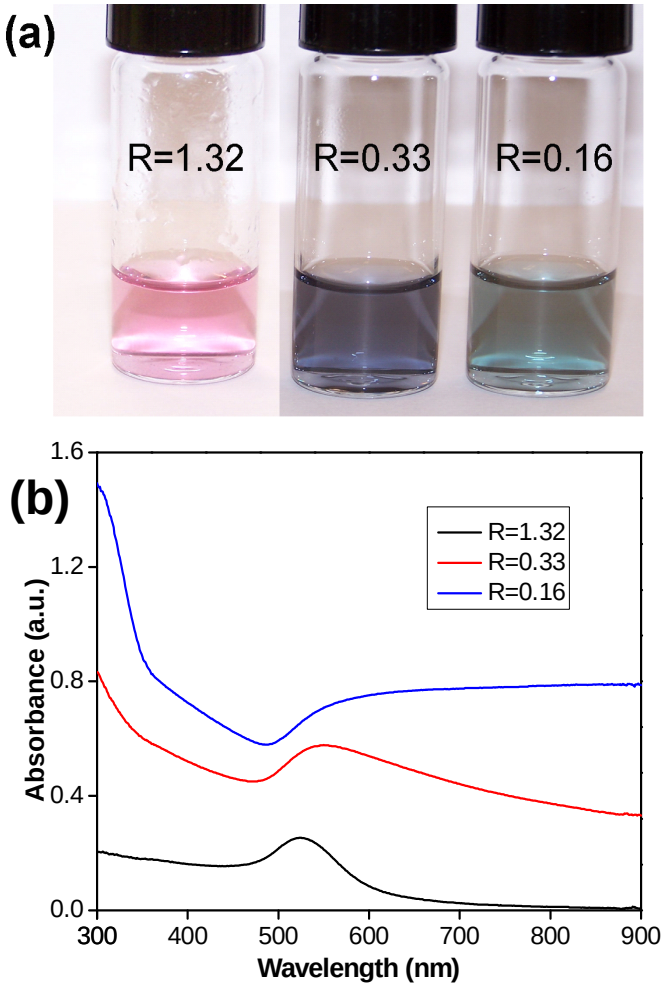

Figure 3.3, Photographs (a) and UV-Visible absorption spectra (b) of the gold nanomaterial solutions prepared under different R values (black curve: R=1.32; red curve: R=0.33; blue curve: R=0.16). Image reprinted with permission from ref. 36, Copyright 2009 Springer Science + Business Media.

3.3.3 Effect of Seeds on the Reaction Kinetics: Acceleration of the Reduction of Gold Precursor

To quantitatively measure the effect of the gold nanoparticle seeds on the citrate reduction of $HAuCl_4$, the reaction rates were evaluated by the consumption of $HAuCl_4$ in

the reaction mixture. We found that the preformed gold seeds accelerated the reduction of $HAuCl_4$ and thus the formation of gold nanomaterials (Fig. 3.4). In the presence of pre-synthesized gold nanoparticles, a significantly accelerated reduction of $HAuCl_4$ was observed, especially at the early stage (first 3 minutes). In other words, $HAuCl_4$ was consumed faster in the presence of gold seeds than without the preformed seeds. There was a fast and continuous color change in the first 3 min in the reaction with the preformed seeds, which was corresponding to the production of nanoscale Au^0 species.[20,168] However, in the reaction mixture without the preformed seeds, there was no color change even after the reaction mixture was boiling for 30 minutes, indicating no nanoparticles were formed, which was confirmed by TEM observation. The colorimetric method showed that the concentration of $HAuCl_4$ was decreased from the original 0.47 mM to about 0.22 mM in the first 30 minutes in the absence of gold seeds (Fig. 3.4). We believe that the decrease of the concentration of $HAuCl_4$ in the absence of the gold seeds was due to the reduction of the Au^{3+} to the colorless Au^+ but not Au^0 due to the limited amount of citrate used in the reaction system (R=0.16). The reaction mixture in the presence of the gold seeds was changed from colorless to light blue under refluxing after 30 min, which is consistent with the TEM observation that single-crystalline gold nanowires were formed (Fig. 3.2c).

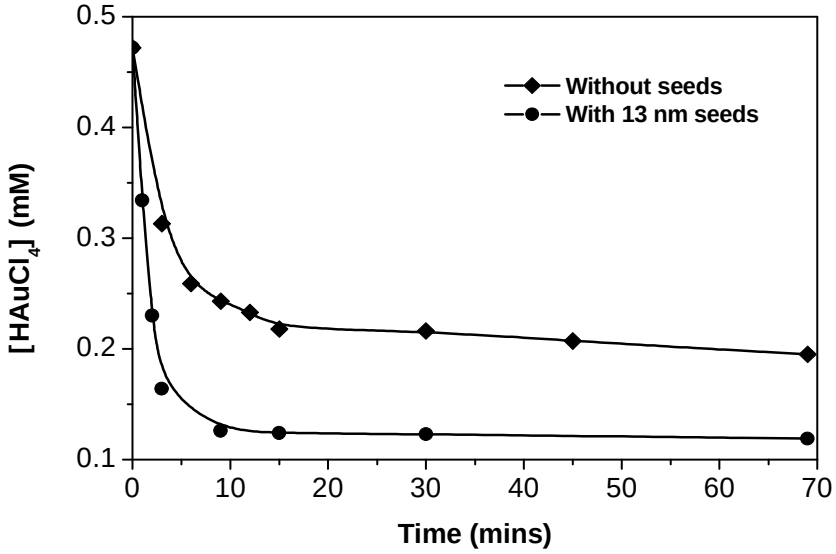

Figure 3.4, The concentration of remained $HAuCl_4$ as a function of time in the absence or presence of gold seeds. Initial concentration of the reagents for the reaction at t=0 min: [$HAuCl_4$] = 0.472 mM, [Citrate] = 0.078 mM; that is, R=0.16. (t=0 min is defined as the point of injecting seed solution into the vial.) Image reprinted with permission from ref. 36, Copyright 2009 Springer Science + Business Media.

3.4 Discussion

Our experimental results clearly showed that, with the same amount of sodium citrate, the preformed gold nanoparticle seeds can significantly accelerate the reduction of $AuCl_4^-$. More importantly, the morphologies of the final products (nanoparticles, nanochains and nanowires) are dependent on the R values. It is well accepted that nucleation is the initial step in the formation of nanoparticles.[184] Small clusters of metal,

more likely charged, are first formed by coalescence of evenly distributed atoms in the solution; larger nanoparticles are then successively growing from these clusters by the addition of atoms. According to Murphy *et al*., nucleation is a slow step, followed by a much faster, self-accelerated growth of nanoparticles.[149] Their work suggests that if pre-synthesized gold clusters are added to the reaction solution before nucleation, the growth rate of nanoparticles will be tremendously raised, and meanwhile, an expansion in the particle size should be observed. This process can clearly explain the accelerated reaction of citrate and $HAuCl_4$ in the presence of gold seeds. This was also confirmed by the TEM results (Fig. 3.2), which show that, in all of the samples derived from the pre-synthesized gold nanoparticles (~13 nm), no particles in the final product are smaller than the seeds. Therefore, we believe that the gold nanomaterials were grown on the basis of the pre-synthesized seeds that served as nuclei, thereby accelerating the nanomaterial growth process. However, in the absence of preformed seeds, the nucleation that was the rate-limiting step was necessary, which would result in a slower reaction and growth rate.

By changing the R values from 1.32, 0.33, to 0.16 and in the presence of gold seeds, we obtained three different morphologies of gold nanomaterials (Fig. 3.2). When R= 1.32, the sodium citrate, which acted as both reducing agent and surface ligands, was in excess, and thus larger gold nanoparticles were grown from the gold seeds. When R=0.33 or 0.16, the sodium citrate was in deficiency (i.e., limited) with respect to $HAuCl_4$ and 1D nanostructures (nanochains or nanowires) were formed through the attachment of the growing nanoparticles. The effect of R values on the morphologies of the final products

could be explained by the change in surface energy at different R values as well as directional dipole-dipole interaction between adjacent nanoparticles. It was first discovered by Kiely *et al.* that alkanethiol-coated spherical gold nanoparticles could fuse into a semi-continuous network when exposed in the ambient air for several months. One of the reasons they suggested was that due to the degradation of alkanethiol molecules (i.e., the surface ligands) over the period, the surface energy of the nanoparticles would increase, so that each particle was connected to particles that were sitting around it to reduce the surface area, consequently reducing the surface energy.

Hence, in our experiments, at the low R values (i.e., with a limited amount of citrate ions available for coating the surface of nanoparticles, e.g., R=0.33), the surface energy of the nanoparticles would also increase, thus the nanoparticles would attach to each other to form a nanochain in order to reduce the surface energy. That is, the surface energy reduction will drive the attachment of nanoparticles to form nanochains. At an even lower R value (0.16), the citrate ions will be more deficient for coating the nanoparticle surface and thus the surface energy of the nanoparticles will be even higher. Therefore, the interface between two adjacent nanoparticles will tend to disappear in order to minimize the surface energy, which will drive the fusion of attached nanoparticles into a single crystalline nanowire (i.e., oriented attachment). The single crystalline gold nanowires (Fig. 3.2c-d) are straighter and have larger diameters than the polycrystalline nanochains (Fig. 3.2b). This is probably because the $HAuCl_4$ concentration in S3 (R=0.16) was two times of that in S2 (R=0.33) while both S2 and S3

had the same amount of sodium citrate and preformed seeds. Therefore, citrate ions in S3 were consumed faster than those in S2, which may lead to a more dramatic increase of surface energy in a unit time and thereby a larger driving force for nanomaterial growth for S3 than S2.

We believe that the dipole–dipole interaction is one of the driving forces for the formation of 1D nanostructures observed in our work (Fig. 3.2). It was reported that small quantum dots or silver nanoparticles could self-assemble into nanowires, which was driven by strong dipole–dipole interaction between adjacent nanoparticles.[163,185] Most recently, a combination of theoretical and experimental work demonstrates that negatively charged gold nanoparticles (14 nm) in aqueous solution could self-assemble to form a 1D nanochain under a proper ionic strength, and the nanochain formation was triggered by short-range anisotropic dipolar interactions between the adjacent nanoparticles.[186] The same work also demonstrates that under some solution conditions, the negatively charged gold nanoparticles will be isolated from each other to unfavor the nanochain formation due to the electrostatic inter-particle repulsion. We believe that in our experiment, at lower R values, the solution condition may favor the aggregation of gold nanoparticles into 1D nanostructures due to the dipolar interaction between adjacent nanoparticles.

The excess $AuCl_4^-$ ions at low R values is a second factor in promoting aggregation of nanoparticles into 1D nanochains and nanowires. It was found that $AuCl_4^-$ ions could preferentially bind to the gold surface in the presence of citrate ions.[187] Earlier detailed study also indicated that the adsorption of $AuCl_4^-$ ions onto the Au particle surfaces would result in an attraction force between two neighboring gold particles.[169] At the

lower R value (R<1, e.g., 0.33 or 0.16), $AuCl_4^-$ ions were in excess amount. As a result, the excess of $AuCl_4^-$ ions in the reaction system will cause the preferential adsorption of $AuCl_4^-$ on the Au nanoparticles and subsequently favor their aggregation into nanowires or nanochains. This explanation could also be supported by the fact that upon addition of $AuCl_4^-$ ions into citrate stabilized gold nanoparticles solution, nanoparticle aggregation occurred.[187] At the higher R values (R>1, e.g., 1.32), at the early stage, the $AuCl_4^-$ ions are not completely consumed and will preferentially bind to the nanoparticle surface. Consequently, the nanoparticles will be aggregated into nanochains temporarily. When reaction is completed, the $AuCl_4^-$ ions will be almost consumed, and the citrate ions will be in excess and bind to the nanoparticle surface as ligands. However, earlier study found that once the citrate ions were coated on the gold, two neighboring gold surfaces will repel each other.[169] Therefore, the temporarily formed nanochains will break up into spherical nanoparticles. This explanation is consistent with the fact that in the reaction of sodium citrate with $AuCl_4^-$ ions, even when the final product was spherical gold nanoparticles, nanochains were found to be a transitional product.[168] Hence, one can see a continuous color change in the preparation of spherical gold nanoparticles by citrate reduction.

Lastly, along with the above two factors, the reduction of surface energy will further drive the aggregation of nanoparticles into 1D nanostructures. It was discovered that spherical gold nanoparticles could fuse into a semi-continuous network driven by the reduction of surface energy in the nanoparticle system.[188] Namely, each particle was connected to particles that were sitting around it to reduce the surface area, consequently reducing the surface energy. In our experiments, as indicated above, at the low R values

(e.g., R = 0.33), gold nanoparticles will tend to aggregate due to the attraction between nanoparticle surfaces. The aggregation of nanoparticles into a nanochain will reduce the surface energy and thus is thermodynamically favorable. Therefore, the surface energy reduction will further drive the attachment of nanoparticles to form nanochains. At an even lower R value (0.16), more excess $AuCl_4^-$ ions will be coated on the gold nanoparticle surfaces to bring the nanoparticles together. Therefore, the interface between two adjacent nanoparticles will tend to disappear in order to minimize the surface energy, which will drive the fusion of attached nanoparticles into a single crystalline nanowire.[189,190] The single crystalline gold nanowires (Fig. 3.2 c&d) are longer and wider than the polycrystalline nanochains (Fig. 3.2b). This is because the $HAuCl_4$ concentration in S3 (R = 0.16) was two times of that in S2 (R = 0.33) while both S2 and S3 had the same amount of sodium citrate and preformed seeds, resulting in the availability of more excess $AuCl_4^-$ ions on the nanoparticles to drive nanoparticle attachment into longer and wider nanowires in S3.

Overall, the aggregation of nanoparticles into the nanochains and nanowires at lower R values is driven by the dipolar interaction, enhanced nanoparticle attraction, and reduction of surface energy. The nanoparticles in the nanochains may further fuse to form the single-crystalline nanowire structures at very low R values. The continuous aggregation of gold nanoparticles at the end of most of the gold nanowires observed (Fig. 3.2c&d) also confirmed this mechanism. In addition, we found that at R = 0.66, rod-like nanoparticles were formed due to the fusion of fewer nanoparticles (Fig. 3.5a). This is probably because when R = 0.66 (i.e., $AuCl_4^-$ ions are just slightly excessive), that is, higher than the R value for the nanochain formation (e.g., R = 0.33, Fig. 3.2b) but lower

than the R value for the spherical nanoparticle formation (e.g., R = 1.33, Fig. 3.2a), there may not be enough excess $AuCl_4^-$ ions to cover the surface of spherical nanoparticles after the reduction of $AuCl_4^-$ ions to Au. When R is reduced to an even lower value (e.g., 0.33 and 0.16), more $AuCl_4^-$ ions will be available to favor the aggregation of nanoparticles,[169] which further enhances the aggregation of nanoparticles into nanochains and nanowires (Figs. 3.2c&d, 3.5b). These results agree with the above explanations.

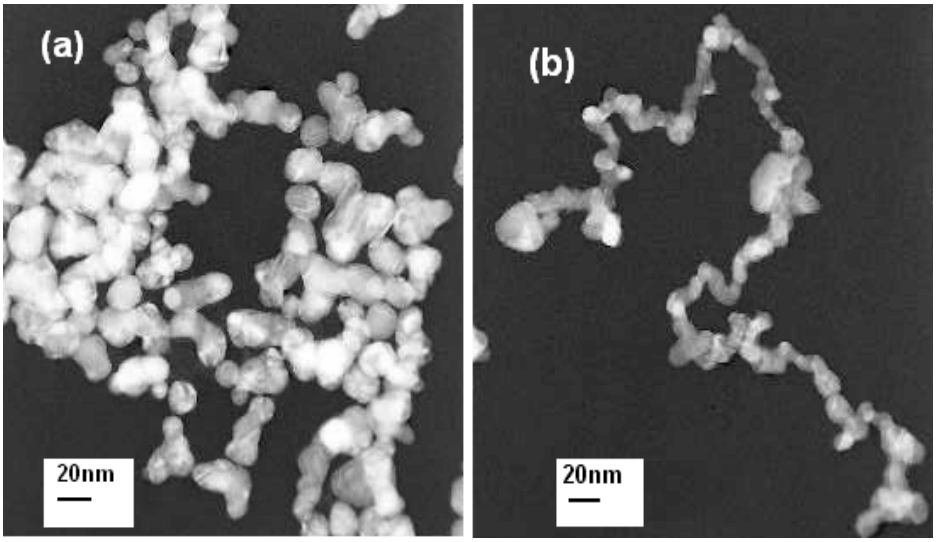

Figure 3.5, TEM images of gold nanomaterials with different citrate/$HAuCl_4$ ratio: (a) R = 0.66, (b) R = 0.33. Image reprinted with permission from ref. 36, Copyright 2009 Springer Science + Business Media.

3.5 Conclusion

In summary, we studied the seed-mediated synthesis of gold nanomaterials using 13 nm gold nanoparticles as seeds. We found that gold seeds can accelerate the reduction of

the gold precursor by sodium citrate that serves as both reducing agent and binding ligand. By tuning the molar ratio of sodium citrate to the gold precursor, different gold nanomaterials can be obtained including spherical nanoparticles, polycrystalline nanochains and single-crystalline nanowires. Without the preformed gold nanoparticles, single-crystalline gold nanowires cannot be formed under a limited amount of citrate. Furthermore, the formation of nanowires was driven by the surface energy reduction and dipole-dipole interaction. Our results indicate that different morphologies of gold nanomaterials can be obtained by simply adjusting the R values in the presence of preformed gold nanoparticle seeds.

CHAPTER 4

Separation of Nanoparticles in a Viscosity Gradient Created by Aqueous Polyvinylpyrrolidone Solution

4.1 Introduction

Non-uniform size distribution can be observed in the chemical synthesis of many types of nanoparticles. To get uniformly distributed nanoparticles, it is necessary to separate them by size. Several size sorting methods have been developed in literature, including size exclusion chromatography,[191] filtration,[192,193] electrophoresis[194,195] and solvent/antisolvent selective precipitation.[196] Recently, direct size separation of nanoparticles in complete liquid phase through centrifugation has been proved to be a more effective method due to its high efficiency, capability of scalable production and free of nanoparticles aggregation.[197-199] Both density based isopycnic centrifugation and velocity related rate zonal centrifugation have been reported. For small nanoparticles (less than 10 nm), their overall density after solvation falls into the density range of gradient medium, thus isopycnic centrifugation can be used to achieve separation. Larger nanoparticles are generally denser than the liquid medium, so they could only be separated by the difference of sedimentation velocity.[197,198] Previously, density gradient, created by iodixanol and CsCl,[197,198] has been employed to differentiate the sedimentation velocity of small and large nanoparticles. In this work, for the first time,

we use a pure viscosity gradient built from polymer aqueous solution to achieve separation of nanoparticles by size.

4.2 Experimental Methods

4.2.1 Preparation of Seed Solution

AuNPs seeds of 10 nm were synthesized by the classic sodium citrate reduction of $HAuCl_4$ in a boiling water bath. The amount of each reagent used are 6 ml 5.9 mM $HAuCl_4$, 45 ml H_2O and 4 ml 38.8 mM sodium citrate. The as-synthesized seed NPs were used directly for preparation of larger NPs without any treatment.

4.2.2 Preparation of Different Sized AuNPs

Size control was realized by fixing the supply of $HAuCl_4$, but changing the amount of seed during the reaction. To a total volume of 5 ml solution, containing 300 mg PVP 10K, 0.5 ml 5.9 mM $HAuCl_4$ and various volumes of seeds solution (4, 2, 1, 0.5, 0.25, 0.10 and 0.04 ml), 50 μl 78.8 mM ascorbic acid was added under vigorous stirring. The reaction will finish in about 10 min. The larger NPs were pre-treated to remove some small nanoparticles that are not nucleated on the seeds, by PVP viscosity gradient. The resultant AuNPs sizes are 15, 18, 21, 27, 31, 44 and 50 nm corresponding to each amount of seeds above.

4.2.3 Preparation of PVP Viscosity Gradient

The PVP aqueous solution of different concentrations was prepared by directly dissolving calculated amount of PVP into water. The dissolution of PVP was assisted by vigorous vortexing and sonication to enhance the homogeneity of the solution. The viscosity gradient was created by loading PVP solutions of high to low concentration consequently into a 15 ml conical centrifuge tube. For example, in the viscosity gradient used in Fig. 4.1, 2 ml 30 wt% PVP was loaded first to the bottom of the centrifuge tube by a Pasteur pipette, following that 25, 20, 15 and 10 wt% PVP solutions were loaded very carefully one after another in 1.5 ml of each. The centrifuge tube was maintained at about a 45^{o} angle during addition of different layers. Concentrated solution of gold nanoparticles of mixed sizes was loaded carefully onto the top of the PVP viscosity gradient and the tube was subjected to centrifuge shortly after the loading. To take digital photos of different time points, the centrifuge was interrupted, and continued with the same sample after the photos were taken.

4.3 Results and Discussions

4.3.1 A Case Study of Separation of Five Different Sized AuNPs in PVP Viscosity Gradient

Polyvinylpyrrolidone (PVP, M.W. 10 K) is a highly water soluble polymer and can be obtained in a relatively low cost, thus it is chosen here to make the viscosity gradient. The gold nanoparticles (AuNPs) of different sizes are synthesized through a

seed-mediated method. To avoid aggregation of NPs during centrifugation separation, PVP is used to stabilize the NPs. The PVP coated AuNPs can maintain the highest stability in the gradient medium, which is highly concentrated PVP, so that the NPs will remain their physical properties after the size separation. As shown in Fig. 4.1a that a small volume of concentrated AuNPs mixture solution, which contains 15, 18, 21, 27 and 31 nm five different sized NPs, was placed on top of the polymer gradient medium that is built up by 10, 15, 20, 25 and 30 wt% aqueous PVP. After centrifuge at 3,400 g for 2.5 h, five fractions of NPs can be seen clearly in the gradient medium. The TEM examination (Fig. 4.1b-f) shows that each fraction contains uniformly distributed NPs, with increasing size from top to bottom layers. In the isopycnic centrifuge, NPs of a particular size and density will stop moving once reaching a liquid layer with a density equal to theirs, and extended centrifuge time will not further shift the relative position of the NPs fractions in the liquid medium. While in the zonal rate centrifuge, because the density of NPs is larger than the highest density of the medium, as long as there is a centrifugal force, NPs will continue moving downwards even after they have been well separated into several fractions by their sizes. In our approach, it can be seen from photos taken at 30 min intervals (Fig. 4.1a) that all NPs had been moving downward continuously during the 2.5 h centrifuge time. Therefore, the separation of AuNPs in the PVP viscosity gradient should be through the rate zonal centrifuge, which is by the settling velocity difference among large and small sized NPs, rather than the density difference.

4.3.2 Role of Viscosity Gradient in Separation of AuNPs

The densities of PVP are only slightly higher than water (1.064 g/ml at 30 wt%) and are very close to each other among different concentrations.[200] The 30 wt% PVP is only about 5% denser than the 10 wt% solution, and there is merely around 1% difference between neighboring layers (Table 4.1). However, the viscosity changes dramatically when the polymer concentration varies. The viscosity of 30 wt% PVP is almost 8 times higher than that of 10 wt% PVP solution.[201] For neighboring layers, the lower layer is 1.6-1.8 times more viscous than the above layer (Table 4.1). Hence, one can find that the aqueous PVP concentration gradient will only lead to the formation of viscosity gradient, rather than the density gradient as may happen in many other cases, such as iodixanol, CsCl and sucrose (although both density and viscosity increase along with increasing concentration in these examples, they are normally referred as density gradient). The PVP viscosity gradient contributes in at least two ways to the successful size partition of AuNPs. First, the significant increase of viscosity at layer interfaces can effectively impede the small NPs from entering the next layer; while larger NPs, although also slowed down, can pass through the interface easily and move toward next layer to achieve separation. Second, the viscosity gradient narrows the band width of each NPs fraction, so that a good separation resolution can be obtained. Practically, when NPs of similar size are travelling in the same PVP layer, where the viscosity is not too harsh for particles to move smoothly, only a very wide fraction can be observed. However, when

the frontier NPs reach the harsh PVP layer, they will experience a sudden decrease of settling velocity; while the following NPs are still moving in the same speed, so at the layer interfaces, same sized NPs will tend to accumulate to form a narrow band (Fig. 4.2). In addition to the viscosity gradient, in a swing arm centrifuge rotor, once the large NPs are slightly separated from the small ones, they will go through a higher centrifugal force g, due to the increase of actual radius of rotation, which will raise the settling velocity of large NPs and further favors partition.

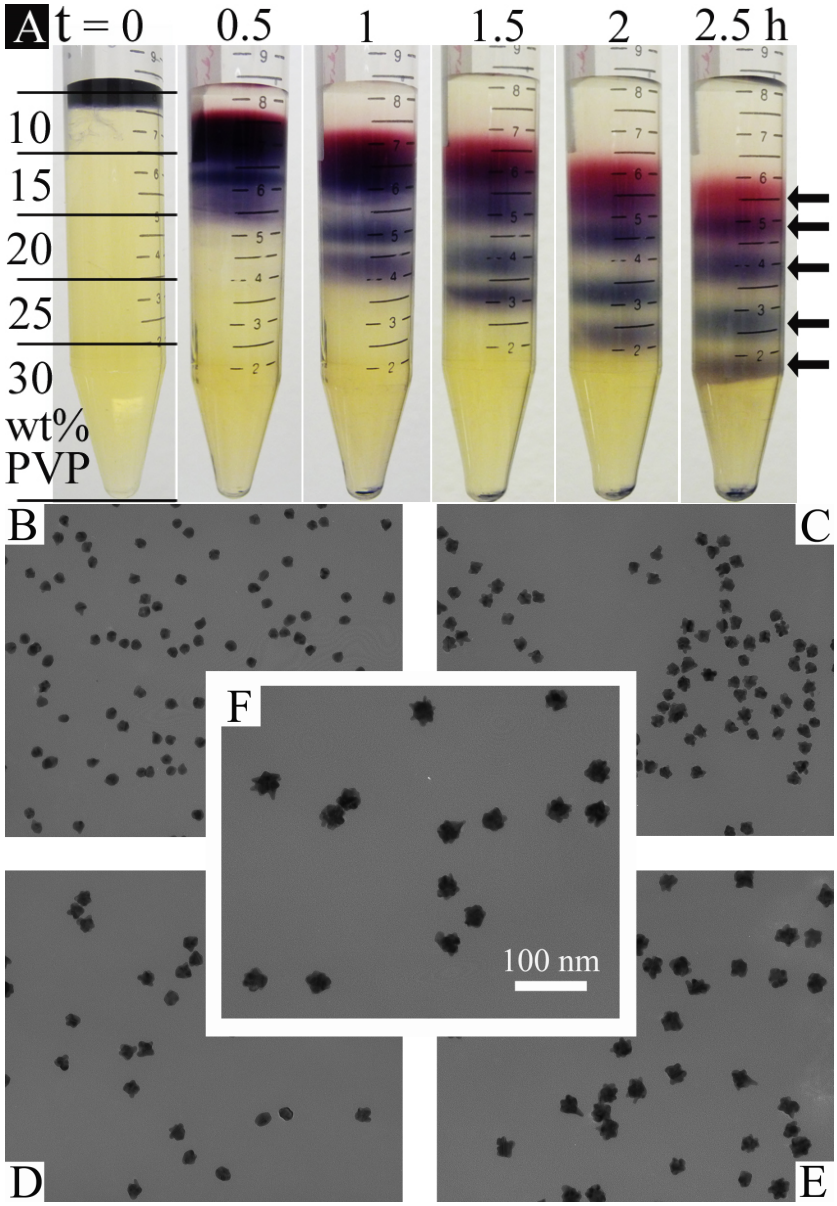

Figure 4.1, Separation of five different sized AuNPs in a PVP 10K viscosity gradient. A) Photographs taken at 0.5 h intervals. Gradient thickness has been indicated by black lines on the leftmost tube. Five NPs fractions, indicated by arrows, can be seen clearly after 2.5 h centrifuge; B-F) TEM images, corresponding to fractions from top to bottom, show NPs size in each fraction. Scale bar in F is applicable to all images.

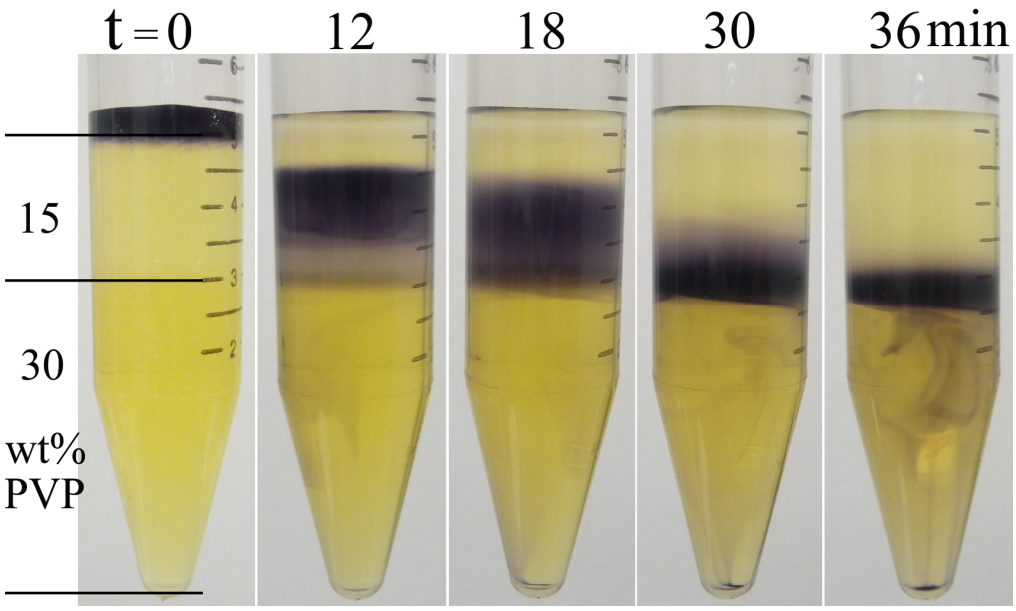

Figure 4.2, A set of photographs showing that viscosity gradient can effectively narrow down the band width of nanoparticles fraction. Uniform 31 nm AuNPs can travel smoothly in 15 wt% PVP 10K under centrifugal force, however, it only resulted in a wide NPs fraction (12 & 18 min). When the frontier AuNPs reach the interface of 15 wt% and 30 wt% gradients, they experienced a sudden decrease of settling velocity, while the following NPs (in 15 wt% gradient, have not yet reach the interface) were still moving down at the same speed, therefore, at the gradient interface, NPs accumulated to form a narrow band, which makes it possible to obtain sharp separation between different sized NPs.

4.3.3 Unique Advantage of Viscosity Gradient in Separation of Larger Nanoparticles

The density gradient has been demonstrated as a very effective method in separation

of small NPs through isopycnic centrifuge, in which the density difference among gradients mainly contributes to the separation. For large NPs, for instance 30 nm or larger AuNPs, their overall density will be much higher than that of the liquid. Separation of NPs can only be realized through rate zonal centrifuge. In such circumstances, the density gradient may not be sufficient to retard particle sedimentation or regulate the fraction band width.

$$v = \frac{d^2(\rho_p - \rho_l)}{18\mu} \; g \qquad (1)$$

Where,

v -- settling velocity of NPs
d -- diameter of NPs
ρ_p -- density of NPs
ρ_l -- density of liquid medium
g -- centrifugal force
μ -- viscosity of liquid medium

The settling velocity of nanoparticles in a viscous medium can be described by Stokes' law in equation (1) above.[202] According to the work by Falabella *et al.* it is very reasonable to assume large AuNPs (more than 10 nm) having density of 5 g/cm^3 or even higher.[203] Since the discussion here is about the contribution of *density* gradient versus *viscosity* gradient in separation of larger NPs, the viscosity of liquid in a density gradient is considered as constant and *vice versa*. Therefore, for same NPs, under same *g*, the settling velocity ratio in *different density* medium will be:

$$\frac{v_1}{v_2} = \frac{\rho_p - \rho_{l1}}{\rho_p - \rho_{l2}} \qquad (2)$$

While in *viscosity gradient*, the equation will be:

$$\frac{v_1}{v_2} = \frac{\mu_2}{\mu_1} \qquad (3)$$

Through a simple calculation, it could be found from equation (2) that the ratio of settling velocity of 5 g/cm^3 NPs in 2 g/ml liquid to that of 1 g/ml liquid will be $\frac{v_1}{v_2} = \frac{5-2}{5-1} = 0.75$. Reminding that 2 g/ml is about the highest density for a typical liquid and 1 g/ml is the lowest for aqueous solution, thus the largest settling velocity difference of 5 g/cm^3 NPs in a *density gradient* will be about 25%.

Now let's consider the situation in *viscosity gradient*. The viscosity data of 30 wt% and 10 wt% PVP can be found in Table 1 above (20.5 and 2.6 mPa·s respectively). As calculated from equation (3), the settling velocity ratio will be $\frac{v_1}{v_2} = \frac{2.6}{20.5} = 0.127$, in other words, the velocity will be reduced by 87.3% in a 30 wt% PVP solution compared to that in 10 wt% PVP.

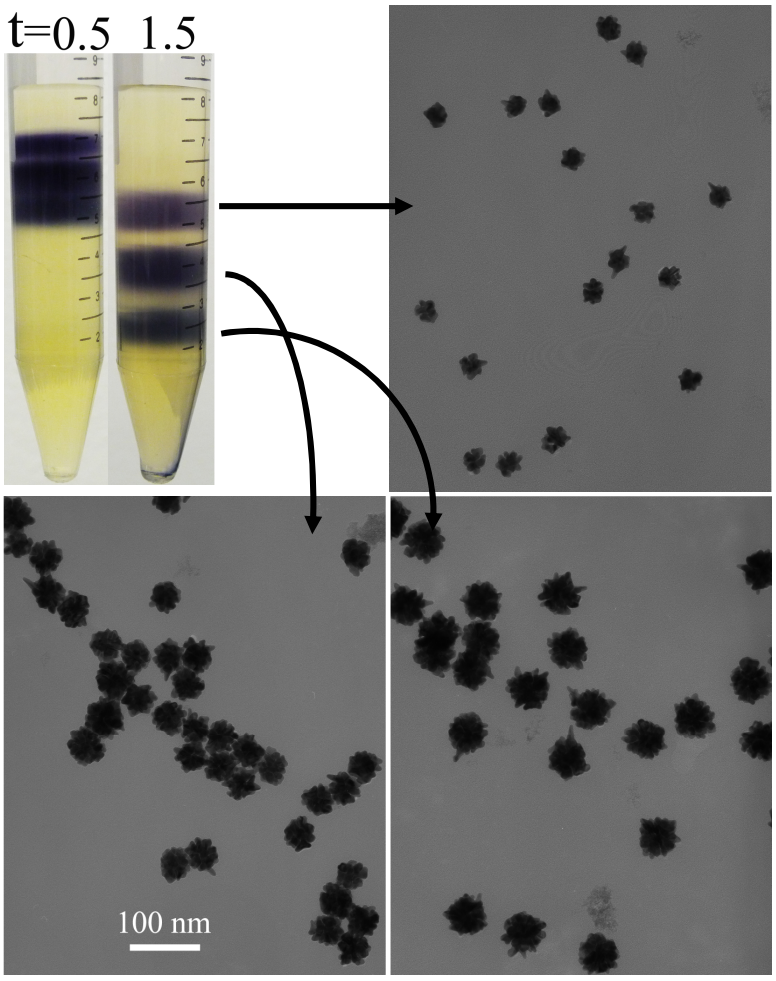

Figure 4.3, Separation of 31, 44 and 50 nm large AuNPs in 20, 25, 30, 35 and 40 wt% PVP 10K viscosity gradient. Photographs show separation at different time points. Three distinct fractions can be obtained after 90 min of centrifuge. TEM images are corresponding to NPs in each fraction. All TEM images share the same scale bar.

It has been discussed in 4.3.2, as well as in literature, that the size separation of NPs is primarily because of the *sharp decrease of NPs' settling velocity at the gradient interface*. Therefore, the viscosity gradient is more likely capable of partitioning large

NPs. As a demonstration, uniform 31, 44 and 50 nm AuNPs were mixed up and centrifuged in 20, 25, 30, 35 and 40 wt% PVP viscosity gradient, three fractions corresponding to each size of NPs can be obtained after centrifuge (Fig. 4.3). It should be noted that previously in literature, all approaches on size separation had focused on NPs below 25 nm, so this is the first trial to separate large NPs.

4.3.4 Extended Study of Viscosity Gradient Created by PVP of a Different Molecular Weight

The viscosity of polymer is dependent on its molecular weight (M.W.). Under the same concentration, polymer of higher M.W. will have a higher viscosity. In other words, to obtain the same viscosity, less concentrated high M.W. polymer can be used; this provides more flexibility to minimize the cost of separation through viscosity gradient. Here, besides using PVP 10K, we also tried to employ PVP 40K for separation of AuNPs (see Table 4.2 for viscosity and density profile). For five sized NPs (same as those in Fig. 4.1), 5.8, 8.7, 11.8, 14.8 and 18.7 wt% PVP 40K, whose viscosities are equivalent to 10, 15, 20, 25 and 30 wt% PVP 10K, were used to build the viscosity gradient. The centrifuge was carried under the same condition, and finally five NPs fractions that are similar to Fig. 4.1 were obtained (Fig. 4.4). More importantly, no destabilization of NPs was found under higher M.W. polymer solution. Similarly, when everything else was remained identical to Fig. 4.3, but the polymer concentration changed to 11.8, 14.8, 18.7, 22.8 and 27.0 wt% PVP 40K, three fractions of larger AuNPs can be observed (Fig. 4.5).

It is expected that with even higher PVP M.W., the concentration needed to build viscosity gradient could be further reduced.

Table 4.1, Viscosity and density profile of aqueous PVP 10K.

Concentration (wt %)	Viscosity * (mPa·s)	Density ** (g/ml)
10	2.6	1.019
15	4.2	1.030
20	6.8	1.041
25	12.1	1.053
30	20.5	1.064
35	40.2	1.075
40	75.0	1.087

Table 4.2, Viscosity and density profile of aqueous PVP 40K.

Concentration * (wt %)	Viscosity * (mPa·s)		Concentration (wt %)	Density *** (g/ml)
5.8	2.6		10	1.02
8.8	4.2		15	----
11.8	6.8		20	1.04
14.8	12.1		25	----
18.7	20.5		30	1.07
22.8	40.2		35	----
27.0	75.0		40	1.09

* Viscosity and equivalent PVP 40K concentration data were determined from the plotted graph in ref. 201.

** Density of PVP 10K of various concentrations was calculated by equation below.

$$d = 0.002263\ c + 0.996$$

This equation was linearly fitted from data in Table 1 of ref. 200, with $R^2 = 0.999$.

*** No density information of aqueous PVP 40K is available in literature, so this set of data was measured by us in the current work. Due to the low accuracy, 10, 20, 30 and 40 wt% concentrations were purposely chosen to get significantly different values. Yet, it can still be deduced that the densities of PVP 40K in the viscosity gradient used for actual NPs separation are very close to each other.

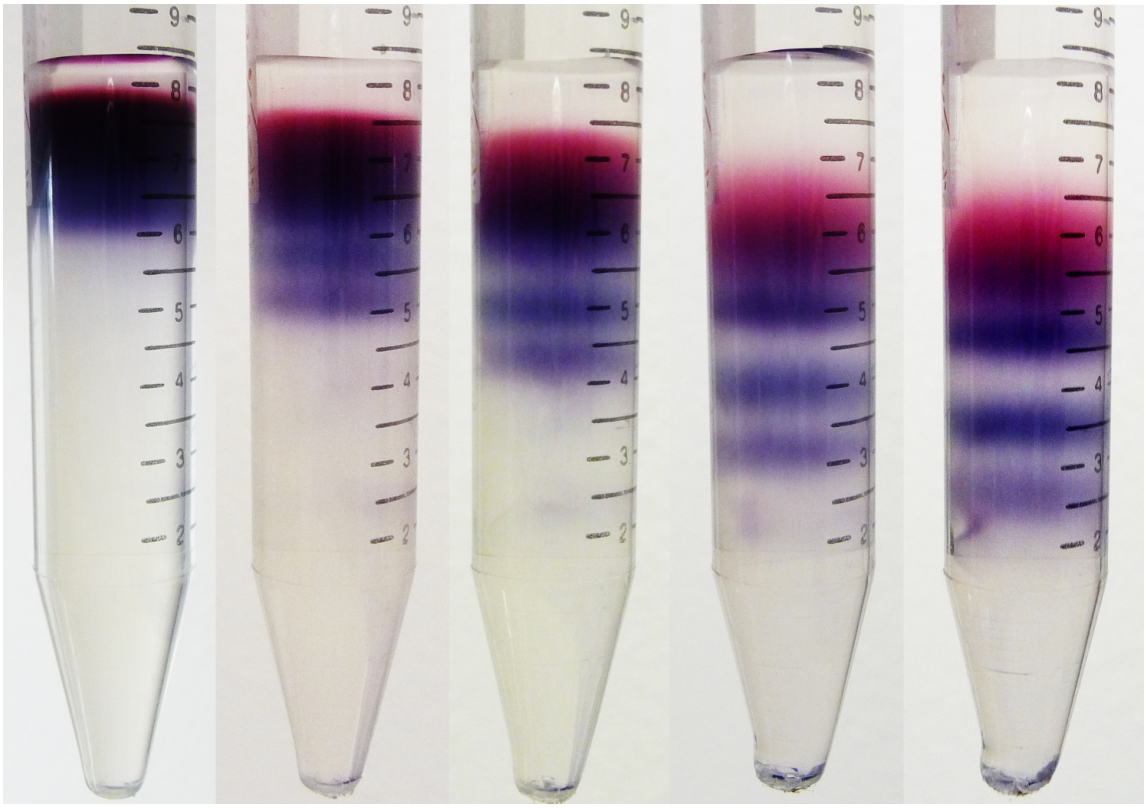

Figure 4.4, A set of photographs taken at different centrifuge time points of the same sample, showing separation of five different sized AuNPs in 5.8, 8.7, 11.8, 14.8 and 18.7 wt% PVP 40K viscosity gradient. From left to right, taken at 0.5, 1.0, 1.5, 2.0 and 2.5 h centrifuge time. NPs sizes and viscosities of each gradient are the same as in Fig. 4.1. The viscosity gradient is built identical to the structure in leftmost of Fig. 4.1A.

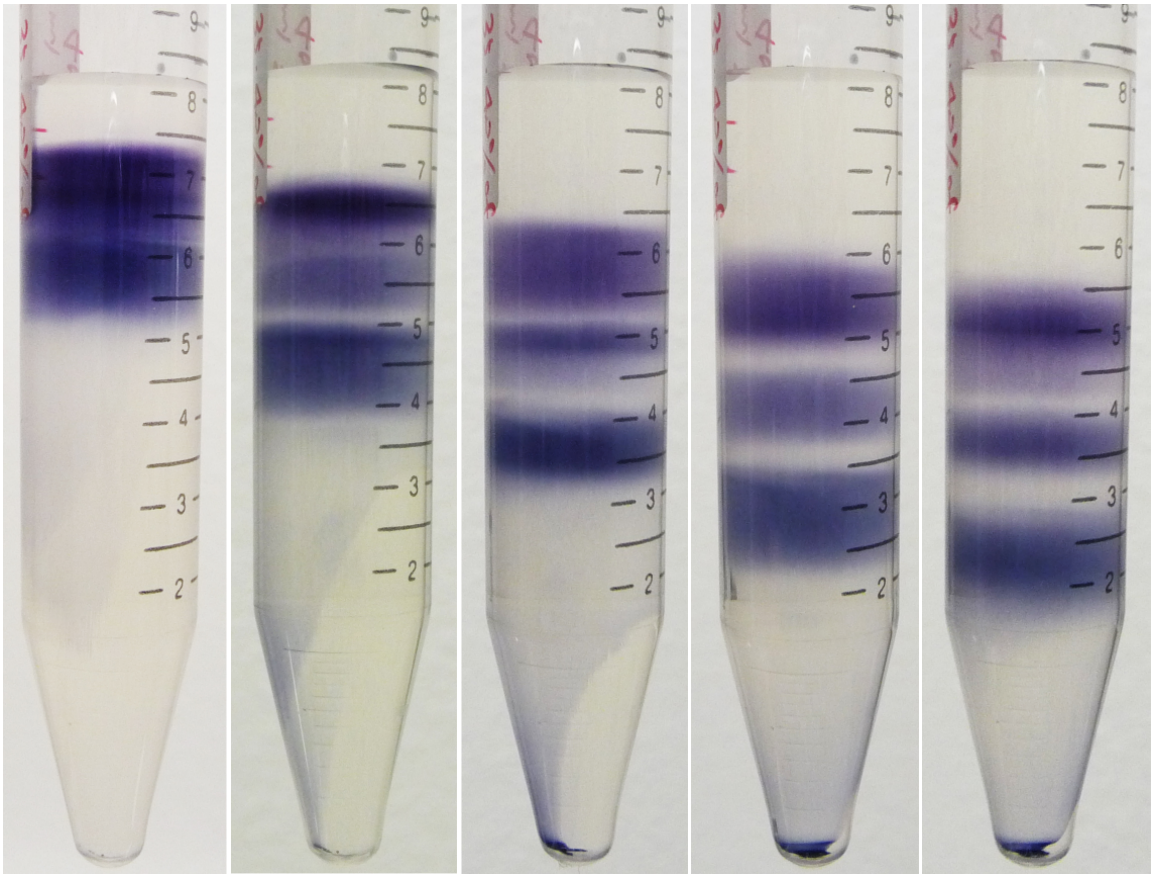

Figure 4.5, A set of photographs taken at different centrifuge time points of the same sample, showing separation of three sized AuNPs in 11.8, 14.8, 18.7, 22.8 and 27.0 wt% PVP 40K viscosity gradient. From left to right, taken at 0.5, 1.0, 1.5, 2.0 and 2.5 h centrifuge time. NPs sizes and viscosities of each gradient are the same as in Fig. 4.3. The viscosity gradient is built identical to the structure in leftmost of Fig. 4.1.

4.4 Conclusion

The weight of 18 nm AuNPs is only 1.73 times of that of 15 nm particles, and 31 nm

particles are merely 1.51 times as heavy as 27 nm particles. The precise separation of tiny size different NPs makes the viscosity gradient very promising in purification of NPs dimers and trimers from individual ones without using high ionic-strength medium, which will destabilize NPs in most cases.[197] Also, many types of NPs have been synthesized with PVP coating and some other sorts of NPs have been stabilized by PVP through ligand exchange or layer-by-layer coating, our unique viscosity gradient should be powerful for purification of those NPs.

CHAPTER 5

Ordered Alignment of Gold Nanorods along Filamentous Biological Templates

5.1 Introduction

Research on gold nanoparticles has recently shifted from their preparation towards their assembly into highly hierarchical and functional structures, due to the unique optical and electronic properties arising from the coupling of individual nanoparticles.[131,204,205] These properties offer potential applications in future waveguides,[206,207] cancer diagnostics,[208] selective detectors[209] and nanoelectronic devices. Among these research work, alignment of gold nanorods (NRs) became particularly interesting because the anisotropic plasmon resonance of gold nanorods along the longitudinal and transversal directions,[48,181,210-212] which could be further used to control the optical response by selectively exciting the long and short axes with polarized light.[213]

Till now, assembly of gold NRs has mainly relied on the ligand replacement method. In this strategy, the thiolated capping reagents were selectively bound to the tips of gold NRs as the thiol groups in the capping reagents have much higher affinity to the tips than the side walls of NRs. The interaction between the thiolated capping reagents allows the end-to-end one dimensional alignment of gold NRs. For example, aligned gold NRs patterns have been achieved by thioalkylcarboxylic acid,[204] cysteine,[214] glutathione,[215] DNA,[216] block copolymer,[217] biotin,[218] and biorecognition molecules.[219] However, the length of aligned gold NR chains from these approaches could hardly go beyond

micrometer scale; most of the current NR chains are less than 1 μm long. The limitation of nanorod chain length will seriously limit the applications when long range plasma coupling is needed. Recently, direct alignment of gold NRs along carbon nanotubes has been developed by Lizmarzán *et al.*[120] However, further modification of carbon nanotubes by using lay-by-layer (LBL) techniques was required in their approach. In this work, we introduced a simple method of assembling gold nanorods into oriented structure by using the biological filaments, namely bacteria flagella, as templates.

5.2 Experimental Methods

5.2.1 Purification of Bacteria Flagella

The flagella were purified from wild type Escherichia coli (E. coli) bacteria (strain SL5928).[258] The cells were cultured in the autoclaved LB broth medium at 37 ^{o}C to OD value around 0.5~0.6 and collected by centrifugation at 2500 × g for 10min. The bacteria were subsequently washed in PBS buffer and water. Following this step, the cells were suspended in distilled water in high concentration (1/100 original volume) and transferred to 1.5 ml eppendorf tube. The tube was subjected to vortex at the highest speed for 3 min, during which sheared flagella were detached from the bacteria surface. Finally, the suspension was centrifuged at 10000 × g for 10 min, leaving bacteria debris as sediment and flagella in the supernatant. The supernatant was collect carefully and stored under -20 ^{o}C.

5.2.2 Preparation of Gold Nanorods Solution

Gold NRs were synthesized following the procedures developed by El-Sayed *et al*.[211] Seed solution was prepared by injecting 600 μl of 100 mM $NaBH_4$ into 10 ml mixture solution which contained 0.25 mM $HAuCl_4$ and 0.1 M CTAB under vigorous stirring. 30 ml gold NRs solution was prepared at each time. Briefly, to a 30 ml growth solution, which contained 0.5 mM $HAuCl_4$ and 0.1 M CTAB, 1050 μl of 4 mM $AgNO_3$ solution and 210 μl of 78.8mM ascorbic acid solution were added in sequence. After gentle shaking, 36 μl as prepared gold seed solution was added. The reaction took place at room temperature and the resultant gold NRs had the aspect ratio of 2-3.

5.2.3 Alignment of Gold Nanorods by Flagella Directly in Solution Phase

Gold NRs solution was centrifuged at 13000 rpm, for 6 min for 2 cycles to remove excess CTAB and re-dissolved into same volume of distilled H_2O. To align gold NRs, various volumes (10-300 μl) of flagella were added to gold NRs solutions that contain same number of particles and placed under room temperature for overnight. The gold NRs/flagella solution was then centrifuged at 2000 rpm for 6 min, the supernatant was removed by pipetting and the sediment was redispersed into distilled H_2O. TEM samples were made by drop casting the solution onto a TEM grid and drying in the air.

5.2.4 Pre-Immobilization Approach of Assembling Nanorods

A drop of flagella solution was cast onto a TEM grid and allowed to concentrate in the air for about 15 min. After that the remaining liquid was wicked by a piece of filter paper. By this process flagella can be immobilized onto the grid. Following that the grid was floated on a drop of gold NRs solution with the side containing flagella in contact

with the liquid. This step last for about 30 min, during which gold NRs were absorbed and assembled along the flagella template. The grid was then washed by floating it on a drop of DI water to get rid of unbound gold NRs. After drying, the grid was directly used for TEM examination.

5.3 Results and Discussions

5.3.1 The Structure of Flagella Templated Nanorods Assembly

Typical TEM images of aligned AuNRs at different magnifications are shown in Fig. 5.1. It can be seen that most of the nanorods have been aligned orderly along flagella into a two string pattern. The nanorods are arranged in a tip-to-tip manner with their longitudinal direction oriented with the long axis of the flagella templates. The inter-particle distance varies dramatically at different sites. Such alignment is highly reproducible and can be prepared in relatively large amount. The electrostatic interaction should be the main source of force that induces the assembly. The gold NRs are synthesized with a bilayer cationic CTAB coating on the surface, thus they are positively charged; while flagella, like many other naturally self-assembled supermacromoleucles, are negatively charged in neutral solution.[220] When the surface charges of gold NRs are reversed by applying a polyelectrolyte wrapping process with PSS (sodium polystyrene sulfonate),[221] no assembly was observed in multiple trials of different conditions. The electrostatic force, as demonstrated in the literature, is strong enough to induce the immobilization, aggregation and assembly of nanoparticles.

Theoretically, in the electrostatic force induced assembly, the rod-like nanoparticles could have either their tips or the long sides in contact with the template. However, in this work, nanorods are predominated with their sides interacting with the flagella. This might be because the surface area of nanorods along the long axes is much higher than that at the tips. Under the same surface charge density, larger are of interaction will likely result in a stronger binding of nanorods onto the template. And thus, the gold nanorods will prefer to assemble into a more stable structure.

In the assembly of nanoparticles into 1D hierarchical structure, inorganic nanowires, especially carbon nanotubes, have been used widely as hard templates. The pristine carbon nanotubes have no charge on the surface and they are not even dispersible in water. A tedious surface modification, including oxidization (by nitric and sulfuric acids) and polymer wrapping (by a multi-step layer-by-layer assembly of polyelectrolytes) has to be carried out to make the nanotubes charged.[120] The biological filamentous templates, flagella, are about 20 nm in diameter and up to 15 μm in length,[222] thus they have dimensions comparable to that of the carbon nanotubes and are suitable to be employed as template for nanoparticles assembly. The flagella can be prepared in relatively large amount through bacteria culture. More importantly they are natively charged, and therefore can be used directly to induce the assembly of nanoparticles. The surface charge density on the flagella can also be manipulated through the well developed genetic engineering process.[223]

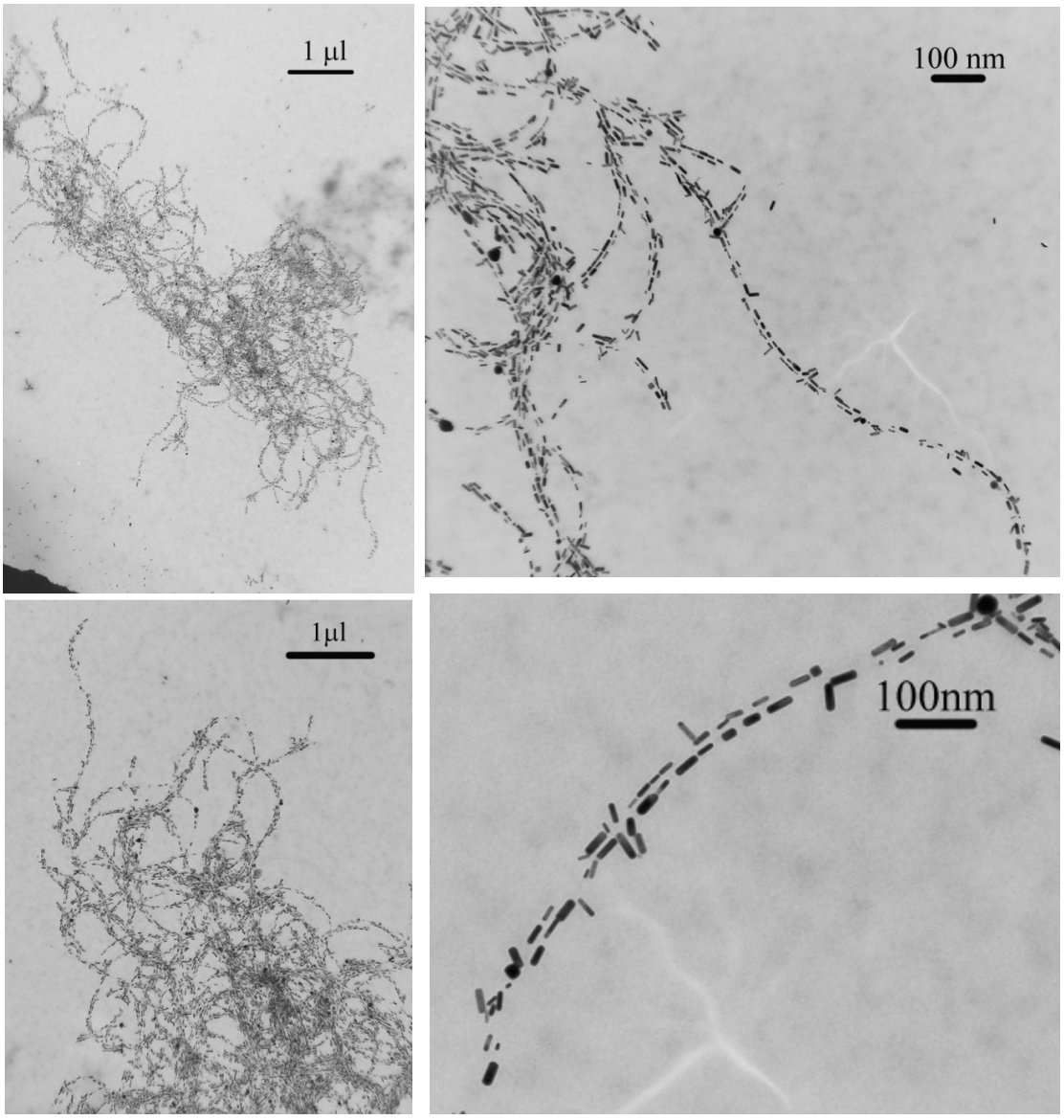

Figure 5.1, TEM images of low and high magnification showing the structure of gold NRs that were aligned by flagella directly in solution phase.

5.3.2 Interaction of Gold Nanorods with Flagella at Different Ratios

From our experience, to obtain the highly ordered alignment of gold nanorods, the

ratio between rods and flagella has to be finely tuned. As shown in Fig. 5.2, we used the same amount of AuNRs, but 300, 100, 20 and 10 μl of flagella solution (named sample A, B, C, and D respectively); after placed on benchtop for overnight, the four tubes appeared very differently. With reducing amount of flagella, they formed stable suspension, flocculation, precipitation and aggregation respectively; the first three samples can be redispersed simply by hand shaking while the last one remained as tiny visible particles. We further investigated the difference among these samples by examining the flagella-AuNRs hybrid structure under the TEM. The typical TEM images are shown in Fig. 5.3, no alignment was observed in samples A and B, most flagella only have a few nanorods standing by them (Fig. 5.3 A&B). Relatively, sample B has slightly more nanorods on each flagellum and nanorods-flagella network like structure was seen on the grid. Sample C showed highly ordered two string alignment of nanorods along the flagella (Fig. 5.3C). Sample D only contained large dense aggregates, without any obvious pattern; however, at the edge of nanorods aggregate, linear arrangement of nanorods could still be seen clearly (Fig. 5.3D).

Based on the above observation, we further interpret the interaction between rods and flagella by the model sketched in Fig. 5.4. The flagella should be in large excess amount in samples A and B. There might be more than one flagellum interacting with single nanorod, which resulted in the network like rods-flagella hybrid structure (Fig. 5.4 A&B). However, due to the strong repulsive force among the charged flagella, the hybrid structure could be stabilized. When the amount of flagella was reduced from 300 μl to

100 μl, the total repulsive force decreased correspondingly; besides, more rods were on average interacting with one flagellum, which increased the density of the hybrid structure, so they slowly flocculated. At the right ratio, nanorods can be assembled along flagella (Fig. 5.4C). Further reducing the amount of flagella turned nanorods into excess. Ideally, the rods would first form ordered alignment, same as in Fig. 5.4C, the excess amount of rods would still interact with the exposed surface of flagella, and bridged multiple aligned flagella into an aggregation (Fig. 5.4D).

Top: Placed overnight on benchtop

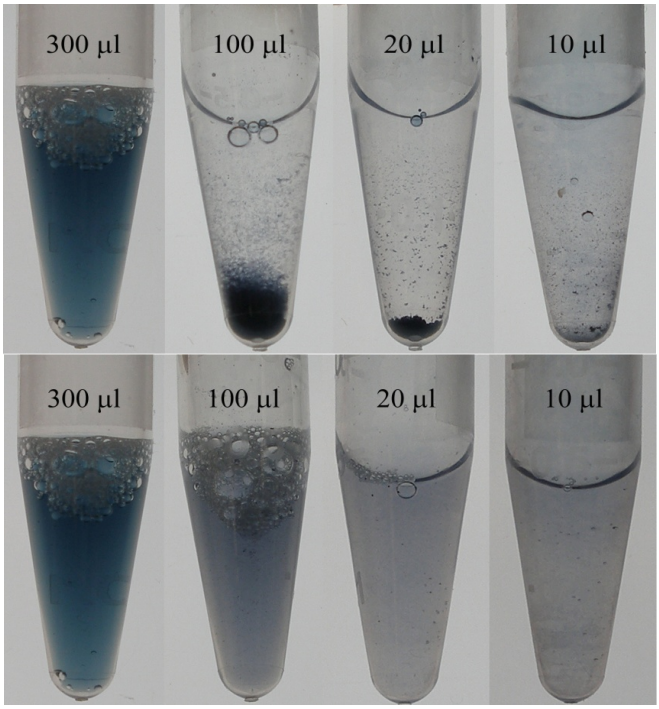

Bottom: Resuspended by hand shaking

Figure 5.2, Photographs of AuNRs-flagella mixed solution at different ratio of the two species: after placed on benchtop for overnight (top) and resuspended by hand shaking (bottom).

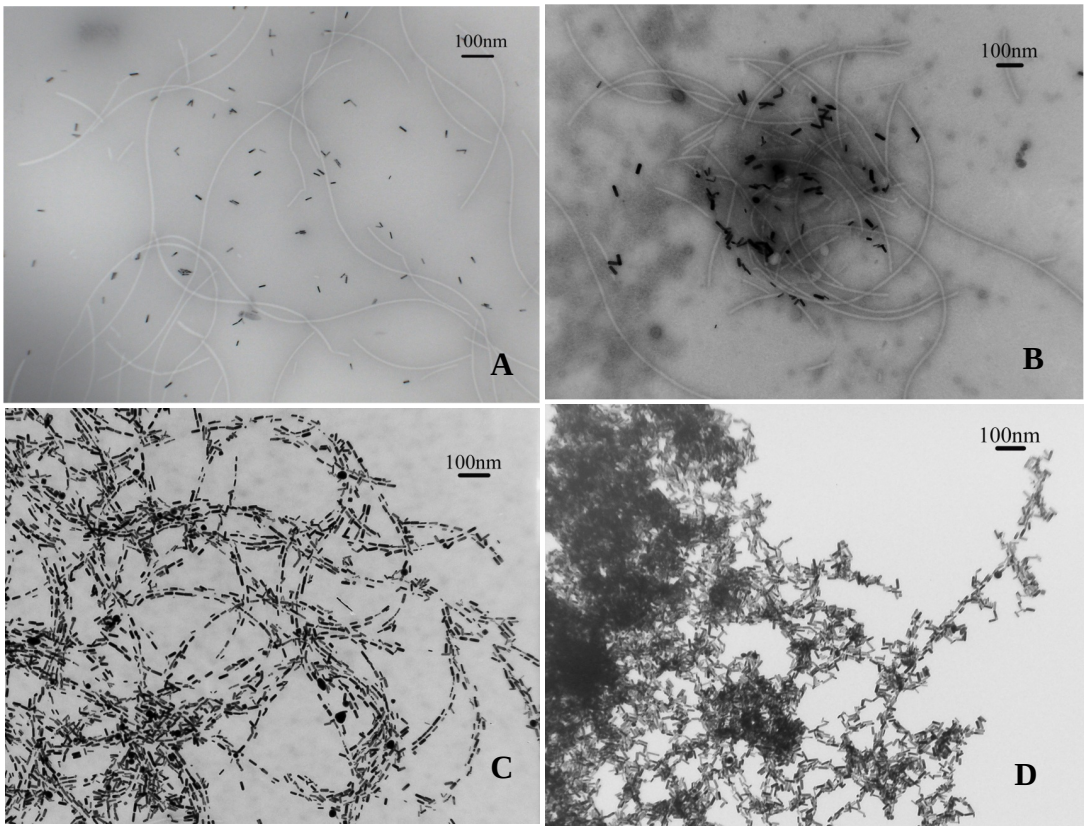

Figure 5.3, TEM images of AuNRs-flagella hybrid structure at different ratios of the two species. (A-D) are corresponding to 300, 100, 20, 10 μl of flagella as in the photographs in Fig. 5.2 respectively.

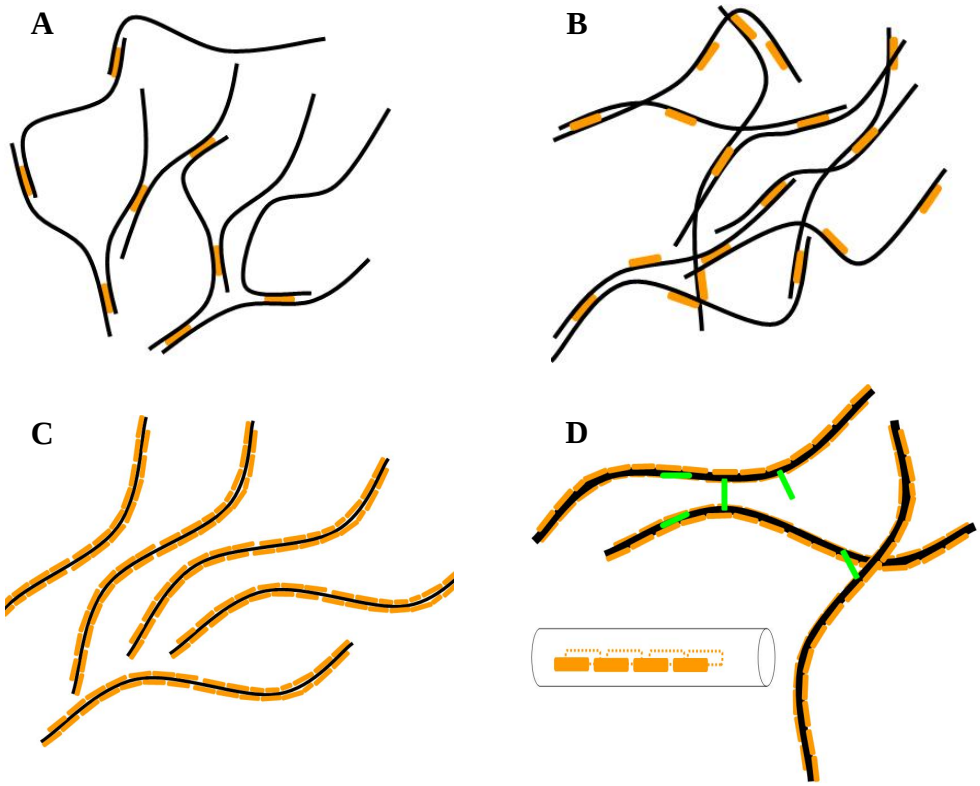

Figure 5.4, Proposed mechanism of interaction between AuNRs and flagella at different amount ratios.

5.3.3 Optical Shift Effect in Assembled Gold Nanorods

The optical property is one of the most important properties on gold nanoparticles.[4,7] Many optical related biological applications, including molecular detection and sensing,[4] biological imaging and diagnostics,[5-7] targeted drug delivery and medical therapy,[8-12] have been explored based on the gold nanoparticles. The optical shift effect associating with the assembly of gold nanoparticles is also an interesting phenomenon that has

attracted intensive studies.[205,224] When gold nanoparticles approach each other within a certain distance, interaction or coupling of their surface plasmon will result in a solution color change, which is reflected as a blue shift in the optical spectrum. Such optical shift is highly dependent on the distance of neighboring nanoparticles, the smaller the distance, the longer the shift. In linearly assembled gold nanoparticles, the surface plasmon coupling has directly led to the propagation of light in spaces where the dimension is smaller than the reflection limit of light.[131]

When the flagella solution was added into gold NRs suspension, the color of the nanoparticles solution was changed immediately. In the absorption spectrum measured before and after addition of flagella, the SPR band corresponding to the transverse direction of nanorods generally remained at the same wavelength (528 nm), but the longitudinal SPR band shifted from 832 nm to 880 nm (Fig. 5.5). In the meanwhile, a significant broaden of the peak was observed at the longer wavelength. As it could be seen from Fig. 5.1 that the tip-to-tip distance between most adjacent nanorods are small enough to induce the plasmon coupling effect, so the solution color change should be the result of assembly of nanorods onto the template. While the gold nanorods are assembled in a tip-to-tip style, plasmon coupling will only take place along the longitudinal direction, rather than the transverse direction.[225] This explains why the absorption peak shift was only observed at the longer wavelength but not at the short wavelength. It has been mentioned that the surface plasmon coupling induced absorption peak shift is highly distance dependent, while the gaps between the tips of adjacent nanoparticles were not

uniform along the template, thus the shifted SPR band would be inevitably widened.[120]

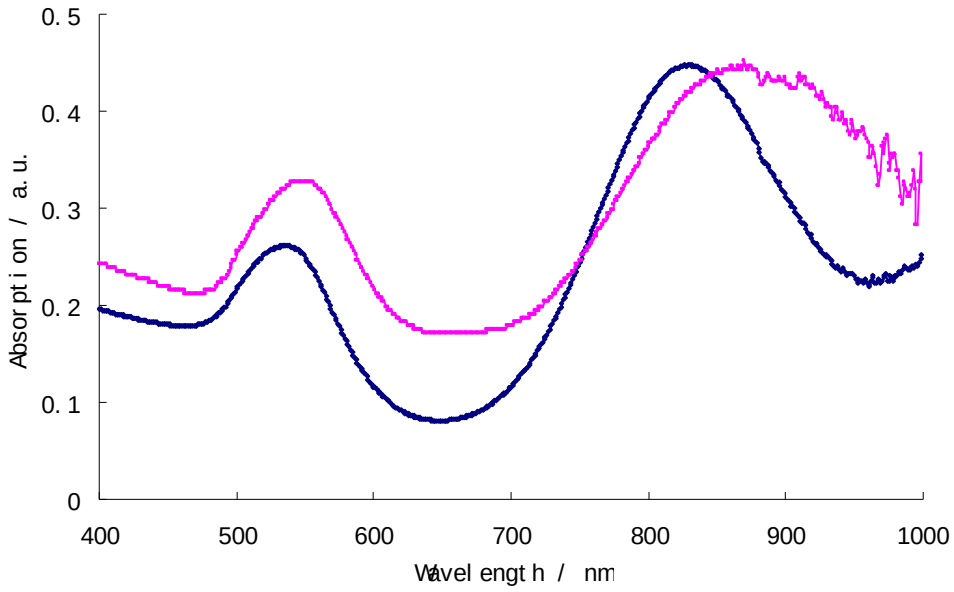

Figure 5.5, UV-Vis spectrum of gold nanorods before (blue line) and after (red line) alignment.

5.3.4 Assembling of Nanorods onto Flagella through the Pre-Immobilized Process

As we discussed above, in order to have nanorods aligned highly ordered along flagella, we had to play carefully with the ratio between them, which is a time-consuming process. This will be especially problematic when nanorods used are not synthesized from the same pot (we have the experience of getting rods of different aspect ratios in two synthesis trials, even all the precursors were added in the exactly same amount). Because of the above reasons, exploring a process that depends less on the amount ratio

of nanorods and flagella is very necessary.

Here, we employed a pre-immobilized process, as described in Fig. 5.6A. Basically, in this process, the flagella will be first immobilized onto the formvar (polyvinyl formal) side of the TEM grid. Following this step, the super-light grid will be floated onto a droplet of AuNRs solution. The formvar itself has no charge on the surface, thus when the TEM grid is floated onto the nanoparticle solution, the pre-immobilized flagella will be the only attractive sites that can uptake nanoparticles through electrostatic force and assemble them along the template into a linear structure. As it can be seen in Fig. 5.6B that AuNRs can also be aligned into two string highly ordered structure which is pretty similar to that made in the solution phase (Fig. 5.1). The assembly of nanorods onto pre-immobilized flagella can take place in a wide concentration range of both the nanoparticles and the template. And thus it is much simpler than the direct assembly in the solution phase as described in 5.2.2. Through the same process, nanorods could be aligned directly onto the flagella of living bacteria (Fig. 5.6C). The flagella on living bacteria are generally longer than those isolated, as in the isolation the vortex force used to detach flagella from the bacteria body would simultaneously break the long fibers into many shorter rods. Thus, direct assembly of nanorods onto the flagella of living bacteria is more likely to produce longer 1D pattern of aligned nanorods. Besides, the direct assembly also enables more manipulation to the hybrid structure, especially in the fabrication of devices. Because the body of bacteria has an overall size on micron scale, while flagella have only nano-sized diameter, the manipulation of a micro object should

be technically much easier than that of a nanoscale object.

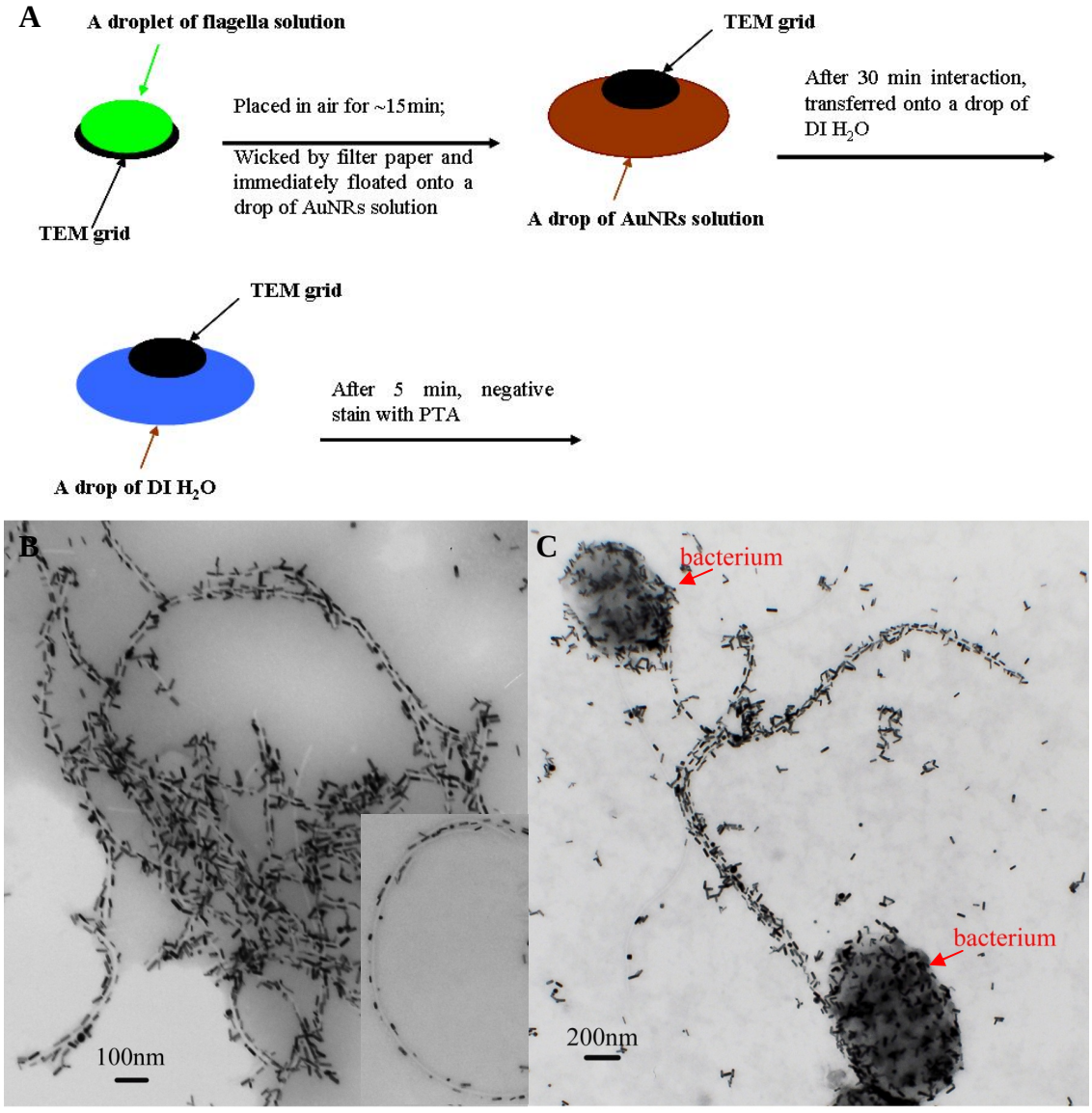

Figure 5.6, (A) Schematic diagram of float grid approach to align AuNRs. (B, C) TEM images of aligned AuNRs onto free flagella and flagella of living bacteria through the pre-immobilization process.

5.4 Conclusion

Oriented assembly of gold nanorods has been achieved by using biological filaments, namely bacteria flagella, as templates. The electrostatic interaction between the positively charge gold nanorods and negatively charged flagella is considered to be the main driving force for the assembly. The effect of concentration ratio of nanoparticles to templates on the final assembled structure was discussed. The optical shift effect arising from the surface plasmon coupling in the tip-to-tip assembly of nanorods along flagella has been investigated. In addition, the pre-immobilized method developed was proved to be a simpler method than the direct mixing in solution phase to assemble nanorods.

CHAPTER 6

Biomimetic Branched Hollow Fibers Templated by Self-Assembled Fibrous Polyvinylpyrrolidone (PVP) Structures in Aqueous Solution

6.1 Introduction

Branched hollow fibers can be found in nature and play a significant role in the functioning of biological bodies. For example, as the most important vessels, capillaries in the blood vessel system own an abundance of branches, which enable the exchange of chemicals and water between the blood and body tissues. Without the bronchial tree in the respiration system, oxygen transportation will be extremely slow and any intensive body movement will need great effort or even become impossible. Branched hollow fibers are also adopted by many types of birds in their feathers.[226,227] The branched structure of feathers can reduce the weight and increase the friction with air, and also act as a thermal insulator.[226] Mimicking unique branched hollow structures in nature will help us to produce novel advanced materials that can find potential technological and medical applications such as microfluidics,[228] artificial blood vessel generation,[229,230] and lung tissue engineering.[231,232] However, synthesis of branched hollow fibers remains a challenge up to date. Non-branched solid and hollow fibers of many types of materials have been prepared in different ways, such as chemical vapor deposition (CVD),[233-235] anodic aluminum oxide (AAO) templating,[236] electrospinning[237,238] and many other wet

chemical synthetic methods.[152] So far, branched hollow fibers were only reported in the fabrication of carbon nanotubes[239,240] and polyaniline nanotubes.[241] The branched carbon nanotubes were prepared by directly templating Y-branched nanochannel alumina using CVD, and self-assembled doped polyaniline was formed from the fusion of micelles containing polyaniline and dopants.

The polymer polyvinylpyrrolidone (PVP) has found its application in many scientific areas. For example, in adhesive industry, PVP offers a unique combination of desired properties including good initial tack, transparency, chemical and biological inertness, and very low toxicity. In material science, PVP has acted as a key factor in the shape controlled synthesis of silver and platinum nanocrystals.[242-244] For the synthesis of these nanomaterials, PVP serves as a polymeric capping agent, which can selectively interact with the {100} facets of Ag and Pt, and shape control was realized through the preferential adsorption of atoms onto poorly protected facets such as {111}.[245] PVP has also been widely used as an additive to manipulate solution viscosity in the production of nanofibers through electrospinning. In addition, in the fabrication of various membrane products, PVP is added to increase the hydrophilicity of the membranes.[246-249] In this work, we discovered that, after a relatively long period of aging at room temperature, PVP could self-assemble to form a macroscopic matrix made of a branched hollow polymer nanofibers in an aqueous solution. By directly templating the silica formation on the self-assembled fibrous network, branched hollow silica fibers were synthesized. Inspired from the self-assembly of PVP into fibrous structures in the solution, we also

studied the self-assembly of PVP-coated nanoparticles into branched fibers. We believe that the self-assembled fibrous PVP structures could be potentially used as a universal template for preparing branched hollow fibers through the synergistic assembly of nanoparticles and PVP in the solution phase.

6.2 Experimental Methods

6.2.1 Preparation of Self-Assembled Hollow Fibrous PVP Structures

In a 15-ml vial, 600 mg of PVP (10 kg/mol) was dissolved into 10 ml distilled water (PVP 5.7 wt. %). The solution was then sonicated for 10 min to ensure homogeneous distribution of the polymer. After this step, the vial was capped and the solution was placed on the bench top at room temperature for about two weeks. During this period of time, tiny polymeric aggregates were found at the bottom of the vial in one week and slowly grew larger and larger in the following week.

6.2.2 Growth of Silica on Self-Assembled Hollow Fibrous PVP Structures

The polymer aggregate made of self-assembled hollow PVP fibers was transferred to a 5 ml vial by Pasteur pipette and washed with distilled water twice to remove free polymer molecules in the solution. The aggregate was then suspended in a 1 ml ethanol-water (4: 1 v/v) solution. To the resultant suspension were added 50 μl

tetraethoxysilane (TEOS) and 50 μl NH_4OH. The suspension was further mixed by gently inverting the vial for several times. In order to form a uniform silica layer onto the polymer aggregate, during the reaction, the vial was placed onto an aliquot mixer rocker for about 2 h. The as-grown silica microfibers were washed twice with ethanol to get rid of the products that might be formed in the hydrolysis reaction other than the silica microfibers.

6.2.3 Preparation of Hollow Gold Fibers by Co-Self-Assembly of PVP-Coated Gold Nanoparticles and Free PVP Molecules

Gold nanoparticles were synthesized through the reduction of gold chloride ($HAuCl_4$) by sodium citrate. The synthesis system included 5 ml 5.9 mM $HAuCl_4$, 3 ml 38.8 mM sodium citrate and 42 ml distilled water. Ligand replacement of citrate ions by PVP on the surface of gold nanoparticles was carried out according to the procedure reported in the literature. 50 ml PVP stabilized gold nanoparticles were centrifuged and re-dispersed into 10 ml or 50 ml PVP aqueous solution (PVP 5.7 wt. %). The mixture was then allowed to stay on the bench top at room temperature for 2 weeks. Gold microfibers were formed through the co-assembly of the PVP-coated gold nanoparticles and PVP.

6.2.4 Characterization

Silica and gold microfibers were characterized by Scanning Electron Microscope (SEM) JEOL 880 at 15 kV in both bundled and individual fibers. The bundles of fibers were prepared by directly placing a bulk piece of as-synthesized silica onto a piece of freshly cleaved mica. Individual fibers were prepared by sonicating the bundles for 2 -3 min, and then casting a drop of suspension onto mica. Gold microfibers were prepared in the same way, except that instead of using mica, silicon wafer was employed as a substrate. Samples of silica were coated with a thin layer of gold platinum by sputter coating prior to SEM imaging; while gold microfibers samples were directly subjected to SEM examination without any additional coating.

6.3 Results and Discussions

6.3.1 Structure of PVP Jellyfish-Like Aggregate

The self-assembled fibrous PVP structure formed in the aqueous solution was a jellyfish-like three-dimensional aggregate with a centimeter scale (Fig. 6.1a). However, when taken out of the solution, the aggregate was collapsed immediately into a semitransparent thin film. The SEM imaging of the film revealed that the aggregate was constructed from a network of branched hollow PVP fibers of micron size (Fig. 6.2a). The collapsed morphology indicated that the fibers formed might be hollow when in the solution. A closer look at the ends of the polymer fibers shows that the fibers are indeed hollow (Fig. 6.2b). The hollow nature of the PVP fibers was also proved by TEM

imaging (Fig. 6.3). To the best of our knowledge, the self-assembled fibrous structure resulting from the self-assembly of PVP in the aqueous solution has never been reported, although it was not a surprise to us that PVP could self-assemble to form this kind of structure.

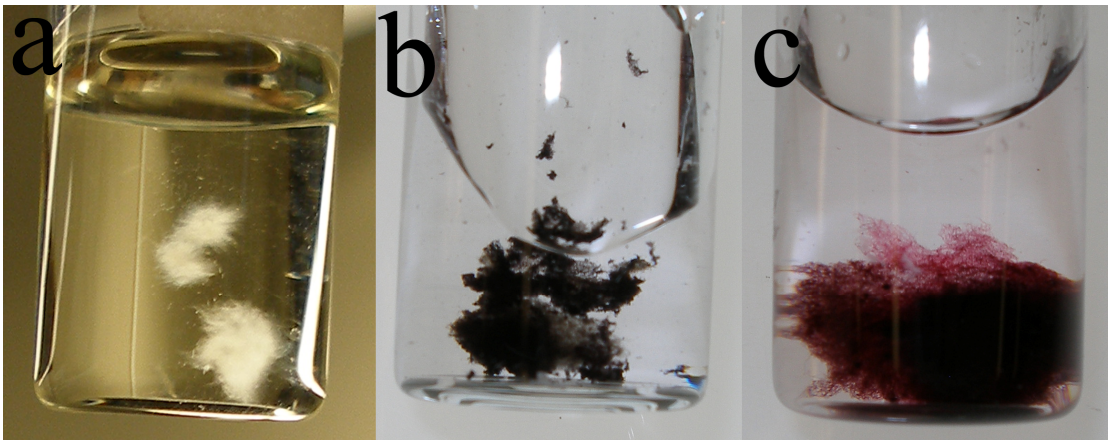

Figure 6.1, Photographs of (a) PVP jelly-fish like aggregate; (b) PVP-gold aggregate co-assembled from PVP and gold nanoparticles with a high concentration; (c) PVP-gold aggregate co-assembled from PVP and gold nanoparticles with a concentration 5 times lower than that in b. Image reprinted with permission from ref. 310, Copyright 2010 American Chemical Society.

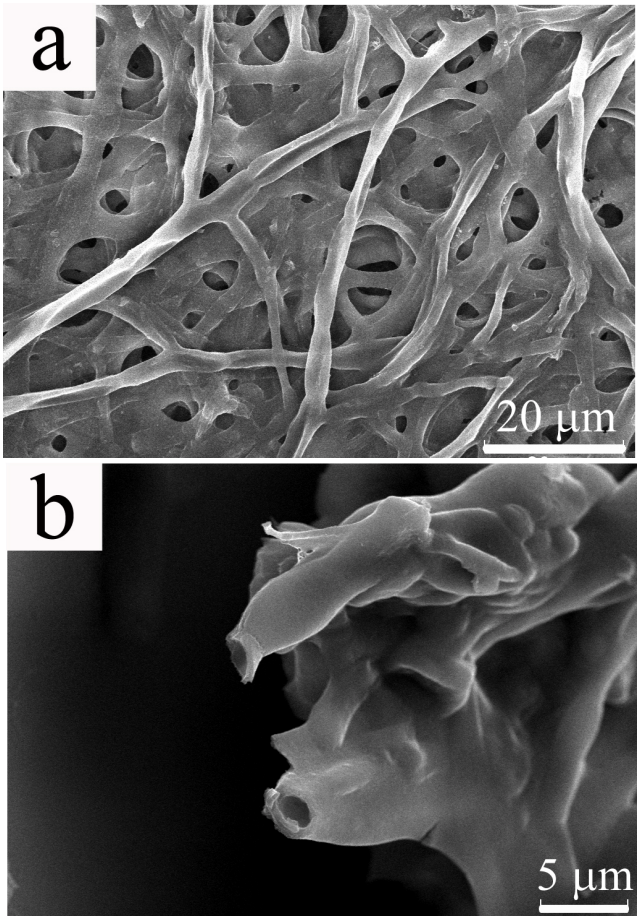

Figure 6.2, SEM images of self-assembled hollow branched PVP fibers. a) An aggregate of branched fibers that may be collapsed upon drying on substrate; b) higher magnification image of the tips of the fibers, showing the hollow nature of the fibers. Image reprinted with permission from ref. 310, Copyright 2010 American Chemical Society.

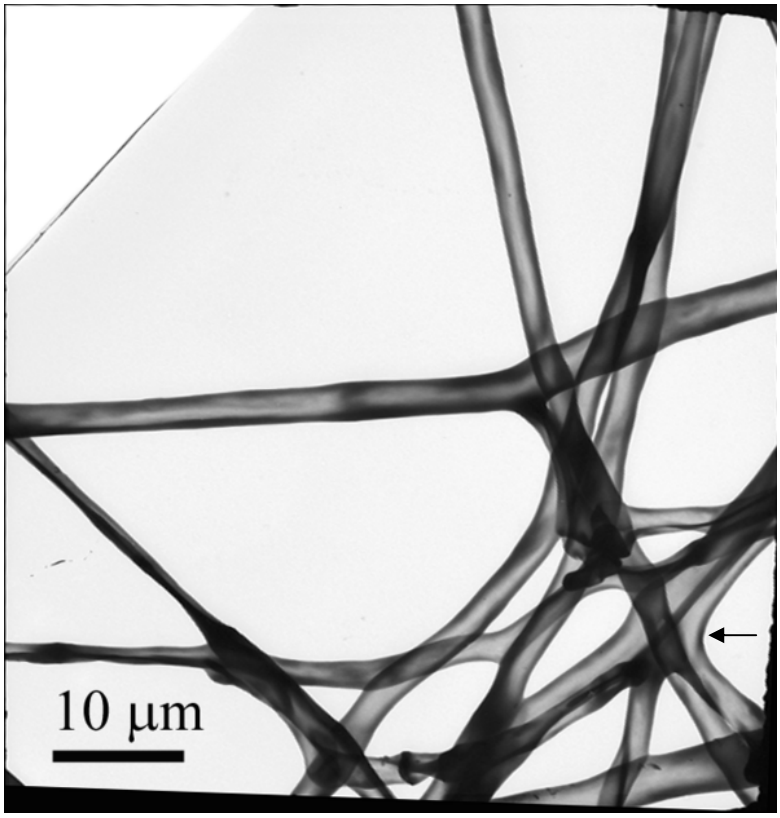

Figure 6.3, A typical TEM image of PVP hollow fibers. The thickness of fiber wall varies, which can be judged from the nonuniform contrast along the axes. Some segments of the fibers have dark contrast at the magnification shown here, but hollow channels can still be observed from these segments under high brightness electron beam. However, images can hardly be taken due to the lack of stability of PVP fibers under high energy beam. A black arrow shows a hollow junction at the branch. Image reprinted with permission from ref. 310, Copyright 2010 American Chemical Society.

6.3.2 The Mechanism of Formation of PVP Aggregate

The association behavior of polymers in a solution phase has been extensively studied for decades. Generally, van de Waals force, hydrophobic and electrostatic interactions as well as hydrogen bonding are the major driving forces responsible for inter- and intra- molecular interaction among polymer molecules.[250] In PVP, both the polymer backbone and methylene groups in the five-member ring provide good sites for hydrophobic interaction, enabling the association of PVP through hydrophobic interaction. In addition, polymer chains with highly electronegative amide groups could be strongly linked together through solvent-mediated H-bonding interaction.[250,251] Earlier, an aggregate of around 100 nm nanoparticles was found to form in a freshly prepared PVP aqueous solution by dynamic light scattering (DLS), however, the detailed structure of the aggregate was not mentioned.[252] Actually, not only PVP, but also other amide containing polymers, such as poly(N,N-diethylacrylamide) (PDEA), could self-assemble to form aggregates, due to their structural similarity.[253]

We believe that the macroscopic PVP structures shown in Fig. 6.2 result from a self-assembly process in which individual polymer chains interact with each other through H-bonding and hydrophobic interaction. To prove this mechanism, we suspended the polymer aggregates into 1 M urea aqueous solution, which is a common reagent used to break H-bonding in protein science. After one week, we observed a dramatic decrease in the dimension of polymer aggregates, indicating that some polymer chains had been

disassembled from the major aggregated structures due to the loss of H-bonding interactions. More detailed mechanism was analyzed by a combination of DLS measurement and SEM imaging.

By using DLS to measure the size distribution of the particles formed during the aging of the aqueous PVP solution, we found that even in the freshly prepared PVP solution, there were particles ranging from 40-80 nm (Fig. 6.4). Given that the individual polymer chain length (M.W. 10 kDa, 91 monomers) should be less than 15 nm, the nanoparticles detected by DLS must be generated from the association of polymer chains. However, after 1 and 4 days, the particle size was increased to 90-160 nm and 210-490 nm, respectively (Fig. 6.4). These facts indicate that the polymer molecules gradually self-assemble into larger particles in the solution. At day 6, the PVP aggregates became visible by naked eyes at the bottom of the vial (around 1 mm in diameter). We further examined the tiny aggregates by SEM (Fig. 6.5). It could be seen clearly that in the center of the aggregates there was a core made of chains of PVP microspheres, from which polymer fibers were grown and stretched toward all directions (Fig. 6.5a). A closer look at the core reveals that hollow microspheres are fused into the chains (Figs. 6.5b&c). Longer hollow fibers were grown from the microspheres at the end of such chains (Fig. 6.5d).

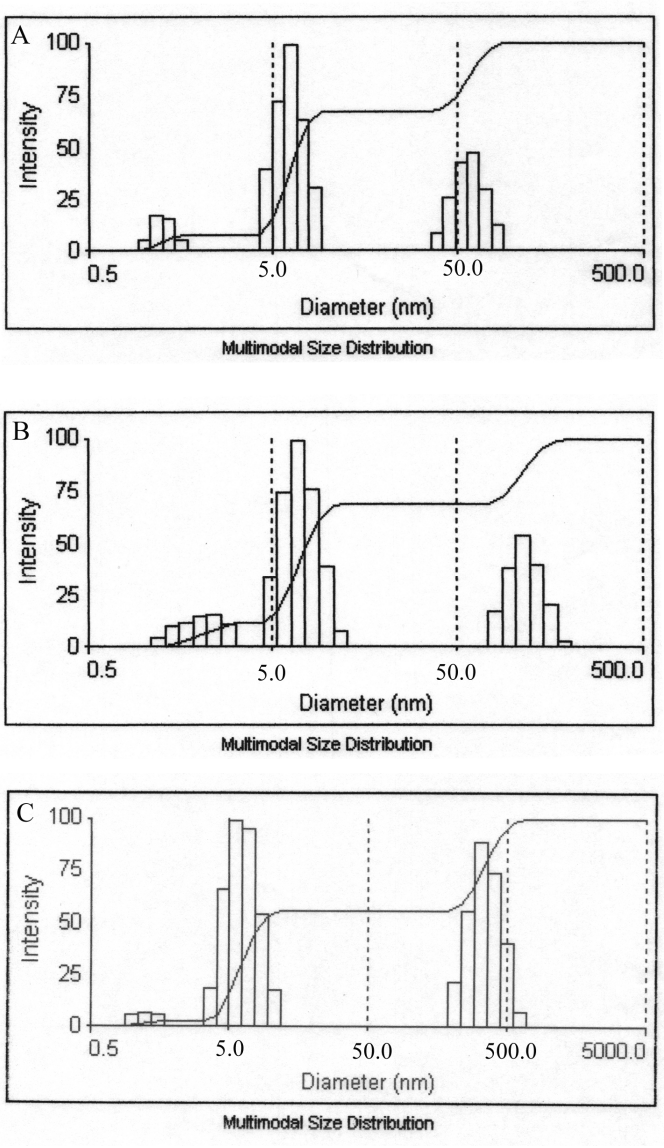

Figure 6.4, Particle size distributions in 5.7 wt. % PVP aqueous solution determined by Dynamic Light Scattering (DLS) measurement. (A) Freshly prepared solution, (B) Solution aged for 1 day, (C) Solution aged for 4 days. The mean diameters for these three time points are 22.0 nm, 39.0 nm and 156.6 nm, respectively. The particles of around 5 nm are corresponding to the individual polymer chains (M.W. 10 kDa). The particles around 50 nm or larger are corresponding to the aggregates formed as a result of the

self-assembly of polymer chains. Image reprinted with permission from ref. 310, Copyright 2010 American Chemical Society.

Based on the DLS and SEM analysis of the early stage during the formation of the jellyfish-like PVP aggregate, the aggregate formation process can be divided into two steps: formation and fusion of PVP microspheres into pearl-necklace-like chains and growth of hollow fibers from the chains. In the chain formation step, the polymer molecules, in the aqueous solution, first interacted with each other to form hollow spheres; when the hollow spheres reached a critical size (typically larger than 2 μm as seen from SEM images), they started to aggregate and fuse into a pearl-necklace-like chain (Fig. 6.5b). Subsequent outgrowth of longer fibers from the chain can be realized through the assembly of free polymer molecules in the solution onto the microspheres at the end of the pearl-necklace-like chains (Fig. 6.5d), rather than through continuous attachment of microspheres, as there was a dramatic morphological difference between the chains (rough, Figs. 6.5b & 6.6a) and outgrowing fibers (smooth, Figs. 6.5d & 6.6b). However, the microspheres at the end of the chains might have been elongated first to facilitate the assembly of PVP molecules (Fig. 6.7). A continuous morphological transition from spherical particles into smooth fibers was observed at the interface of pearl-necklace-like chains and outgrowth fibers. With increasing distance from the central chains, the PVP hollow microspheres underwent the change into ellipsoids, rods and eventually smooth fibers. The hollow microspheres (Fig. 6.5c) constituting the chains

may eventually be fused into hollow fibers, which might be the same process of hollow nanoparticles fusing into nanotubes.[241] The branched character of the fibers was originated from the attachment of microspheres, which did not take part in the chain formation or was generated after the formation of the chain, onto the sidewall of outside fibers (Fig. 6.8). Once the attached microspheres were fused with long fibers (i.e., stems), free polymer molecules in the solution would also assemble onto the new site, and this will lead to the growth of a branch from the microspheres.

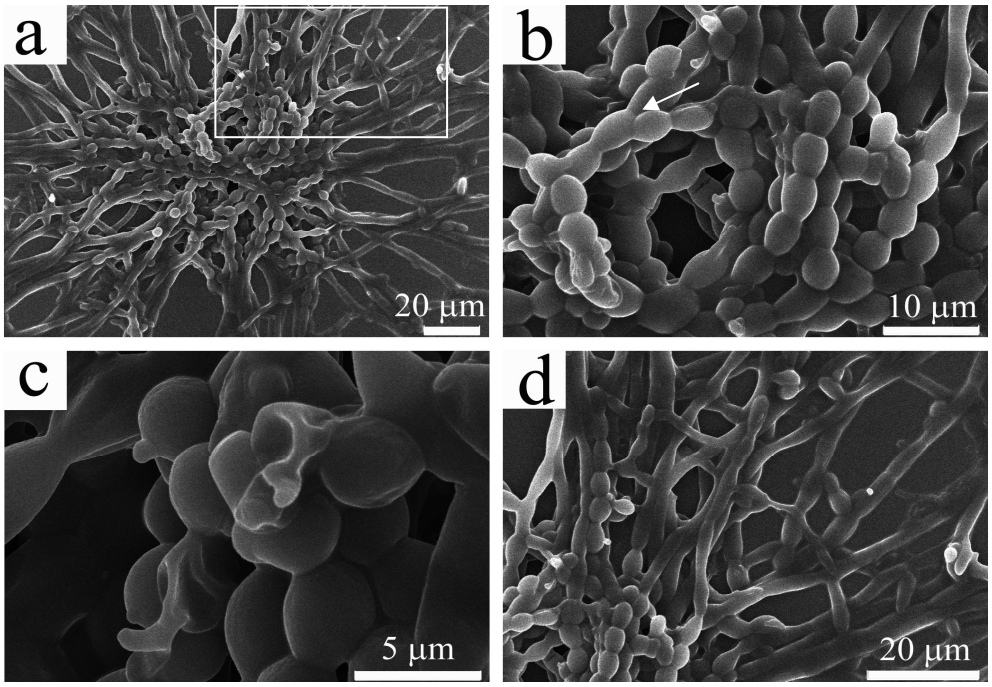

Figure 6.5, SEM images of PVP aggregates formed at the early stage. (a) An overall view of an aggregate with a core (made of pearl-necklace-like linear chains) from which all the fibers were grown; (b) A closer view of the core from the aggregate shown in (a), highlighting that the formation and fusion of PVP microspheres into pearl-necklace-like chains (It should be noted that the branched structures are found in the core, as indicated by the arrow); (c) The pearl-necklace-like chains with some broken microspheres highlighting the hollow nature of PVP microspheres; d) A closer view of the area highlighted by a white square highlighted in (a), showing that free PVP molecules in the aqueous solutions continued to assemble onto the microspheres at the end of the pearl-necklace-like chains, and finally resulted in the formation of jellyfish-like large aggregate. Image reprinted with permission from ref. 310, Copyright 2010 American Chemical Society.

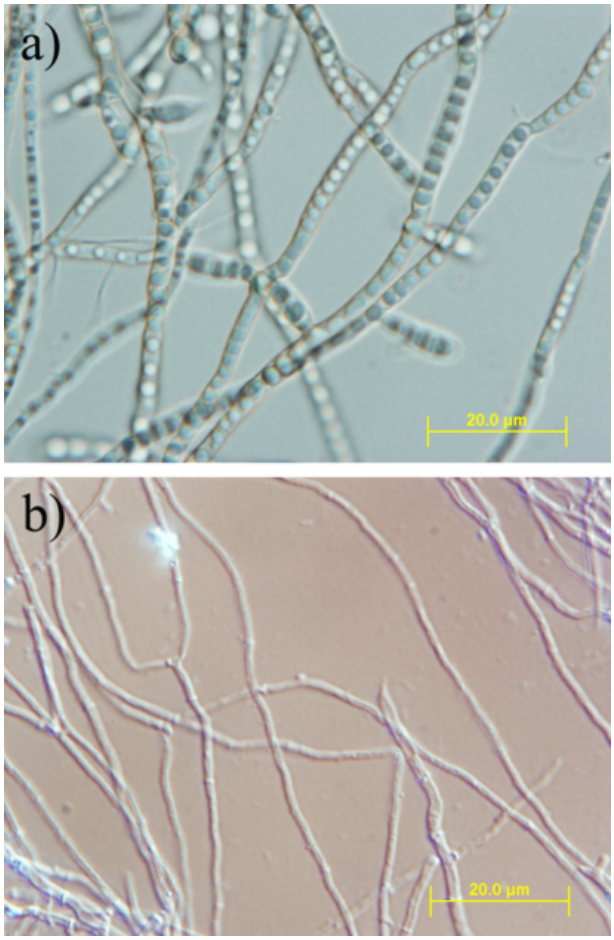

Figure 6.6, PVP fibers imaged directly in the solution phase under optical microscope. (a) Fibers which are formed at the early stage and later become the core (corresponding to Fig. 6.5b). The image shows that the fibers were initially formed as a result of the aggregation of PVP microspheres and appeared to be pearl-necklace-like chains. (b) Fibers formed at later stage and outgrown from the core. The outgrown fibers have a smoother surface, indicating that outgrowth occurs through the assembly of free PVP molecules in the solution onto the end of pearl-necklace-like chains, rather than through the continuous aggregation of PVP microspheres. Image reprinted with permission from ref. 310, Copyright 2010 American Chemical Society.

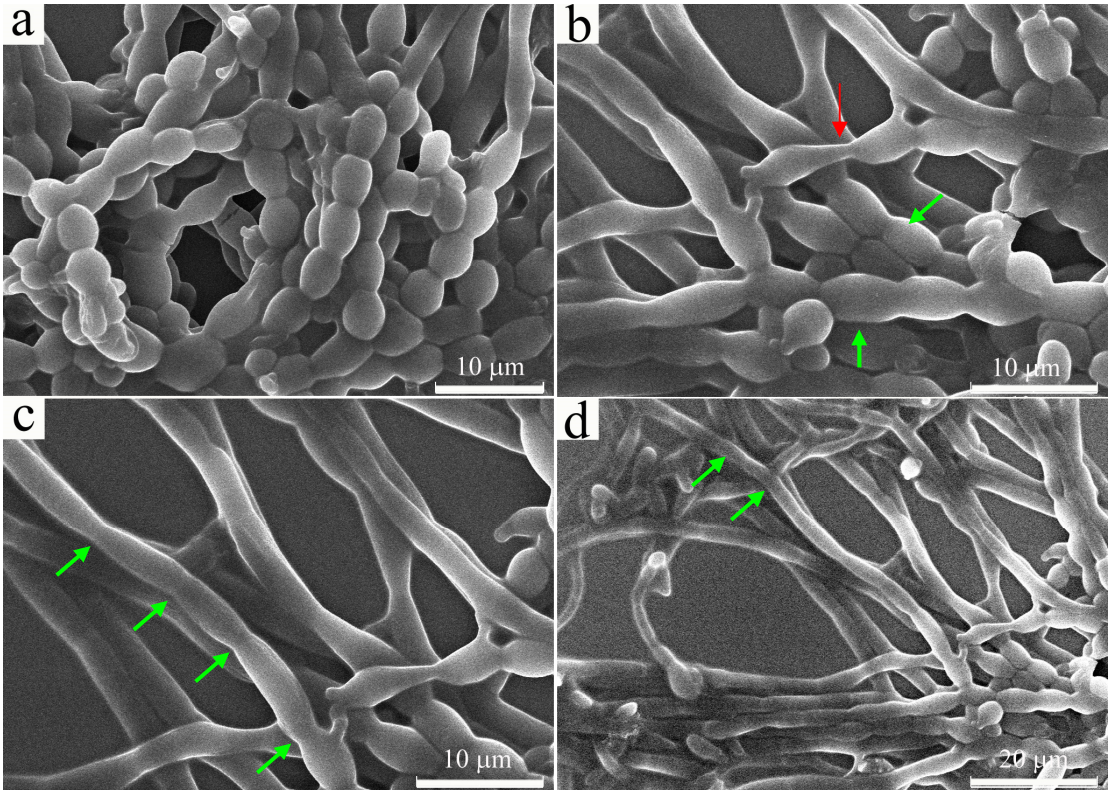

Figure 6.7, A continuous morphological transition of PVP microspheres at the end of pearl-necklace-like chains. (a) At the center of the chain (same image as Fig. 6.5b); (b) Slightly away from the center, spheres became ellipsoids (green arrows), red arrow shows an ellipsoid further elongating into rods; (c) further away, ellipsoids became rods, green arrows show the junction of each rods; (d) rods finally transited into smooth hollow fibers (green arrows) at even further distance from the central chains. (b-d) were imaged at the same fiber but different spots of interest. Image reprinted with permission from ref. 310, Copyright 2010 American Chemical Society.

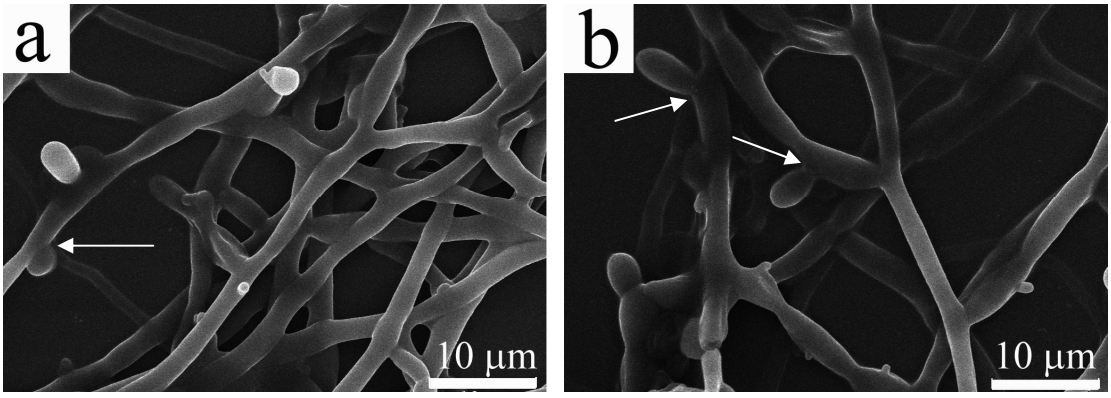

Figure 6.8, SEM images showing the early stage of branch formation. (a) A PVP microsphere highlighted by an arrow that has just settled onto the sidewall of a fiber and a PVP branch may grow from this microsphere; (b) Branches indicated by arrows that have grown longer. Image reprinted with permission from ref. 310, Copyright 2010 American Chemical Society.

The self-assembly behavior of PVP in the aqueous solution should be a general phenomenon, independent of their molecular weight. To prove this claim, we tried the same experiment with PVP of a higher molecular weight (40 kDa). Interestingly, same branched hollow structures were observed by SEM (Fig. 6.9). However, the average diameter had been increased from 2-3 μm to around 5 μm. Such increase is reasonable because polymers with an increased polymer chain length may lead to a larger dimension of self-assembled microspheres and the consequent larger diameter of the resultant long fibers grown on the basis of the microspheres.

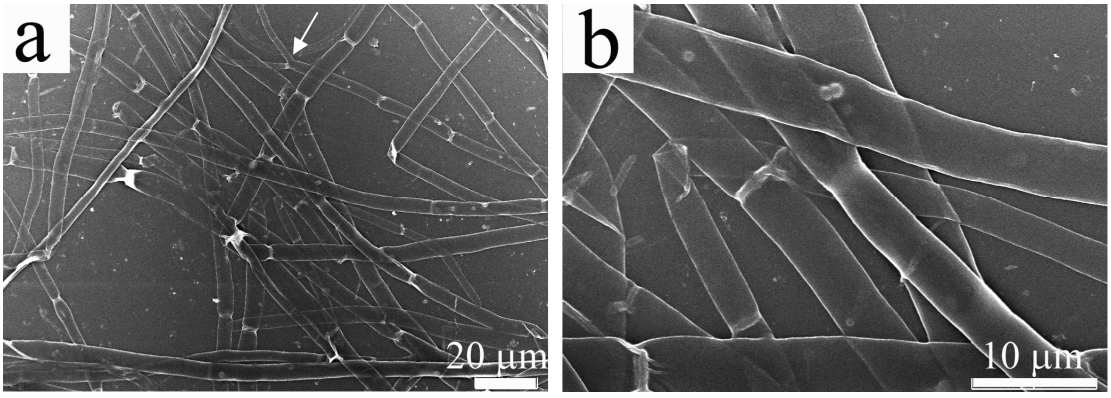

Figure 6.9, SEM images of fibers resulted from the self-assembly of PVP with a molecular weight of 40 kDa. Compared to PVP with a lower molecular weight (10 kDa), their average diameter had been increased from 2-3 μm to around 5 μm. (a) Low magnification; (b) Higher magnification. A branched structure is highlighted by an arrow in (a). It should be noted that the aggregate has been sonicated to get isolated fibers for imaging purpose and during this process the branches may be separated from the stems. Image reprinted with permission from ref. 310, Copyright 2010 American Chemical Society.

6.3.3 Silica Branched Hollow Fibers by Directly Templating the PVP Aggregate Structure

The formation of self-assembled branched hollow PVP fibers encouraged us to use them as a template to synthesize inorganic branched hollow fibers. Templating methods using chemical or biological templates have been actively used in the synthesis of various

nanomaterials, including nanowires,[254,255] nanotubes,[256-258] and hollow spheres,[259] and in the ordering of nanoparticles.[97] The idea is that a molecule or material with a high affinity to PVP, when added to the branched hollow PVP fiber networks in the suspension, should attach to the walls of networked PVP fibers and form a uniform coating layer, which will result in the replication of branched hollow fibrous PVP structure. Silica was chosen for this attempt for two reasons: first, silica is a biocompatible biomineral existing in many mineralized biological systems,[260] and thus the synthesis of branched hollow silica fibers may find application in biomedicine; second, silica is known to have strong hydrogen-bonding interaction with PVP[261] and silica formation on PVP coated nanoparticles has been demonstrated in the synthesis of core/shell nanoparticles[262] and core/sheath nanowires.[263]

The self-assembled fibrous PVP structure was stable, with no visible destruction of the jellyfish-like bulk structure, when transferred from pure aqueous to ethanol aqueous solution (see experimental section). After silica deposition on the hollow PVP fibers, the mechanical strength of self-assembled PVP structures was enhanced. This was evidenced by significantly reduced collapse of the structures upon drying on the mica substrate. Also, unlike pure PVP hollow fibers in the semitransparent film, silica-coated PVP fibers appeared as a large white aggregate on mica. As shown in Fig. 6.10a, large bundles of silica fibers were produced by using self-assembled branched PVP fibers as templates. In contrast to PVP fibers in Fig. 6.2, most silica fibers maintained their cylindrical morphology, which is consistent with the above observation that the silica-coated PVP

fibers had a much less structural collapse than the self-assembled pure PVP fibers when transferred from a solution phase to a solid substrate. The hollow character of PVP fibers was also duplicated by the silica fibers due to the formation of silica on the hollow PVP fiber surface (Fig. 6.10b). Our investigation on the growth mechanism of silica onto PVP fibers demonstrated that the silica coating was actually occurring simultaneously on both outer and inner walls of the PVP fibers, though the silica growth rate on the outside surface might be faster than on the inner surface as the diffusion of the precursor to the outside surface is easier. This was evidenced directly from the fact that when the concentration of the silica precursor (TEOS) was increased, solid fibers without hollow channels were observed, suggesting the complete occupation of silica in the hollow channels due to silica deposition on the inner wall of the PVP fibers.

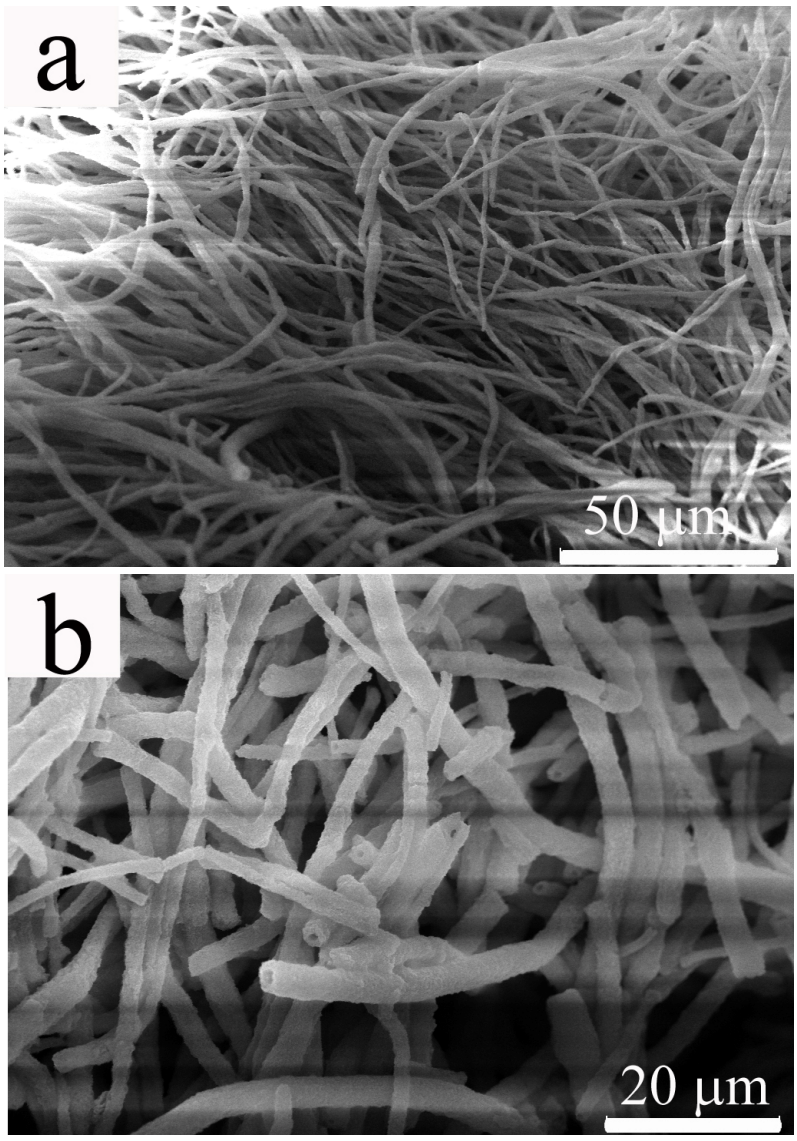

Figure 6.10 SEM images of silica fibers formed by silica deposition on the branched hollow PVP fibers shown in Fig.6.2. a) bundles of silica fibers; b) higher magnification showing that these fibers are hollow. The branched structures of individual fibers are not obvious due to the close packing of the branched fibers. Image reprinted with permission from ref. 310, Copyright 2010 American Chemical Society.

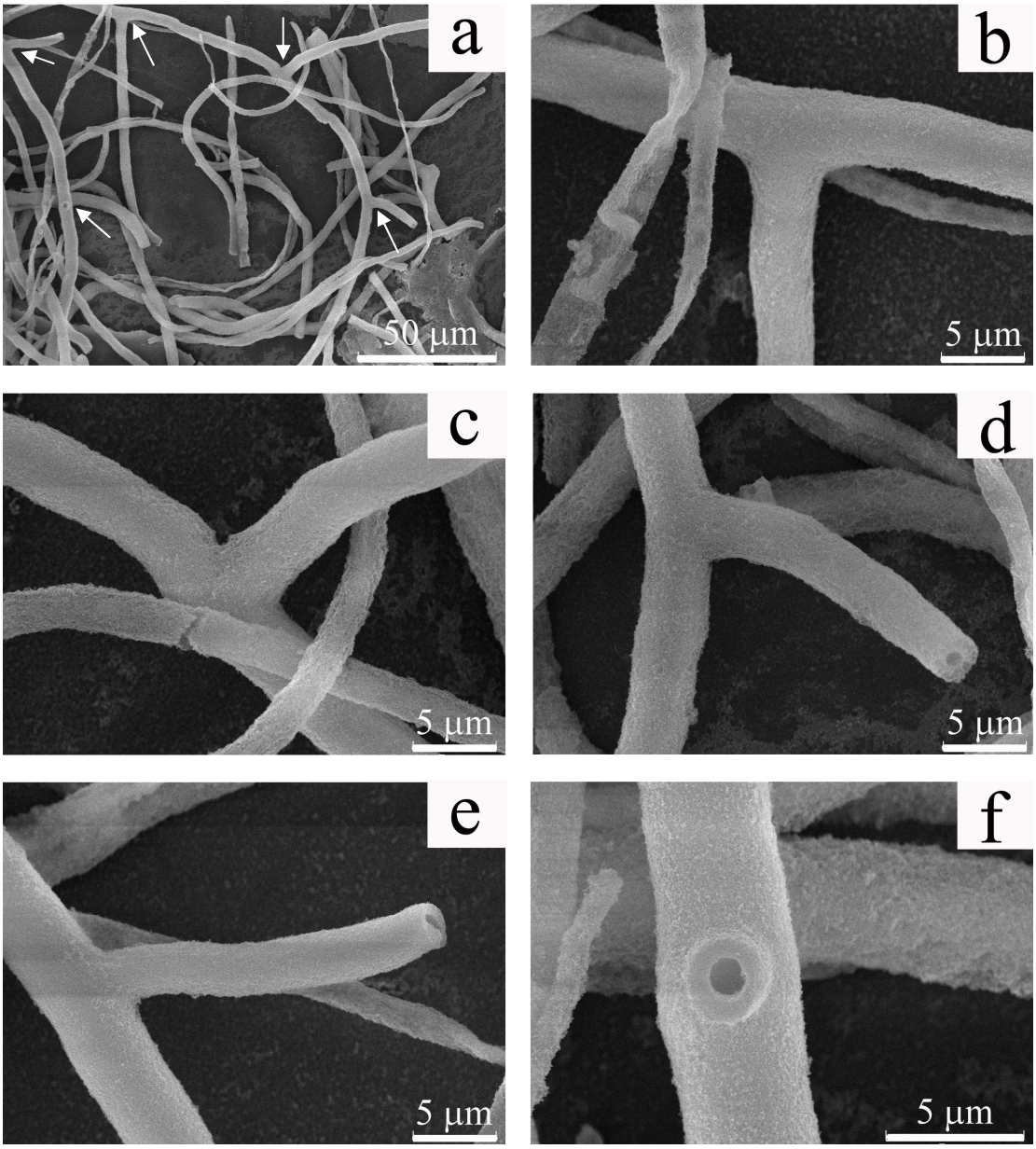

Figure 6.11, SEM images of individual silica fibers separated from the samples shown in Fig. 6.10 by sonication. a) low magnification image showing two branched fibers; b-d) higher magnification of three branches of the fiber in upper center of image shown in a; e, f) higher magnification of two branches of the fiber on the left side of image shown in a. Branches are indicated by arrows in image a. Image reprinted with permission from ref. 310, Copyright 2010 American Chemical Society.

The silica fibers in Fig.6.10 are closely packed, which prevents us from visualizing the actual branched structure easily. For this reason the silica coated PVP aggregate was treated with ultrasound in order to break up the bundles into individual fibers for verifying the branched structures of the silica fibers by SEM (see experimental section). It turned out that the branched nature was ubiquitous for long fibers. Fig. 6.11a showed a typical image of branched long silica fibers. A three-branched fiber and a two-branched one are highlighted by arrows in the image. The angles between branches and main fiber axes were not fixed, but almost exclusively fell into a range of 45°~ 90° (Figs. 6.11b-f). This is of dramatic difference from the branched polyaniline and carbon nanotubes, in which angles between the branches and stems were all less than 45°.[239,240] Non-branched fibers were also observed when the fibers were short, which indicates that they might be derived from the breaking of branched long fibers at the connection point between the branches and the stems. It should be noted that some non-fibrous silica products and flat fibers (Fig. 6.11b) also exist on the mica substrate but they are very uncommon. They might arise from the negative effect of ultrasound, which caused the detachment of silica from some fibers and further disassociation of the fibers into tiny particles.

6.3.4 Co-Assembly of PVP-Covered Gold Nanoparticles with Free PVP Molecules to Form Branched Hollow Fibers

Although direct templating of the preformed self-assembled fibrous PVP structures can produce nice branched hollow fibers, unlike silica, most materials do not have such

strong interaction with PVP in solution phase. For example, in an attempt to use the branched hollow PVP fibers as a template to form gold, $HAuCl_4$ was added to the PVP fibers and reduced with either sodium citrate or $NaBH_4$. However, no gold was formed on the inner or outer walls of the PVP fibers. In order to take advantage of the self-assembly of PVP and extend the use of the self-assembled PVP structures as a universal template for synthesizing branched hollow fibers, self-assembly of PVP-coated nanoparticles was adopted as an alternative. We hypothesize that PVP-coated nanoparticles, when dissolved in PVP solution, will co-assemble with the free PVP molecules to form branched hollow fibers with the nanoparticles embedded in the solid walls of the fibers. Generally, in the co-assembly of nanoparticles with PVP, the surface coat of the pre-synthesized nanoparticles (which could be any type of inorganic nanoparticles) was ligand replaced by PVP and the resultant PVP-coated nanoparticles were re-dispersed into a PVP aqueous solution (typically 5.7 wt. % in this work). Since PVP can self-assemble to form a network of nanofibers (Fig. 6.2), PVP on the surface of nanoparticles and the free PVP molecules in the solution will co-self-assemble to form branched fibers due to the inherent self-assembly behavior of this polymer.

Gold nanoparticles were used as a model to demonstrate the co-assembly process. The PVP-coated gold nanoparticles were prepared by following a reported procedure.[262] The self-assembled structure formed through the co-self-assembly of the PVP-coated gold nanoparticles and the free PVP in the solution was similar to that in the case of only PVP, but it was black (Fig. 6.1b) when in solution and golden in color when dried on

silicon wafer. As shown in Fig. 6.12, gold fibers were very similar to the PVP nanofibers shown in Fig. 6.2 in terms of hollow and branched character, indicating that they were formed under a similar self-assembly mechanism. The Energy Dispersive X-ray Spectrum (EDS) (Fig. 6.12d) showed an intensive peak corresponding to gold (The highest silicon peak was from the silicon wafer substrate; due to the limitation of X-ray detector used in our work, only elements beyond oxygen can be detected, so PVP was "invisible" under EDS).

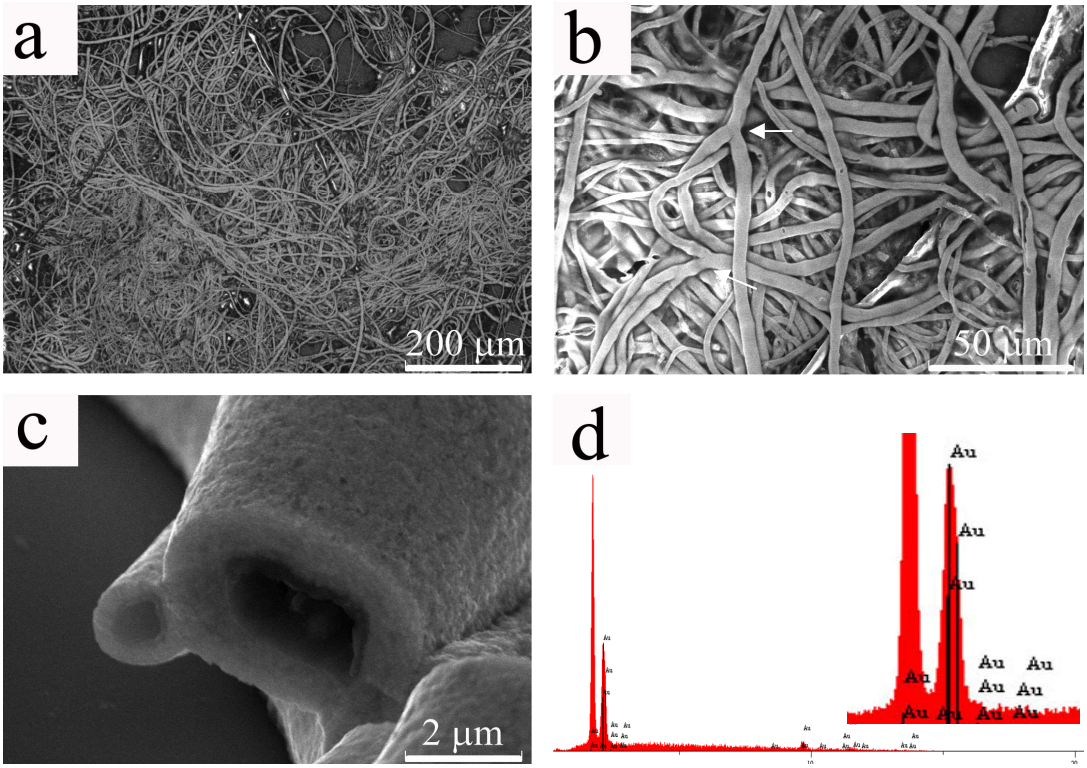

Figure 6.12, SEM images of hollow gold fibers formed throught the co-self-assembly of PVP-coated gold nanoparticles with free PVP in a solution. a) low magnification; b) higher magnification showing the branched nature of fibers (branches are indicated by arrows); c) higher magnification of the tip of the fibers showing that the fibers are hollow and have smooth cross section; d) EDS spectrum showing the existence of gold in the fibers (inset is an amplification of the gold peak, the highest peak is from silicon substrate). Image reprinted with permission from ref. 310, Copyright 2010 American Chemical Society.

We found that the original gold nanoparticles solution was wine red in color whereas the fibrous PVP-gold aggregate showed a black color (Fig. 6.2b). So we believe that the gold nanoparticles in the fibers are in close proximity, which will lead to strong plasmon

coupling between neighboring nanoparticles.[224] To further confirm this, we sonicated the PVP-gold aggregate for 15 min. After this treatment, the remained visible aggregate was discarded and a TEM sample was prepared from the solution containing fiber debris. As can be seen from Fig. 6.13a, the fibers are still composed of nano-sized gold particles. Therefore, the black color of the PVP-gold aggregates must have arisen from the close packing of nanoparticles. Further evidence could also be found directly from the end of a broken fiber where only a few layers of gold nanoparticles were left (Fig. 6.13b) and from debris that were stripped from the fiber sidewalls (Fig. 6.13c). In addition, when the concentration of gold nanoparticles was decreased by 5 times, we could only obtain a red-colored jelly-fish like PVP-gold aggregate, which was of the same color as the initial nanoparticle solution (Fig. 6.1c; Fig. 6.14). This fact is consistent with the explanation given above. Namely, a lower concentration of gold nanoparticles increased inter-particle spacing of gold nanoparticles in the PVP fibers, which further weakened or cancelled the plasmon coupling between nanoparticles.[129]

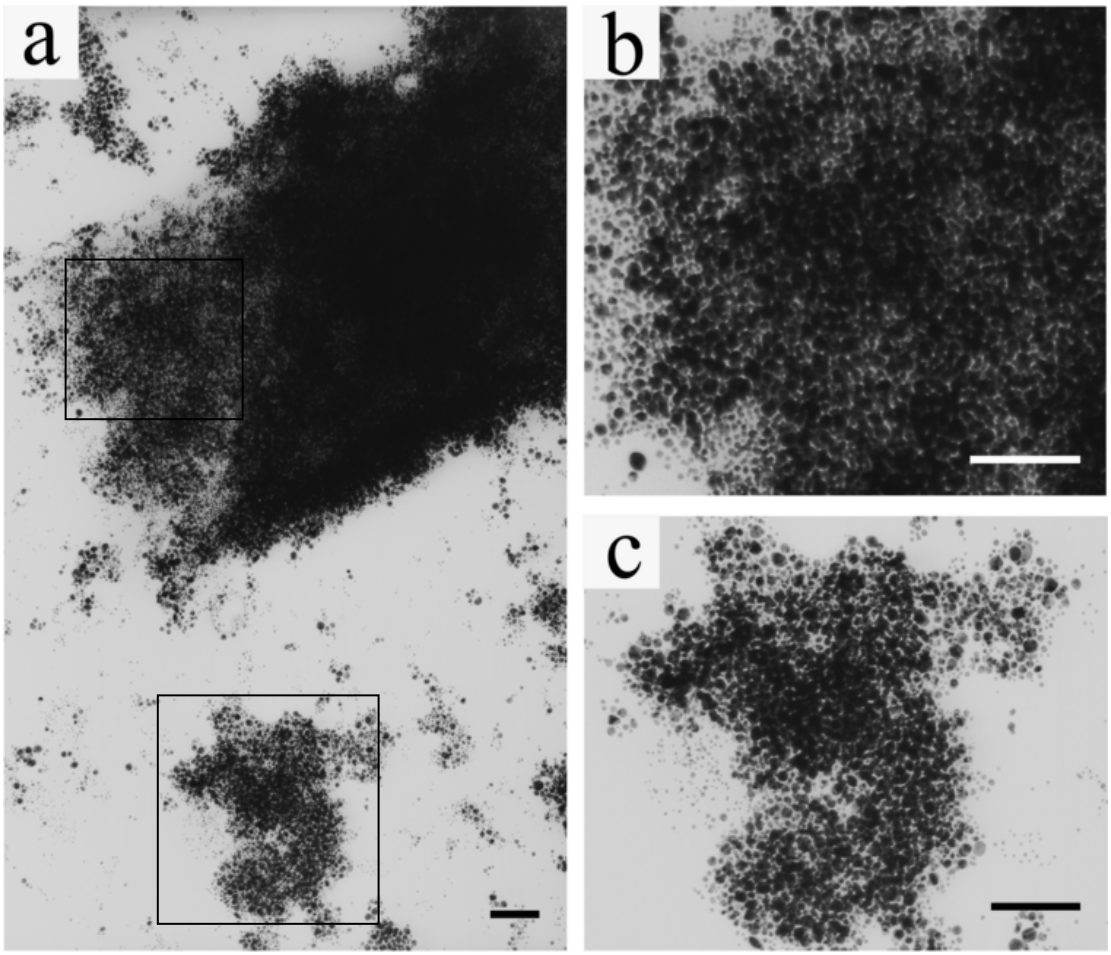

Figure 6.13, TEM images of debris of PVP-gold fibers after the fibers were sonicated for 15 min. a) The fibers were still composed of nano-sized gold particles, which were not fused into larger particles; b, c) Higher magnification showing dense packing of gold nanoparticles in the fibers highlighted by a square in top left and bottom, respectively. The gold aggregate shown in the bottom in (a) was detached from the PVP-gold fibers due to sonication. All scale bars are 200 nm. Image reprinted with permission from ref. 310, Copyright 2010 American Chemical Society.

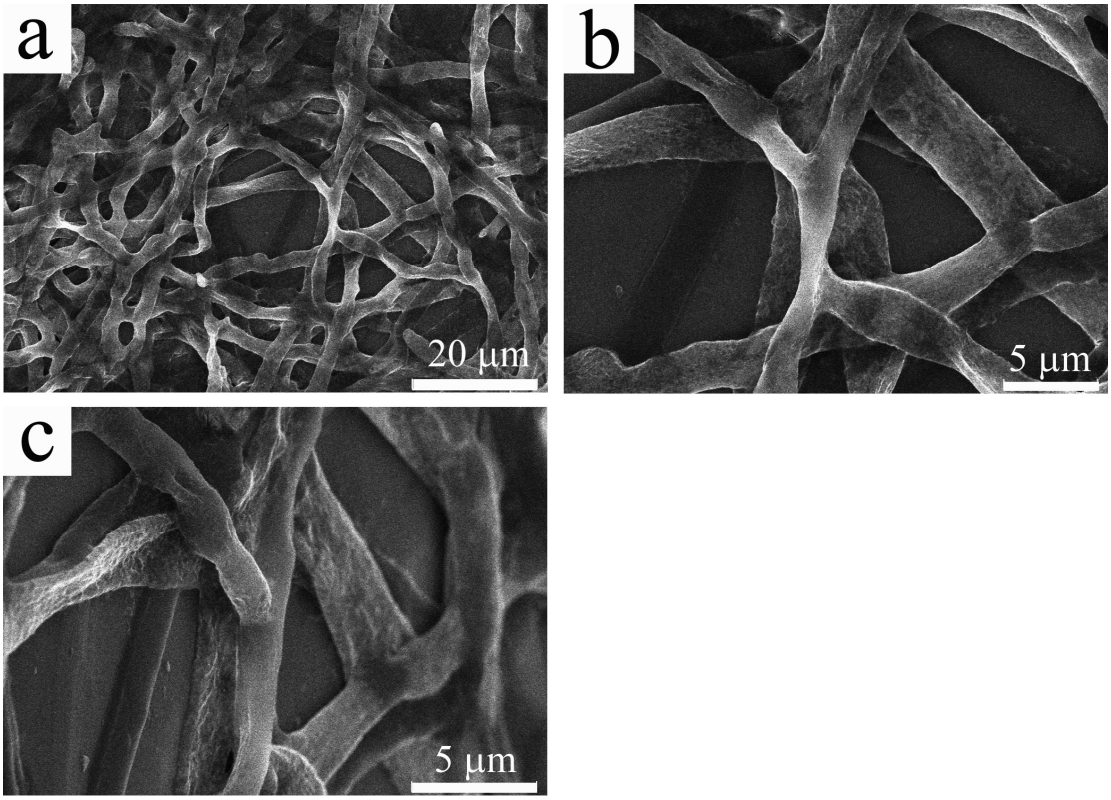

Figure 6.14, SEM images of PVP-gold fibers, co-assembled from the solution, in which the gold nanoparticles concentration was 5 times lower than that used in Fig. 6.12. (a) Low magnification view; (b) higher magnification view showing branches of the fibers; (c) A 60^{o} tilted view of b. Image reprinted with permission from ref. 310, Copyright 2010 American Chemical Society.

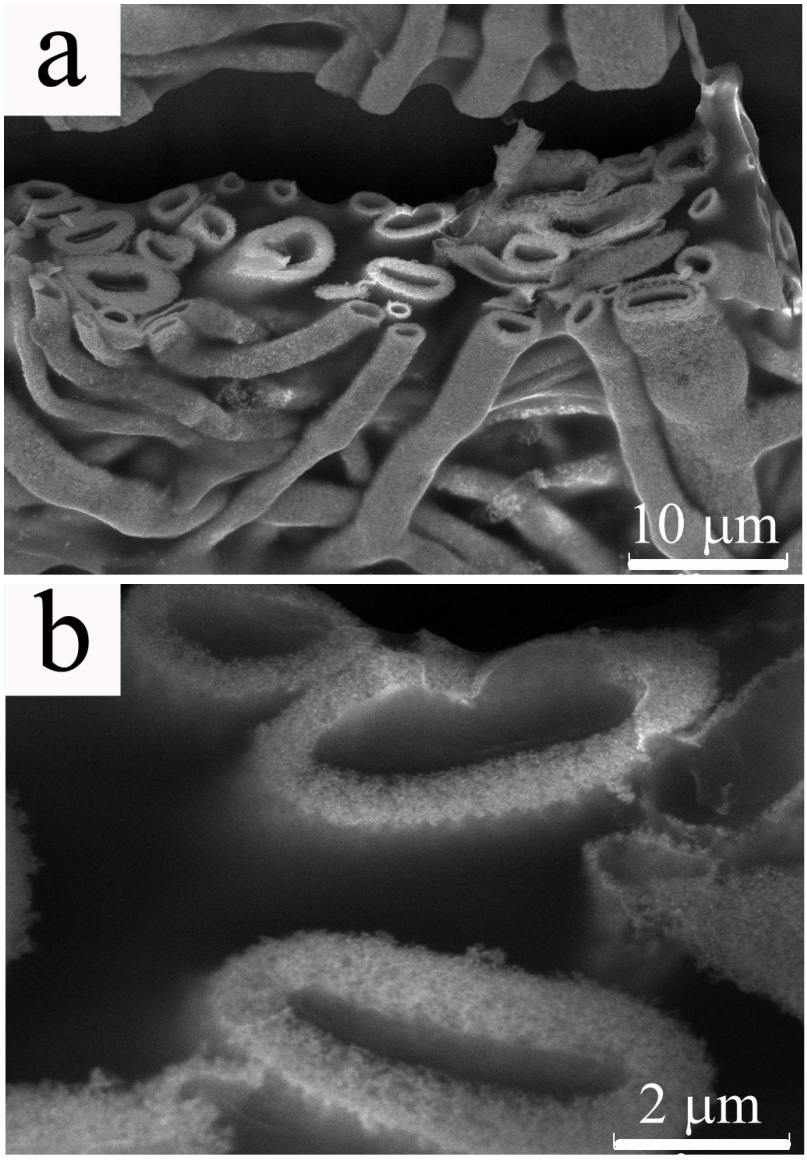

Figure 6.15, SEM images of gold fibers that have been treated in the oven at 220 ^{o}C for 24 h. a) fiber structure is not destroyed by heating upon the glass transition temperature of PVP; b) after PVP has been melted away, the cross sections of the fibers become porous. Image reprinted with permission from ref. 310, Copyright 2010 American Chemical Society.

To investigate whether gold can form a fibrous structure when PVP matrix was damaged, PVP-gold fibers shown in Fig. 6.12 were treated in an oven at 220 ^{o}C for 24 h, which was far above the glass transition temperature of the polymer. Under this condition, pure self-assembled fibrous PVP structure was found to be completely deformed into a continuous film without any fibrous character. A polymer film was also observed after heating the gold fibers, indicating that there was phase separation of melted PVP matrix from gold. Nevertheless, the main structure of gold fibers was intact. As shown in Fig. 6.15a, hollow character was maintained in almost all the fibers, although they were slightly collapsed from cylindrical into elliptical shape. A significant difference was seen at a higher magnification. Before heating, the gold-PVP fibers had a smooth cross section (Fig. 6.12c), which became porous after heating (Fig. 6.15b). Based on the above observations, it is reasonable to conclude that (1) PVP-coated nanoparticles co-assemble with PVP to form branched hollow fibers in the solution phase; (2) in the as-prepared gold fibers, gold nanoparticles had a very high density in the PVP matrix; and (3) upon heating above the glass transition temperature of PVP, PVP was gradually melted away, and meanwhile, gold nanoparticles are fused together to form porous fibers.

6.4 Conclusion

In summary, jellyfish-like self-assembled fibrous PVP structure was observed after a relative long-term aging of PVP solution under room temperature. By directly templating

the formation of silica on the self-assembled fibrous PVP structure, branched hollow silica fibers were synthesized for the first time. To demonstrate that PVP can be potentially employed as a universal template to prepare branched hollow fibers of various materials, branched hollow gold fibers were synthesized from PVP-coated gold nanoparticles through the synergistic self-assembly of PVP-coated gold nanoparticles and the free PVP molecules in the solution phase. The gold fibers were structurally stable when heated above the glass transition temperature of the polymer. The branched fibers produced in this work may serve as new templates for the synthesis of fibers or tubes of other materials.

CHAPTER 7

Oil Phase Evaporation Induced Self-Assembly of Hydrophobic Nanoparticles into Spherical Clusters with Controlled Surface Chemistry in an Oil-in-Water Dispersion and Comparison of Behaviors of Individual and Clustered Iron Oxide Nanoparticles

7.1 Introduction

The self-assembly of nanoparticles into hierarchical 2-D or 3-D structures has been extensively studied for potential applications in various fields.[206,264-267] The self-assembly behavior can take place both at the interfaces and *in situ*. Assembly at the interfaces of liquid-air and liquid-liquid often results in mono- or multi-layered nanostructures.[268-271] *In situ* aggregation results in the formation of nanoparticle clusters (NPCs) which are larger particles containing a finite number of nanoparticles.[26,272,273] In literature, the *in situ* assembly of nanoparticles has been almost exclusively induced by introducing specifically designed stimulating molecules into the nanoparticles suspension. For example, by adding dodecanethiol into oleylamine capped gold nanoparticles in cholorform, clusters of gold nanoparticles can be assembled due to their reduced stability after ligand exchange.[273] However, a particular type of stimulus may only be good for specific nanoparticles having certain surface ligands. Here we report a simple and general method of assembling hydrophobic nanoparticles into water-dispersed spherical NPCs. In this method, the formation of NPCs is achieved without adding any stimulating reagents

by selective evaporation of the organic phase in an oil-in-water micelle system. The surface chemistry of NPCs can be readily tuned by using different polymers. The method used here can also be extended to make NPCs containing multiple types of nanoparticles.

CTAB is a well-known surfactant and has been widely used in nanoscience. CTAB can aid in the synthesis of many types of nanoparticles with controlled morphologies.[48,136,274-276] One important application in nanoscience is its use as a phase transfer reagent. Many types of nanoparticles have been transferred from the organic to aqueous phase with the assistance of CTAB.[264,277-281] However, in all of these works, only individually dispersed nanoparticles could be obtained after the phase transfer process and no cluster structure has so far been reported under similar CTAB concentration. In this work, we found that if the concentration of nanoparticles is increased to a certain level within CTAB micelles, the NPCs can be formed via evaporation of the organic phase during the phase transfer process.

NPCs exhibit collective properties which individual nanoparticles do not have. Clusters of metallic nanoparticles that are rich in surface plasmon such as gold and silver can create Raman hotspots in between the closely spaced particles due to local electromagnetic coupling.[129,282] Such an effect results in an enhancement of Raman signals from analytes in orders of magnitude.[282-285] Unlike single superparamagnetic iron oxide nanoparticles which exhibit low magnetization and are thus difficult to manipulate with a magnet, NPCs have a much higher response to magnetic fields and are therefore better suited for drug delivery and separation.[286] In addition, clusters of superparamagnetic iron oxide nanoparticles have shown improved contrast enhancement

compared to individual nanoparticles in magnetic resonance imaging (MRI).[26,287-290] Various methods have been employed for synthesizing iron oxide NPCs for MRI applications. Generally, these methods fall into two categories. One type involves block copolymers, either bihydrophilic or amphiphilic.[288,291,292] The other category utilizes simultaneous cluster formation with a silica coating process.[26,289,290] In most of these reported works, a relatively low concentration of iron oxide nanoparticles was used for cluster formation which may prevent them from scalable production. The micelle system we have selected in this current work can result in a final NPCs concentration of 5 mg/ml in an aqueous phase, which is approximately 5 times higher than the highest reported concentrations from previous works.[287,289,290] In addition, the density of iron oxide nanoparticles inside the cluster is much higher than reported values.

7.2 Experimental Methods

7.2.1 Synthesis of Oil Dispersed Fe_3O_4, CdS and Au Nanoparticles

Fe_3O_4 nanoparticles were synthesized and purified following the procedure done by Sun et al.[293] Nanoparticles of 3 nm and 6 nm in diameter could be obtained directly by controlling the solvent and reaction temperature. Larger Fe_3O_4 nanoparticles (12 nm and 15 nm in diameter) were produced by seeded growth based on the 6 nm nanoparticles. Nanoparticles derived from 2 mmol iron acetylacetonate were redispersed into hexane at a concentration of 20 mg/ml where the concentration of the nanoparticles used for NPC

formation could be diluted or re-concentrated from the stock solution.

CdS nanoparticles were synthesized following the reported method in literature with slight modifications.[294] A mixture of cadmium chloride (91.66 mg, 0.5 mM) and oleylamine (5 ml) was heated to 150 ^{o}C under N_2 flow. When $CdCl_2$ was completely dissolved (in about 20 min), 0.5 mM elemental sulfur dissolved in 2.5 ml of oleylamine was quickly added into the hot solution. The reaction was maintained at 150 ^{o}C for an additional 8 hours. Next, it was quenched by quickly adding 15 ml of toluene. Nanoparticles were purified by washing three times with ethanol. Finally, they were suspended into 2 ml of hexane and used for NPCs formation.

Au nanoparticles were synthesized by mixing 100 μl 0.1 M $HAuCl_4$ with 5 ml oleylamine and heated at 150 ^{o}C for about 25 min. The nanoparticles were then washed twice with ethanol and finally dispersed into 0.2 ml hexane.

7.2.2 Synthesis of NPCs Using CTAB as an Emulsifier

A small volume of hexane-dispersed nanoparticles (200 μl, concentration varies from 1-100 mg/ml) was added to 4 ml of 0.1 M CTAB aqueous solution. All of the liquid was then gently mixed by hand shaking followed by sonication for 2 min to form a stable micelle suspension. Afterwards, the mixture was heated in a 80 ^{o}C water bath and stirred at 500 rpm for 5 min to have the majority of the hexane evaporated. Alternatively, hexane evaporation can be done by stirring under the ambient condition for several hours. The solution was then removed from the heat and stirred under a vacuum for 30 min to

completely remove the hexane. In the preparation of Au-CdS hybrid NPCs, 50 μl AuNPs was mixed with 150 μl CdS nanoparticles and sonicated before being added to the CTAB solution.

7.2.3 Synthesis of NPCs Using Polymers as Stabilizers

A volume of 200 μl of hexane-dispersed iron oxide nanoparticles (2 mg/ml) was added to 4 ml of 12 wt% polymer solution. The mixture was then sonicated continuously for 2 h. The water bath of the sonicator was initially set at 40 ^{o}C, however, the temperature was increased to around 70 ^{o}C after 1 h due to the heating effect of ultrasound. After sonication, the solution was also treated by vacuum for 30 min. The molecular weights of the polymers used are as follows: polyacrylic acid (PAA, 15 k, sodium salt, 35 wt%), polyethyleneimine (PEI, 25 k, branched) and poly(styrenesulfonate) (PSS, 70 k).

7.2.4 Silica Coating of CTAB Stabilized Fe_3O_4 NPCs

The process of coating NPCs with silica was modified from the method described in literature.[295] Generally, the as-prepared CTAB covered NPCs (1 ml) were centrifuged at 15,000 rpm for 20 min, and redispersed into 4 ml of 0.02 M CTAB aqueous solution. The pH of the solution was adjusted to around 11 by 0.1 M NaOH. Finally, tetraethyl orthosilicate (TEOS, 20 μl) was added and the resultant solution was stirred for 24 h for complete hydrolysis and condensation of TEOS.

7.2.5 Preparation of Aqueous Individually Dispersed NPs

The hexane-dispersed 6 nm iron oxide NPs were resuspended into toluene at a concentration of 10 mg/ml. In a three-neck flask, 500 mg of polyvinylpyrrolidone (PVP, 10 K) was dissolved into 8 ml of DMSO, followed by adding 2 ml of toluene-dispersed NPs. A homogeneous clear solution could then be obtained. This solution was then heated, under N_2 flow, to 189 ^oC at a temperature increase rate of about 4 ^oC/min. The temperature was remained at 189 ^oC for another 30 min, and then cooled to room temperature. The resulting transparent solution was then dialyzed against water (cutoff of the dialysis membrane, 5 kDa) for 24 h, after which aqueous individually dispersed, PVP-stabilized iron oxide NPs could be obtained. Silica-coated individual NPs were prepared by NH_4OH catalyzed hydrolysis of TEOS in an ethanol/water mixed solvent (4:1 v/v).

7.2.6 Characterization

The size and morphology of as-prepared NPCs were characterized by Transmission Electron Microscope (TEM). All the TEM images were obtained on JEOL 2000FX microscope, operated at an accelerating voltage of 200 kV. The surface morphology of NPCs was examined on a Nano-R2 Atomic Force Microscope (AFM) by Pacific Nanotechnology. The magnetic properties of individual and clustered NPs were measured on a Quantum Designs MPMS2 cryogenic susceptometer. The T2-weighted MR images

were obtained on a Bruker Biospec 7.0 T, 30 cm horizontal-bore imaging spectrometer.

7.3 Results and Discussions

7.3.1 Synthesis of NPCs in CTAB Emulsion

The experimental design is shown in Scheme 7.1. The idea of making NPCs was inspired by the concept of emulsion in which two immiscible liquids can coexist as a stable dispersion under the assistance of an emulsifier or surfactant in the form of micelles, either oil-in-water (used in this work) or water-in-oil. Oil will appear as tiny droplet suspended in bulk water. In oil-in-water emulsion, the surfactant molecules (CTAB in this work) will line up at the oil/water interface to reduce the surface tension of the tiny oil droplets which would otherwise assemble themselves into large drops.[296] If there are NPs initially dispersed in the bulk oil phase, they will remain inside the oil droplet after emulsification due to their hydrophobic nature. Due to its low boiling point, the oil phase can be removed by evaporation, leading to the condensation of NPs inside the micelles. When oil is completely evaporated, NPs inside each micelle will form a larger cluster. However, the NPs within the cluster will not be fused because the long carbon chains on the NPs surface give rise to a steric barrier that effectively leaves each particle isolated.[271] The surface of the resultant clusters is fully covered by surfactant molecules, with the charged head groups in direct contact with water and the tails interacting with the long carbon chains of NPs in the outer layer (this statement will be

validated by the water compatibility and surface charge of NPCs in the next paragraph), similar to the interaction involved when using surfactant to transfer hydrophobic nanoparticles into individual dispersions in water.[281] In this manner, the NPCs are prevented from aggregation and precipitation in the same way as stabilization of individual NPs in aqueous solution.

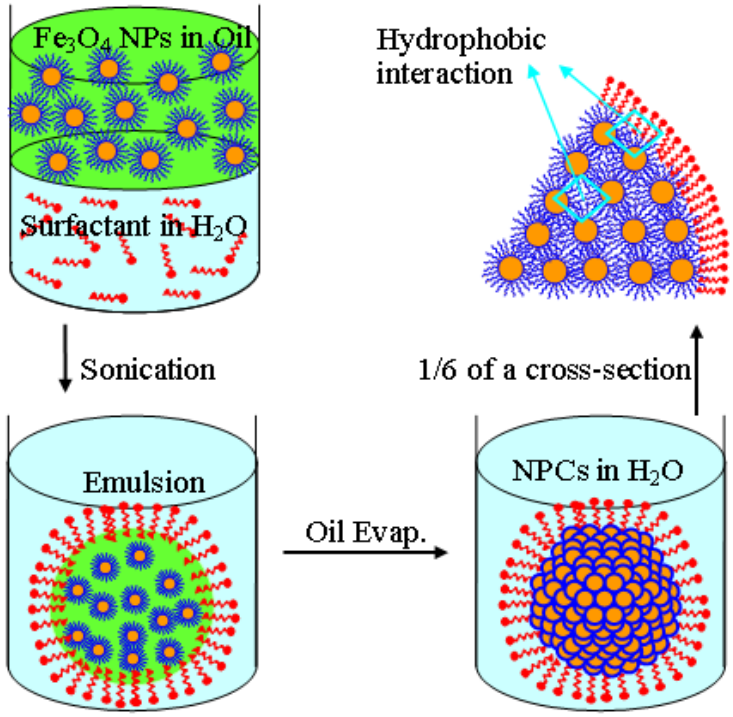

Scheme 7.1, Schematic diagram of the formation of NPCs. Image reprinted with permission from ref. 204, Copyright 2010 American Chemical Society.

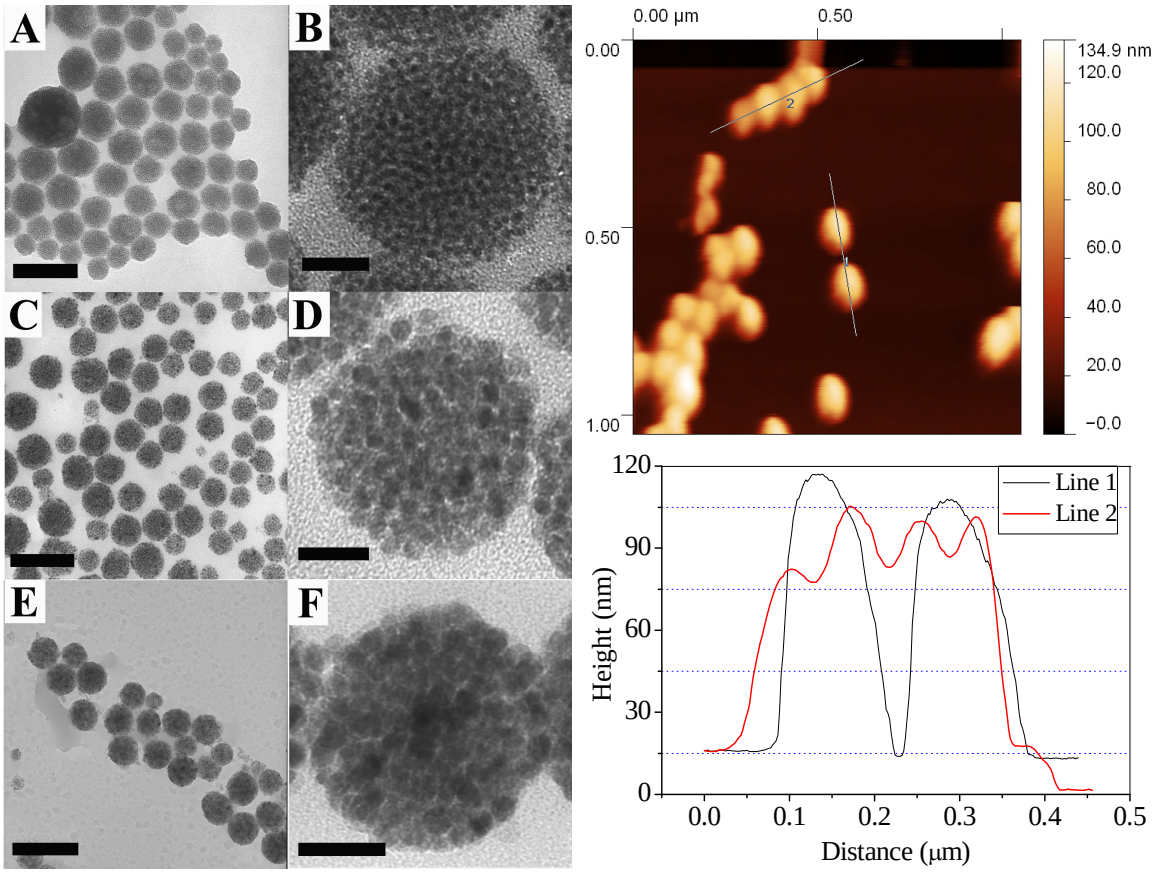

Figure 7.1, Left: (A-F) TEM images of low and high magnification of iron oxide NPCs using CTAB as an emulsifier. The initial sizes of nanoparticles in the organic phase were: (A, B) 3 nm, (C, D) 6 nm, and (E, F) 12 nm respectively. Scale bars: A, C, 150 nm; B, D 20 nm; E, 300 nm; F, 40 nm. Right: top: AFM image of NPCs made from 6 nm iron oxide NPs; bottom: extracted height information from two isolated clusters (line 1) and four contacting clusters in a row (line 2). The TEM images along with AFM characterization indicate that the NPCs were spheres composed of densely packed individual nanoparticles. Image reprinted with permission from ref. 204, Copyright 2010 American Chemical Society.

NPCs made from Fe_3O_4 NPs with an initial individual particle size of 3 nm, 6 nm and 12 nm respectively are shown in Fig. 7.1. The morphology of NPCs was studied by the atomic force microscope (AFM). As it can be seen from the TEM images in Fig.7.1, the individual NPs could be differentiated clearly inside the clusters and no fusion is observed in any of the three different sized NPs. The line profile obtained from AFM contains the height information which has been widely used to study the surface morphology of materials. We collected line profiles across two isolated clusters as well as four contacting clusters in a row. In both cases, smooth curves typically for spherical particles were observed (Fig. 7.1 right). The NPCs obtained in the CTAB-mediated emulsion could be suspended very stably in water, and no aggregation between NPCs was observed once they were centrifuged and resuspended into water. Considering the hydrophobic nature of NPCs, their high water compatibility should originate from the surface protection of the CTAB molecules, which is the only hydrophilic species in the solution. Moreover, the NPCs have a zeta potential of +49 mV, which provides further evidence that the NPCs are stabilized by CTAB, the only positively charged species in the solution. It should be pointed out that although previous micelles created by diblock copolymers were used to make NPCs, the structure reported here is much more closely packed and thus, has a much higher nanoparticle density.

The number density of NPs in the organic phase which is defined as the number of nanoparticles in a unit volume of solution is very important for the formation of NPCs as well as the morphology of clusters. For iron oxide NPs with 6 nm diameter, the NPCs

could hardly be seen at a concentration of 1 mg/ml. When the concentration was increased to 4 mg/ml, about 80% of NPs, which was estimated from the darkness of the supernatant after centrifuge, were in the form of clusters. Morphologically, however, the clusters contained both spheres and large film-like multilayered structures (Fig. 7.2a). At the concentration of 20 mg/ml, more than 98% of NPs existed as spherical clusters after the phase transfer process (Fig. 7.2b). In contrast, for 20 mg/ml of 15 nm NPs, where the number density was calculated to be 16 times less than that of 6 nm NPs under the same mass concentration, only a small portion were seen to be clusters (Fig. 7.2c). Therefore, in order to form NPCs during the phase transfer, the number density of NPs in the oil phase has to reach a certain high level which is dependent on the size of the NPs. However, in previously reported works where CTAB was used as the phase transfer reagent, relatively low concentrations of hydrophobic NPs were used. This provides an explanation as to why no clusters of NPs were obtained previously even though the experiments were carried out through a similar method as used in this work.

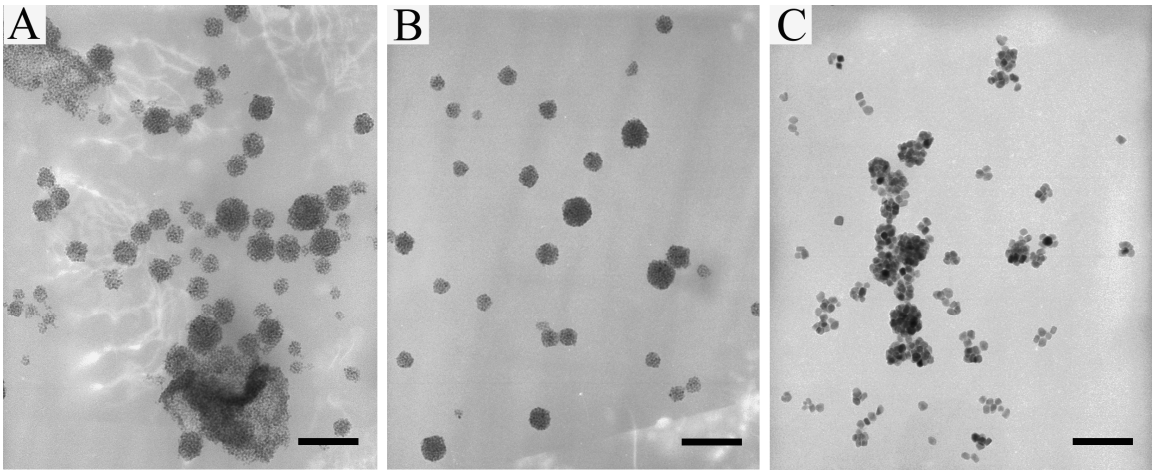

Figure 7.2, Dependence of NPCs yield and morphology on the number density of NPs dispersed in the oil phase. (A) NPCs made from 6 nm NPs at 4 mg/ml, more than 80% were clusters, however, non-spherical assembly was also observed; (B) NPCs made from 6 nm iron oxide NPs at 20 mg/ml, all spherical with more than 98% yield; (C) NPCs made from 15 nm NPs at 20 mg/ml, which is calculated to have about 16 times lower number density than that of 6 nm NPs. NPCs were produced at a very low yield with many individual NPs. Scale bars: 100 nm. Image reprinted with permission from ref. 204, Copyright 2010 American Chemical Society.

7.3.2 Size Selection, Scalable Production and Silica Coating of NPCs

The resultant spherical NPCs obtained through selective phase evaporation were widely distributed from several nm up to 150 nm in diameter. However, the size distribution of NPCs can be narrowed by using differential centrifugation in a pure water medium. Clusters assembled from 3 nm Fe_3O_4 NPs were given here as a demonstration. In the first centrifugation run at 10,000 rpm for 5 min, NPCs larger than 50 nm could

generally be separated (Figs. 7.3a&b) and the average diameter of this fraction was 78 nm. Smaller clusters could then be spun down from the supernatant of the first centrifugation run at 15,000 rpm for 20 min, resulting in a fraction of NPCs with an average diameter of 33 nm (Figs. 7.3c&d). A very small portion of even smaller NPCs remained in the supernatant and could not be spun down. The size of nanoparticles has been one of the greater concerns for *in vivo* applications. The exclusion and capture of nanoparticles by organs have a great impact on their circulation in the blood. Nanoparticles that are smaller than 10 nm will be filtered by the kidney. In addition, they will be captured by the liver, if they are larger than 100 nm. Thus, the optimum nanoparticle size required is 10-100 nm for *in vivo* applications.[297-299] The NPCs should be suitable for *in vivo* applications after the size selection procedures. We believe that the size distribution of NPCs could be further narrowed down by using a density gradient centrifugation.[197,198]

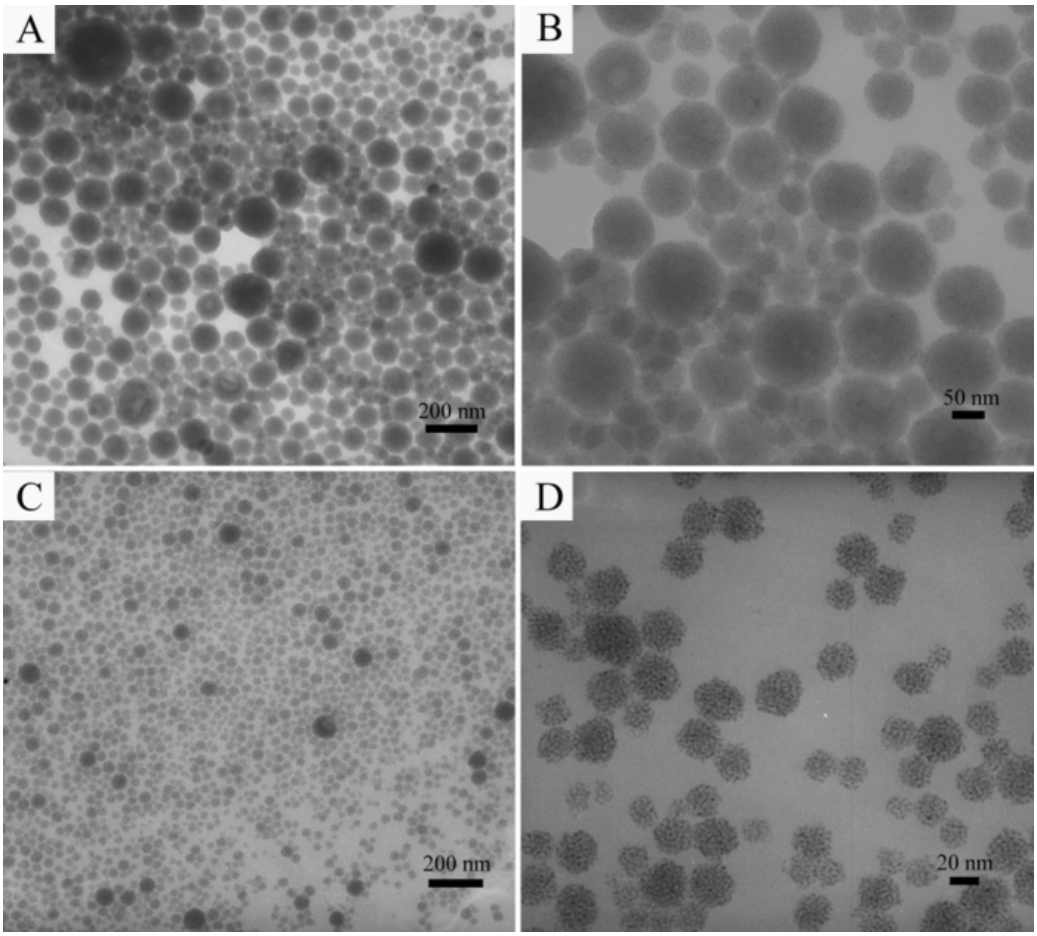

Figure 7.3, Size selection of Fe_3O_4 NPCs by differential centrifuge. (A, B), low and high magnification TEM images of NPCs made from 3 nm NPs, showing that NPCs larger than 50 nm can be collected in the first centrifuge run at 10,000 rpm for 5 min; (C, D), low and high magnification TEM images of NPCs showing that smaller ones will be spun down in the second round centrifuge at 15,000 rpm for 20 min. Image reprinted with permission from ref. 204, Copyright 2010 American Chemical Society.

Mass production of hierarchical nanostructures of interest has always been a challenge in nanoparticles assembly. Most often, the assembly suffers from either low

yields or poor reproducibility. In this work, the potential for a scalable production of NPCs via the CTAB-based emulsion method was investigated. We kept the volume ratio of hexane to water at a constant value of 0.2 ml over 4 ml but changed the concentration of nanoparticles in the oil phase. Several different concentrations (between 20 to 100 mg/ml) of 3 nm iron oxide NPs were tried. In all of these trials, NPCs were produced in a nearly 100% yield indicated by the supernatants being almost colorless after centrifugation at 15000 rpm. A TEM study showed that all of the clusters were composed of closely-packed nanoparticles where no coagulation was observed. Also, there was not a significant increase of cluster size even at a higher initial concentration. When the total volume was expanded by 10 times (100 mg/ml iron oxide NPs in 2 ml hexane and 40 ml water), we generally did not observe any remarkable difference in the NPC size distribution and morphology compared to clusters formed in the 4 ml water system. It should be noted that in current literature, relatively low concentrations of iron oxide NPs were used to synthesize NPCs. Mostly, the initial concentration of NPs in the organic phase was below 10 mg/ml while the final concentration of NPCs in the aqueous phase was less than 1 mg/ml.[290] The initial and final concentrations can reach up to 100 and 5 mg/ml respectively in the current work, which makes it more promising for the scalable production of NPCs.

The as-prepared NPCs were very stable for further surface modification. Polyelectrolyte wrapping through electrostatic interactions has been one method for manipulating the surface charge of nanoparticles.[300,301] The CTAB capped NPCs can be

wrapped with multiple layers of polyelectrolytes without destroying their cluster structure. Moreover, silica can be coated uniformly around the NPCs in a basic solution (Fig. 7.4). The NPCs/silica core/shell structure enables greater functionality on the particles by the well-developed silica modification chemistry.[302,303] For example, fluorescent dyes have been linked onto silica through covalent bonding between amine groups from 3-aminopropyltriethoxysilane (APTES) and isothiocyanate or succinimidyl-ester groups on the dyes; the dye-silica-magnetic NP complex particles can be used as dual probes for both fluorescent imaging and MRI. [304,305]

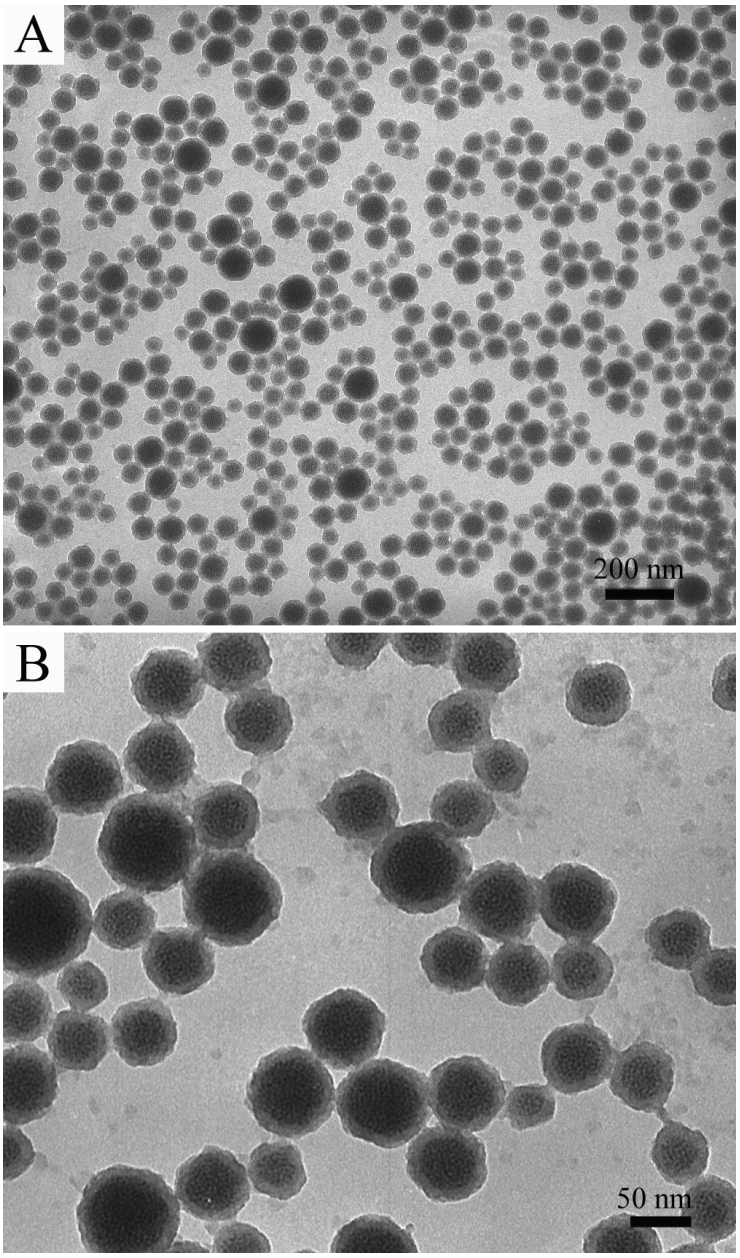

Figure 7.4, Silica coating of 3 nm iron oxide NPCs derived from CTAB as surfactant. No size selection was applied to the NPCs before silica coating. Image reprinted with permission from ref. 204, Copyright 2010 American Chemical Society.

7.3.3 Generality of the Method

The method we developed here can readily be applied to produce NPCs of varying

materials from their hydrophobic nanoparticles. As representatives of semiconductive and metallic materials, CdS and gold NPCs are prepared in CTAB micelles through the same procedures as making NPCs of magnetic particles. In order to explore the potential of preparing multiple-component particles by our method, hydrophobic CdS and Au NPs were first mixed together in hexane followed by selective phase evaporation in CTAB micelles. In all three types of NPCs, a spherical morphology and dense packing of NPs, similar to those of Fe_3O_4 NPCs, were observed (Figs. 7.5, 7.6 & 7.7). The fluorescent property of CdS nanoparticles was retained after the formation of clusters. The size distribution of CdS NPCs could also be narrowed by the differential centrifugation (Fig. 7.5). The absorption spectrum of gold NPCs was red shifted compared to that of the individually dispersed AuNPs (Fig. 7.6).

For CdS and many other semiconductor nanocrystals, the size-dependent fluorescence due to a quantum confinement effect can only be observed when the size of the particles is smaller than the exciton Bohr radius[306], which is the characteristic distance between the electrons and the holes in a bulk semiconductor material (e.g., below 10 nm for commonly used CdSe nanocrystals). However, *in vivo* imaging and diagnostics prefers NPs of larger sizes (10-100 nm).[297,299] For instance, blood vessels in tumor tissue are leakier and have larger pores than those in normal tissue. A larger particle can be selectively delivered to tumor tissue for therapeutic or diagnosis purposes due to enhanced permeability and retention (EPR) effect.[299] Therefore, it is difficult to obtain semiconductor NPs having both fluorescence and a desired size for *in vivo*

applications simultaneously. NPC structure provides a means for increasing the particle size, while still retaining the fluorescence capability that only belongs to smaller nanoparticles. Forming NPCs from NPs could potentially be a better solution than surface modifications of NPs, which only slightly increases the particle size, as a means for solving the size-fluorescence paradox of semiconductor nanocrystals. The red shift in the absorption spectrum of Au NPCs is contributed by the surface plasmon coupling of adjacent NPs inside the clusters. Such a coupling effect can be used for enhancing the signal intensity of analytes in surface enhanced Raman scattering (SERS) detection. The composite clusters that contain more than one type of nanoparticles have more functionalities, and thus can be used for multiple purposes. For example, Fe_3O_4 and CdSe nanoparticles were successfully embedded into a silica particle, which makes it possess both magnetic and fluorescent properties that could be potentially employed in MRI and fluorescent imaging.[307,308]

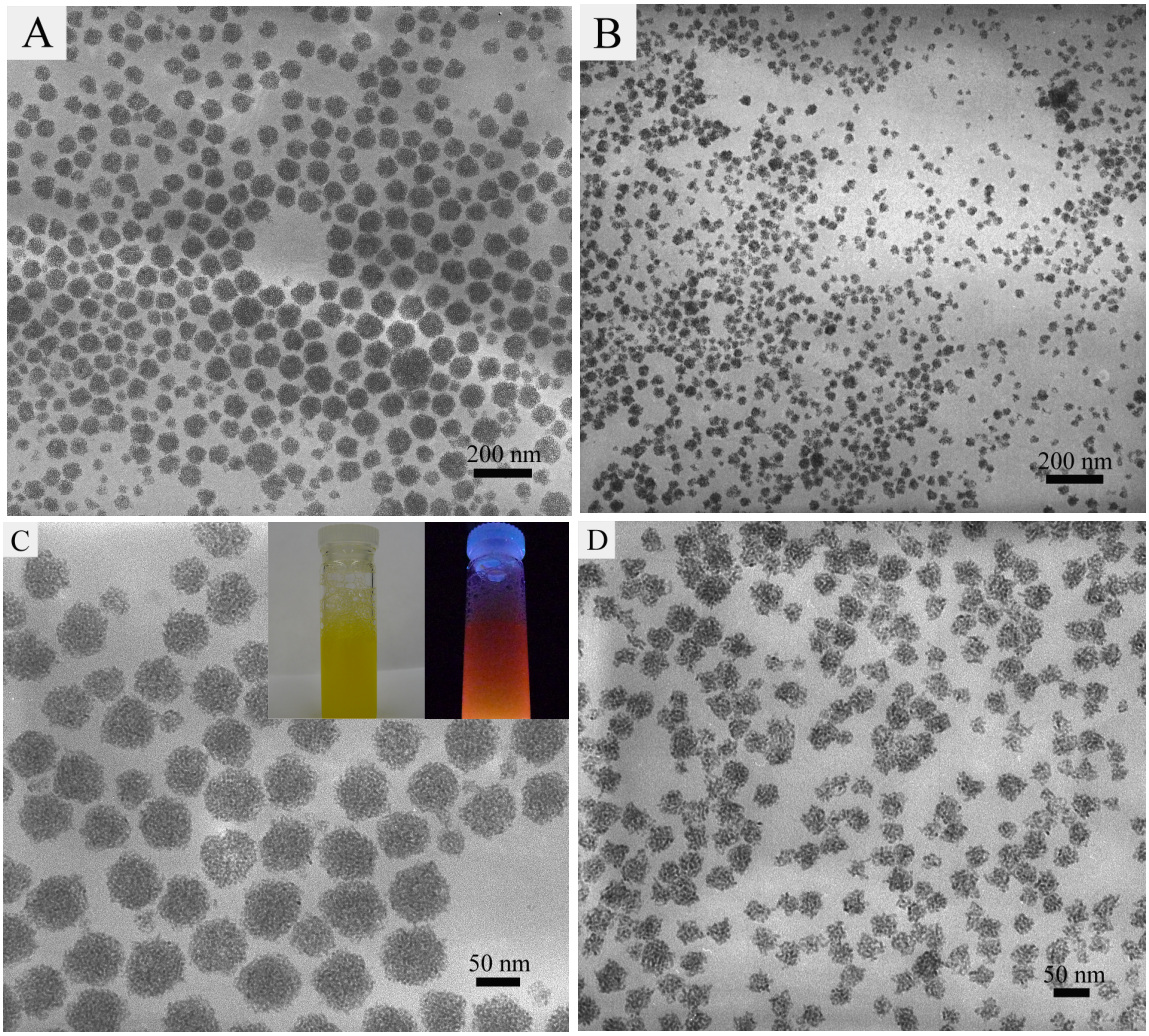

Figure 7.5, CdS NPCs can be prepared in the same way from hexane dispersed 3 nm CdS NPs. TEM images show size selection of CdS NPCs by differential centrifuge. (A, C) and (B, D) are corresponding to low and high magnification of NPCs from the first centrifuge run at 10,000 rpm for 5min and the second run at 15,000 rpm for 20 min respectively. Photograph shows fluorescence of CdS NPCs in C. Image reprinted with permission from ref. 204, Copyright 2010 American Chemical Society.

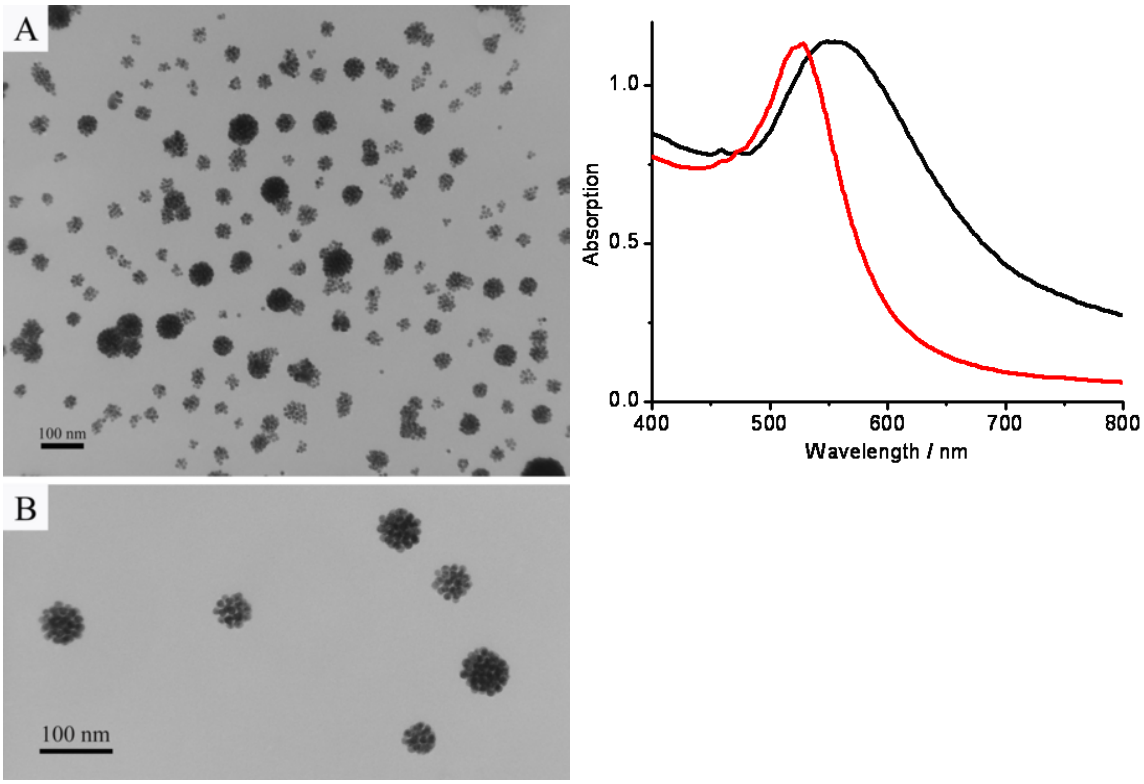

Figure 7.6, Gold NPCs: (A, B) low and high magnification of TEM images; (C) UV-Vis spectrum of individual AuNPs (red line) and Au NPCs (black line) indicating the coupling of surface plasmon upon the formation of clusters. Image reprinted with permission from ref. 204, Copyright 2010 American Chemical Society.

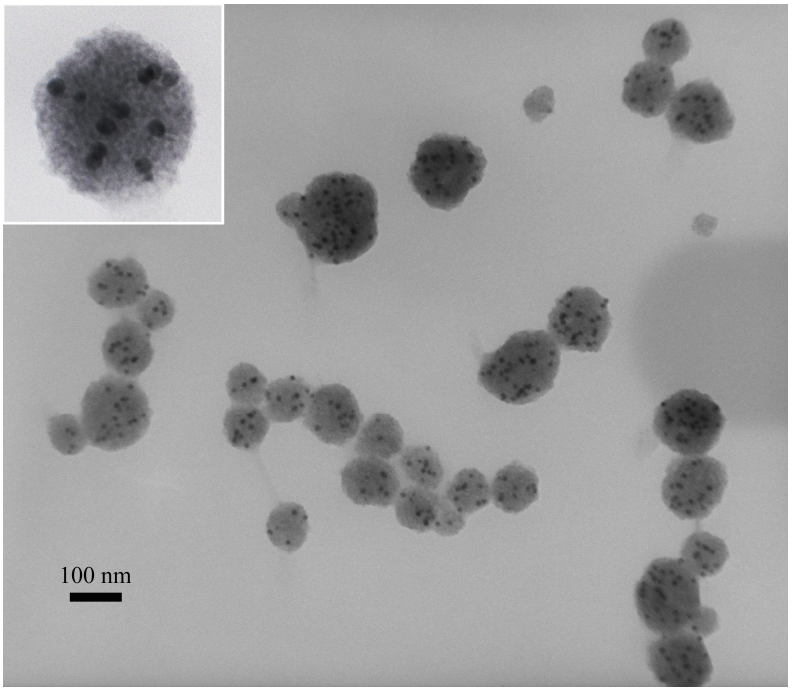

Figure 7.7, Hybrid NPCs containing both AuNPs (black spots) and CdS NPs (self assembled to form the gray area in the image). Image reprinted with permission from ref. 204, Copyright 2010 American Chemical Society.

7.3.4 Control of Surface Chemistry of NPCs

In practice, especially for biological applications, NPs often require further modifications with functional molecules. For example, in targeted delivery, the drug molecules will be immobilized onto the NPs surface.[11] Typically, two strategies can be employed for the immobilization of desired molecules onto NPs: electrostatic interactions between two oppositely charged species and chemical bonding (covalent conjugation with surface functional groups, like $–NH_2$ and –COOH).[11] Both methods require

sophisticated control over the surface chemistry of NPs. For this reason, it is always interesting to prepare NPs with controllable surface charge and functional groups. Here, we demonstrate our ability to manipulate the surface chemistry of NPCs by employing functional polymers, including PEI, PAA, and PSS, instead of CTAB as surface capping reagents. Morphologically, the polymer stabilized NPCs were similar to those obtained from CTAB emulsion (Figs. 7.8, 7.9 & 7.10). The PEI stabilized NPCs showed positive charges; while NPCs covered by PAA and PSS exhibited negative charges as indicated by the zeta potential measurement. In addition, amine (from PEI) or carboxylic acid (from PAA) groups were also present on the surface of the NPCs. The size of polymer stabilized NPCs could also be regulated by differential centrifugation (Table 7.1). In the CTAB micelles, small NPCs (below 100 nm) can be prepared even at an initial NPs concentration of 100 mg/ml. In the polymers solution, however, small NPCs could only be produced when the initial NPs concentration was much lower (2 mg/ml as used in the experiment). At a higher NPs concentration (20 mg/ml), most of NPCs were greater than 500 nm in diameter, which makes them unsuitable for biological applications. These polymers are not emulsifiers, so no stable oil-in-water dispersion can be formed. Therefore, it was necessary to place the mixture solution under sonication throughout the entire experiment in order to prevent the coagulation of oil droplets. However, in terms of stabilization of NPCs, the polymers behave similar to the CTAB. Their hydrophobic backbone can interact with long carbon chains on the NPCs and their hydrophilic side groups can provide compatibility with the aqueous phase.[251,309] The controllable surface

chemistry of NPCs makes them capable of linking molecules through both electrostatic interaction and covalent bonding.

Table 7.1, Surface charge density and average diameter of NPCs using different stabilizers.*

Stabilizer	Zeta Potential (mV)	Ave. Dia. (nm)	
		First**	Secondary**
CTAB	+49	78	33
PEI	+33	88	42
PAA	-56	72	30
PSS	-64	65	28

* The NPCs were made from 3 nm hydrophobic iron oxide nanoparticles in hexane.

** First= first centrifuge run at 10,000 rpm for 5 min; Second= second run at 15,000 rpm for 20 min.

Table reprinted with permission from ref. 204, Copyright 2010 American Chemical Society.

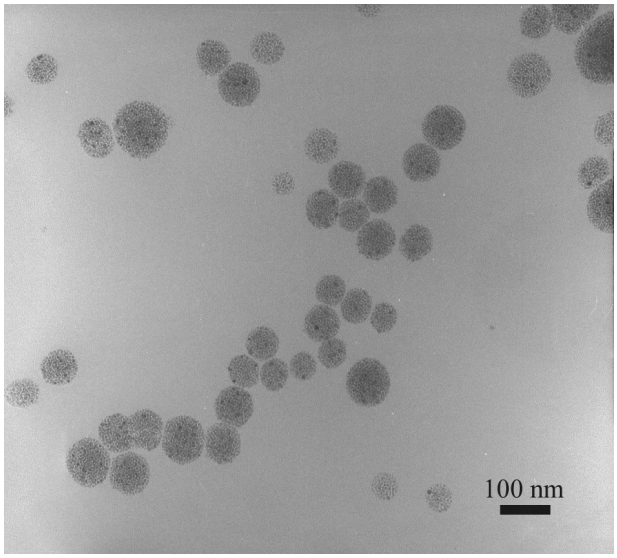

Figure7.8, Fe_3O_4 NPCs using PAA as emulsifier. Clusters were collected by 10,000 rpm for 5 min. Image reprinted with permission from ref. 204, Copyright 2010 American Chemical Society.

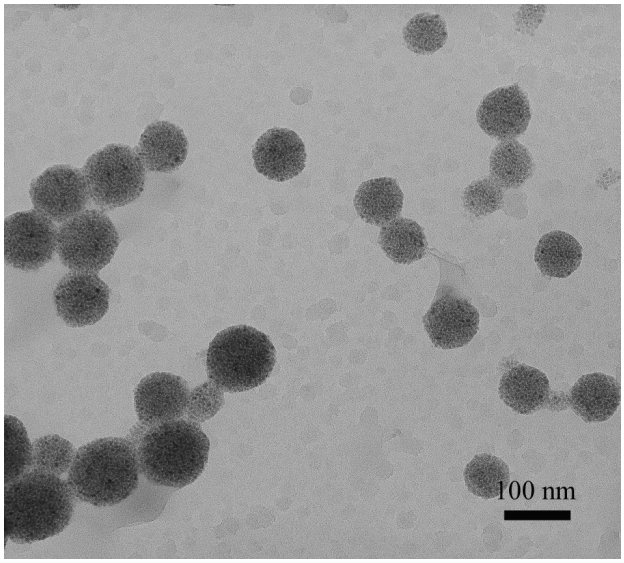

Figure 7.9, Fe_3O_4 NPCs using PEI as emulsifier. Clusters were collected by 10,000 rpm for 5 min. Image reprinted with permission from ref. 204, Copyright 2010 American Chemical Society.

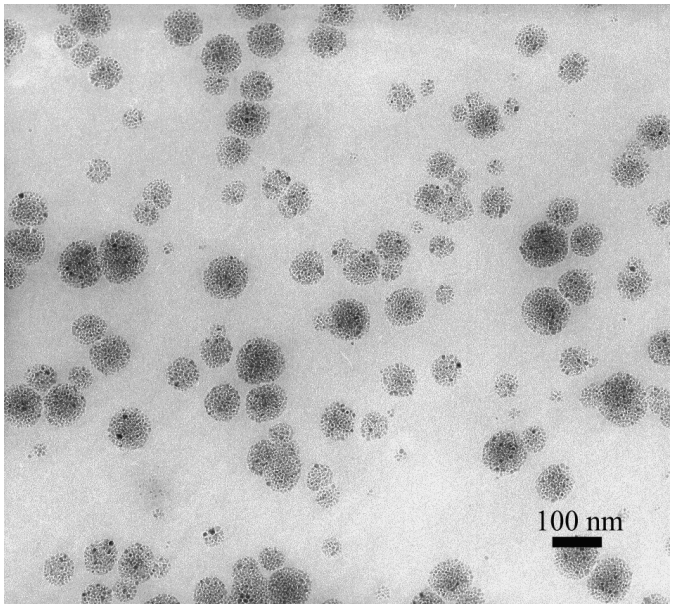

Figure 7.10, Fe_3O_4 NPCs using PSS as emulsifier. Clusters were collected by 10,000 rpm for 5 min. Image reprinted with permission from ref. 204, Copyright 2010 American Chemical Society.

7.3.5 Comparison of Behaviors of Individual and Clustered Iron Oxide NPs

In order to make comparisons between NPs in both individual and clustered forms, hydrophobic iron oxide NPs (i.e., those used for preparing clusters), were transferred into water as individually dispersed particles (Fig. 7.11a). Their magnetic response to an external field was measured at 5 K and 300 K sweeping between -10 kOe and 10 kOe. Both types of particles showed superparamagnetic behavior at 300 K without coercivity. At 5 K, a typical ferromagnetic-like hysteresis loop was observed (Fig. 7.12a). The NPCs and individual NPs had very close coercivity (31 vs. 27 Oe). In the zero-field-cooled/ field-cooled (ZFC/FC) magnetization measurements, the blocking temperature

significantly increased from 111 K (corresponding to individual NPs) to 181 K after the cluster formation (Fig. 7.12b). It is well accepted that for assembled nanoparticulate structures, magnetic dipole-dipole interactions are much stronger than those of individual nanoparticles as a result of the distance dependent nature of such interactions.[310] The anisotropy coupling of dipoles, such as nanoparticles densely packed in 1-D pores, results in a ferromagnetic effect which strongly enhances the coercivity. However, non-oriented dipole-dipole interactions, as in most random nanoparticle aggregates, have been demonstrated both experimentally and theoretically to result in decreased coercivity because of the antiferromagnetic coupling effect.[311,312] In our work, neither a significant increase nor decrease of coercivity of NPCs as compared to individual NPs was observed. This is likely due to the presence of both anisotropic and random dipole-dipole interactions within the clusters, which makes NPCs behave like a non-interacting system. During the formation of NPCs, the kinetically fast condensation due to the quick evaporation of hexane inside the micelles as well as the high thermal energy originating from the high experimental temperature could inevitably cause random assembly. On the other hand, since the liquid was homogenized under magnetic stirring through the entire process, the NPs were magnetized, which could have introduced some anisotropy to the assembly through the partial alignment of magnetic moments of NPs.[313-315] Thus, the sum of the negative contributions from the random assembly and positive contributions from anisotropic assembly within the NPCs may result in a magnetization curve similar to that of non-interacting individually dispersed NPs. The blocking temperature shifting

effect in the ZFC/FC measurement is consistent with the results reported in the literature, which show that inter-particle magnetic coupling can suppress the thermal fluctuation of magnetic spins and raise the ferromagnetic to superparamagnetic transition to a higher temperature.[312,316-318]

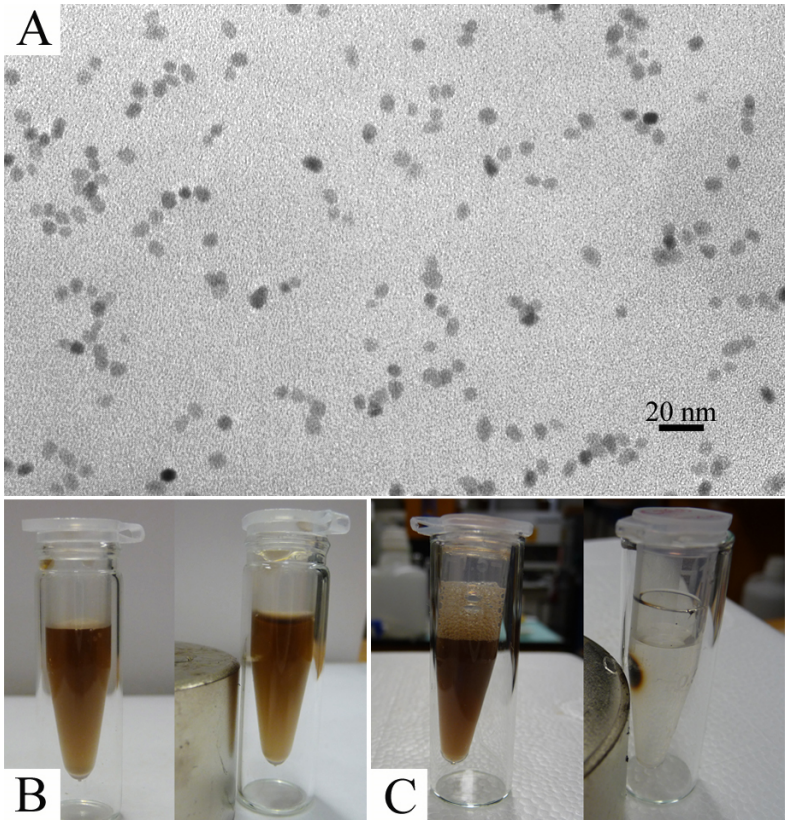

Figure 7.11, Comparison between NPCs and individually dispersed iron oxide NPs of their response to an external magnetic field. (A) TEM images of individually dispersed 6 nm iron oxide NPs, identical to those used to form clusters after being transferred from oil to water; (B) Photos show that no visible movement of individual NPs was observed in 12 h, indicating a very weak magnetic moment of individual NPs; (C) Photos show that all the NPCs were attracted to the magnet in just a few minutes, indicating a strong

magnetic moment resulting from the collective effect of nanoparticles in NPCs. Image reprinted with permission from ref. 204, Copyright 2010 American Chemical Society.

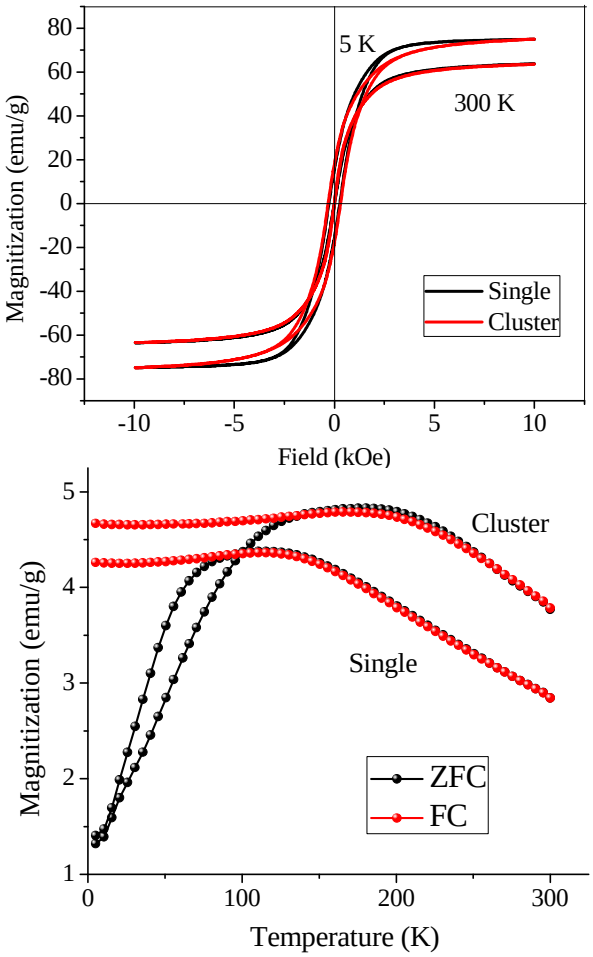

Figure 7.12, Magnetization curves of NPCs and individual iron oxide NPs. Top: Mass magnetization as a function of field strength measured at 300 K and 5 K. At 300 K, both NPCs and individual NPs showed superparamagnetic behavior. Typical hysteresis loops were observed at 5 K, and NPCs exhibited coercivity very close to the individual NPs, probably because of the coexistence of anisotropic and random assembly of NPs during the cluster formation process; Bottom: ZFC/FC measured at 50 Oe, the blocking

temperature had shifted from 111 K to 181 K after cluster formation, which indicates that strong dipole –dipole interactions had taken place among nanoparticles inside the clusters. Image reprinted with permission from ref. 204, Copyright 2010 American Chemical Society.

The single cluster has a much higher magnetic moment than individual iron oxide NPs, which was theoretically predicated earlier by Ge et al.[286] In this work, since we are able to transfer the hydrophobic Fe_3O_4 NPs into stable aqueous dispersions in both clustered and individual forms, direct comparison of the magnetization difference between both forms (and hence their response to an external field) could be made more straightforward. Both Fe_3O_4 NPCs and individually dispersed NPs solutions were placed beside a magnet and observations were periodically made. For individually dispersed iron oxide NPs, we did not observe any visible movement of NPs towards the magnet in 12 h (Fig. 7.11b). However, all the NPCs could be collected by the magnet within just a few minutes (Fig. 7.11c). In order to be able to manipulate the movement of particles in solution by a magnet, the magnetic energy on the particle should be larger than the thermal energy, which is the cause of Brownian motion.[310] This behavior for individually dispersed Fe_3O_4 NPs in an external magnetic field is consistent with theoretical result that the magnetic moment of single NPs is so weak that it could not even overcome the random Brownian motion in solution. Since a cluster is made of many individual NPs, the magnetic moment is a collective result of the individuals; therefore,

the magnetic force on a cluster is increased many times than that on non-clustered NPs.[286] Consequently, there will be a net positive magnetic force driving the clusters toward the magnet.[310] From this comparison, NPCs could be better suited for applications like drug delivery and molecular separation compared to individual NPs. In these applications, target molecules are often linked onto the particle surface and transported or collected by the movement of magnetic particles in the external field.[315,319-323]

Superparamagnetic iron oxide NPs are well known for being able to shorten the transverse relaxation time of water protons and have been used as a negative contrast agent in MRI.[323] Recently, aggregated or assembled iron oxide NPCs are drawing greater attention in MRI applications because they can provide even higher contrast than individually dispersed magnetic NPs.[287-291,305] In order to test the contrast enhancement effect from the clustering of NPs, we measured the T_2-weighted MR images with different iron concentrations in aqueous dispersion. Both individual and clustered particles exhibited a sensitive concentration-dependent darkness in MR images, where the higher the concentration, the darker the image was. However, under the same iron concentration, darker contrast was observed with NPCs (Fig. 7.13). Moreover, the clustered nanoparticles showed a transverse relaxivity (r_2) value of 277.6 s^{-1} mM^{-1} Fe, which is remarkably higher than that of individual NPs (15.4 s^{-1} mM^{-1} Fe). This suggests that NPCs could likely be used as a better contrast enhancer in T_2-weighted MR imaging than individual magnetic NPs.

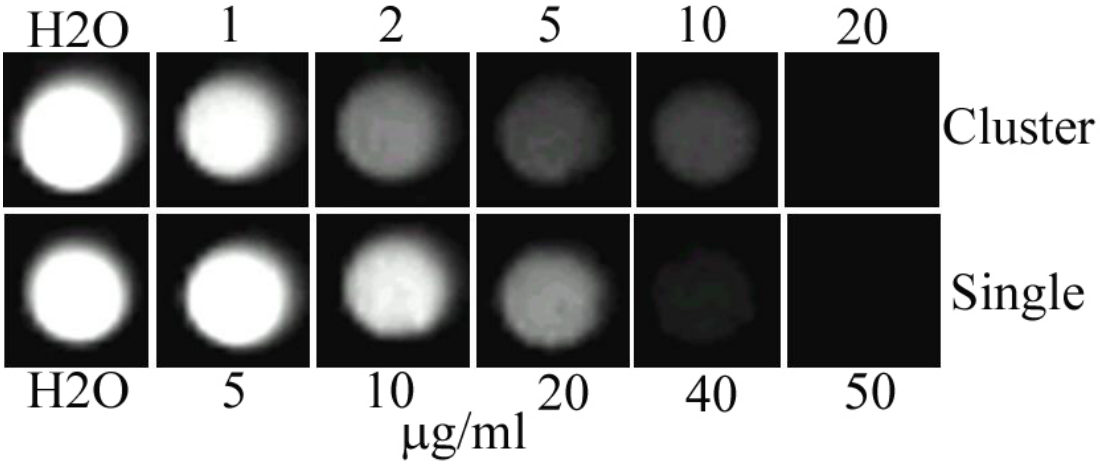

Figure 7.13, MRI images of NPCs and individual NPs with different concentrations in water. The darker contrast shown at a lower concentration for NPCs indicates that in the clustered form, a lower concentration of Fe is needed to obtain a desired contrast. Image reprinted with permission from ref. 204, Copyright 2010 American Chemical Society.

7.4 Conclusion

In summary, a general method for making NPCs was developed in a CTAB-mediated oil-in-water emulsion system, where previously only individual NPs were obtained, by increasing the concentration of NPs dispersed in the organic phase. Although NPCs have a wide range of diameters, differential centrifugation can be used to narrow their size distribution. The final concentration of NPCs produced by our method is about 5 times higher than the highest value reported in literature. Moreover, NPCs can be obtained in nearly 100% yield. Therefore, our method for producing NPCs is scalable. The surface

chemistry of NPCs can be manipulated by employing different polymers rather than CTAB, to stabilize them under constant sonication. Iron oxide NPCs have a much higher magnetic moment than individual NPs, making them better suited for separation and drug delivery purposes. In MRI, a significant increase in transverse relaxivity from NPCs also indicates that a lower concentration of iron can be used to give a reasonable contrast.

CHAPTER 8

Summary and Outlooks

The current research aims at developing new synthetic strategy to prepare structurally complex gold nanoparticles and new size sorting method to separate nanoparticles of larger size, as well as studying the assembly of nanoparticles into novel hierarchical structures through both template-assisted and template-free strategies.

Dendritic gold nanoparticles were prepared through a seed-mediated process in ethanol in **Chapter 2**. Size control of the nanodendrites could be achieved by simply adjusting the ratio of $HAuCl_4$ to total number of seeds added. The surface of nanoparticles is capped by the hexadecylamine ($C_{16}H_{33}NH_2$). The carbon chain length of alkylamines ($C_nH_{2n+1}NH_2$) has great effect on the generation of gold nanodendrites. The dendritic structure can be observed only when $n \geq 12$. In the hexadecylamine-ethanol system, the dendritic structure could be produced on seeds of different shapes, including spherical, rod-like and flat triangular nanoparticles. The future direction of this work should emphasize on both synthesis and application of the dendritic gold nanoparticles. In the current synthetic system, ethanol was used as solvent for the seeded growth of gold nanodendrites. However, the polarity of solvent may have impact on the assembly of shape-defining reagent, hexadecylamine, and consequently on the structure of the resulting gold nanoparticles. Therefore, the solvent effect on the formation of gold nanodendrites should be studied. Compared to the solid spherical nanoparticles of the similar size, the dendritic gold nanoparticles have much higher surface area, thus they can be used to enhance the loading of drug molecules in the drug delivery applications.

Besides, light absorbed by the gold nanoparticles can be converted into heat, which is high enough to trigger the release of drug molecules on the surface of the nanoparticles. The dendritic gold nanoparticles have absorption in the near infrared range, and light of this range is capable of penetrating the human tissues, thus *in vivo* controlled drug release can be achieved by using laser of the corresponding wavelength. Finally, the large surface-to-volume ratio of the dendritic gold nanoparticles makes them better suited for catalysis applications than the solid nanoparticles.

We studied the shape evolution of gold nanoparticles in a seed-mediated growth as well as the kinetics of reduction of $HAuCl_4$ in the presence of seeds in **Chapter 3**. The reduction of the gold precursor by sodium citrate was accelerated due to the addition of pre-synthesized seed nanoparticles. The investigation of shape evolution was carried out by manipulating the molar ratio (R) of sodium citrate to the gold precursor, $HAuCl_4$. Nearly single-crystalline gold nanowires were formed at a very low R value (R = 0.16) in the presence of the seeds as a result of the oriented attachment of the growing gold nanoparticles. At a higher R value (R = 0.33), gold nanochains were formed due to the non-oriented attachment of gold nanoparticles. At a much higher R value (R = 1.32), only larger spherical gold nanoparticles grown from the seeds were found. In the absence of gold seeds, no single-crystalline nanowires were formed at the same R value. Our results indicate that the formation of the 1D nanostructures (nanochains and nanowires) at low R values is due to the attachment of gold nanoparticles along one direction, which is driven by the surface energy reduction, nanoparticle attraction, and dipole–dipole interaction between adjacent nanoparticles.

We developed a novel method of separating nanoparticles of different sizes in a

viscosity gradient in **Chapter 4**. The viscosity gradient was created by stacking gradient concentration of polyvinylpyrrolidone (PVP) aqueous solutions. Previously, such size separation was all achieved in the density gradient, while the hidden contribution of viscosity difference inside the density gradient was not well recognized. Through this work, it is clarified that the viscosity can contribute as importantly as density in the size sorting of nanoparticles through rate zonal centrifuge. It was also demonstrated both experimentally and mathematically that the viscosity gradient is more effective in separation of larger sized nanoparticles. In the current work, all the demonstrations of nanoparticles size separation were based on the PVP-covered AuNPs, which are very stable in the PVP viscosity gradient. In practice, nanoparticles are synthesized with many different surface capping molecules in the solution phase; while most of these non-PVP covered nanoparticles will be destabilized in the PVP viscosity gradient. The future work should aim to extend the viscosity gradient to the size separation of non-PVP stabilized nanoparticles without destabilization. A possible approach that can be employed to solve this issue is to use different polymers. Besides PVP, for many other polymers, such as polyethylene glycol (PEG), polyacrylic acid (PAA) and poly (diallyl dimethyl ammonium chloride) (PDDA), their aqueous solutions of different concentrations have similar densities, but significantly different viscosities, thus they are also suitable to build the viscosity gradient. These polymers contain typical functional groups that appear on the surface of nanoparticles. Therefore, it is possible to find a suitable polymer solution in which nanoparticles capped by a certain type of molecules can be dispersed stably.

We investigated the oriented 1-D assembly of gold nanorods by using bacteria flagella as templates in **Chapter 5**. This biological filamentous template was purified

from the *Escherichia coli* bacteria. The assembly took place through electrostatic interaction between the positively charged gold nanorods and the negatively charged flagella. Two approaches were carried out to obtain the assembled structures. In one approach, nanorods and flagella were mixed directly in the solution phase; while in the other one, flagella were first immobilized onto a TEM grid, which was then floated on a drop of nanorods solution to allow adsorption. Both approaches generated well aligned gold nanorods structures. The optical shift of aligned gold nanorods was also studied. The flagella could potentially be a better template than the previously used carbon nanotubes, since carbon nanotubes involve tedious surface modification to get charges, while flagella are naturally charged and the charges could also be manipulated through genetic engineering. The future work will focus on the large scale oriented assembly of gold nanorods on a substrate and the assembly of other nanoparticles, like gold/silica core/shell nanoparticles, into 1-D structure based on the flagella templates. To assemble gold nanorods into large scale oriented structure, the template, flagella, should first form ordered pattern on a substrate, which could possibly be achieved by the shear force or by an external electric field. And nanorods can then be assembled onto the patterned substrate to form a large scale oriented assembly. The gold/silica core/shell nanoparticles can be synthesized with well-controlled silica shell thickness. When the core/shell nanoparticles are assembled into 1-D arrays, the core-to-core distance can be manipulated by controlling the thickness of the shell. For gold nanoparticles, the manipulability in the inter-particle distance provides a means to control the optical shifting of the assembled 1-D structure.

Novel branched hollow microfibers that were co-assembled from PVP stabilized

gold nanoparticles and free PVP molecules in the solution were revealed in **Chapter 6**. Initially, we discovered that PVP could self-assemble into branched hollow fibers in an aqueous solution after aging under room temperature for about two weeks. On the basis of this finding, we demonstrated two approaches (one is through direct deposition of silica onto the PVP aggregate and the other is through co-assembly of PVP covered gold nanoparticles with free PVP molecules) by which the self-assembly behavior of PVP could be exploited to template the formation of branched hollow inorganic fibers. Our work suggests that the self-assembly of the PVP molecules in the solution can serve as a general method for directing the formation of branched hollow inorganic fibers. The future work includes both the fabrication of branched hollow fibers of other functional materials and the application of current silica and gold based branched hollow fibers. Besides silica, other inorganic oxide materials, like ZnO and TiO_2, can also be prepared by the base-catalyzed hydrolysis reaction of their corresponding organic alkoxides compounds. Thus, branched hollow ZnO and TiO_2 fibers could be prepared in the same way as the fabrication of silica fibers. Silica is a bio-compatible and bio-decomposable material, the overall size of the fibrous structure is on the centimeter scale and the diameter of the individual fibers is comparable to the size of cells, therefore, the silica branched hollow fibers can be used as 3-D substrates, as substituents to the conventional 2-D substrates, for the cell culture. The gold nanoparticles in the co-assembled fibers are very close to each other, resulting in a strong surface plasmon coupling between adjacent nanoparticles. Thus, the gold branched hollow fibers are suitable as substrates for the surface enhanced Raman scattering (SERS) based highly sensitive molecular detection.

A general method for template free assembly of nanoparticle into clusters (NPCs) in an oil-in-water emulsion system was investigated in **Chapter 7**. The assembly was mediated by cetyl trimethylammonium bromide (CTAB) where previously, only individual nanoparticles were obtained. NPCs of magnetic, metallic and semiconductor nanoparticles have been prepared to demonstrate the generality of the method. The NPCs were spherical and composed of densely packed individual nanoparticles. The number density of nanoparticles in the oil phase was found to be critical for the formation, morphology and yield of NPCs. The method developed here is scalable and can produce NPCs in nearly 100% yield at a concentration of 5 mg/ml in water which is approximately 5 times higher than the highest value reported in literature. The surface chemistry of NPCs can also be controlled by replacing CTAB with polymers containing different functional groups via a similar procedure. The reproducible production of NPCs with well defined shapes has allowed us to compare the properties of individual and clustered iron oxide nanoparticles including magnetization, magnetic moments and contrast enhancement in magnetic resonance imaging (MRI). We found that due to their collective properties, NPCs are more responsive to an external magnetic field and can potentially serve as better contrast enhancement agents than individually dispersed magnetic NPs in MRI. The future work will focus on the *in vivo* application of the iron oxide NPCs as MRI contrast enhancing reagent. The surface of the NPCs should be modified so that they can bind specifically to a target, for instance, a tumor site. Considering the simplicity in the surface modification, silica coated NPCs will be better than the as prepared NPCs. In addition, through nanoparticles engineering, the NPCs can be functionalized for multi-mode *in vivo* imaging purposes. For example, gold

nanoparticles can be immobilized onto the silica shell through electrostatic interaction and fluorescent dye molecules can be linked onto silica through covalent bonding. Both these modification methods are well developed. The gold nanoparticles and dye functionalized iron oxide NPCs are capable of imaging the target site through three different modes, including magnetic resonance (magnetic nanoparticles), light scattering (gold nanoparticles) and light emission (dye) modes.

References

[1] Xia, Y.; Xiong, Y. J.; Lim, B.; Skrabalak, S. E., "Shape-Controlled Synthesis of Metal Nanocrystals: Simple Chemistry Meets Complex Physics?", *Angewandte Chemie -International Edition*, **2009**, 48, 60.

[2] Xia, Y.; Yang, P.; Sun, Y.; Wu, Y.; Mayers, B.; Gates, B.; Yin, Y.; Kim, F.; Yan, H., "One-Dimensional Nanostructures: Synthesis, Characterization, and Applications", *Advanced Materials*, **2003**, 15, 353.

[3] Daniel, M. C.; Astruc, D., "Gold Nanoparticles: Assembly, Supramolecular Chemistry, Quantum-Size-Related Properties, and Applications toward Biology, Catalysis, and Nanotechnology", *Chemical Reviews*, **2004**, 104, 293.

[4] Rosi, N. L.; Mirkin, C. A., "Nanostructures in Biodiagnostics", *Chemical Reviews*, **2005**, 105, 1547.

[5] El-Sayed, I. H.; Huang, X.; El-Sayed, M. A., "Surface Plasmon Resonance Scattering and Absorption of Anti-Egfr Antibody Conjugated Gold Nanoparticles in Cancer Diagnostics: Applications in Oral Cancer", *Nano Letters*, **2005**, 5, 829.

[6] Huang, X.; El-Sayed, I. H.; Qian, W.; El-Sayed, M. A., "Cancer Cell Imaging and Photothermal Therapy in the near-Infrared Region by Using Gold Nanorods", *Journal of the American Chemical Society*, **2006**, 128, 2115.

[7] Jain, P. K.; Huang, X.; El-Sayed, I. H.; El-Sayed, M. A., "Noble Metals on the Nanoscale: Optical and Photothermal Properties and Some Applications in Imaging, Sensing, Biology, and Medicine", *Accounts of Chemical Research*, **2008**, 41, 1578.

[8] Sperling, R. A.; Rivera, G. P.; Zhang, F.; Zanella, M.; Parak, W. J., "Biological Applications of Gold Nanoparticles", *Chemical Society Reviews*, **2008**, 37, 1896.

[9] Han, G.; Ghosh, P.; Rotello, V. M., "Functionalized Gold Nanoparticles for Drug Delivery", *Nanomedicine*, **2007**, 2, 113.

[10] Paciotti, G. F.; Kingston, D. G. I.; Tamarkin, L., "Colloidal Gold Nanoparticles: A Novel Nanoparticle Platform for Developing Multifunctional Tumor Targeted Drug Delivery Vectors", *Drug Development Research*, **2006**, 67, 47.

[11] Ghosh, P.; Han, G.; De, M.; Kim, C. K.; Rotello, V. M., "Gold Nanoparticles in Delivery Applications", *Advanced Drug Delivery Reviews*, **2008**, 60, 1307.

[12] Lal, S.; Clare, S. E.; Halas, N. J., "Nanoshell-Enabled Photothermal Cancer Therapy: Impending Clinical Impact", *Accounts of Chemical Research*, **2008**, 41, 1842.

[13] Chen, M.; Goodman, D. W., "Catalytically Active Gold: From Nanoparticles to Ultrathin Films", *Accounts of Chemical Research*, **2006**, 39, 739.

[14] Shipway, A. N.; Katz, E.; Willner, I., "Nanoparticle Arrays on Surfaces for Electronic, Optical, and Sensor Applications", *ChemPhysChem*, **2000**, 1, 18.

[15] Li, Y.; Wu, Y.; Ong, B. S., "Facile Synthesis of Silver Nanoparticles Useful for Fabrication of High-Conductivity Elements for Printed Electronics", *Journal of the American Chemical Society*, **2005**, 127, 3266.

[16] Bruce, P. G.; Scrosati, B.; Tarascon, J. M., "Nanomaterials for Rechargeable Lithium Batteries", *Angewandte Chemie International Edition*, **2008**, 47, 2930.

[17] Link, S.; El-Sayed, M. A., "Size and Temperature Dependence of the Plasmon Absorption of Colloidal Gold Nanoparticles", *Journal of Physical Chemistry B*, **1999**, 103, 4212.

[18] Kelly, K. L.; Coronado, E.; Zhao, L. L.; Schatz, G. C., "The Optical Properties of Metal Nanoparticles: The Influence of Size, Shape, and Dielectric Environment", *Journal of Physical Chemistry B*, **2003**, 107, 668.

[19] Jain, P. K.; Lee, K. S.; El-Sayed, I. H.; El-Sayed, M. A., "Calculated Absorption and Scattering Properties of Gold Nanoparticles of Different Size, Shape, and Composition: Applications in Biological Imaging and Biomedicine", *Journal of Physical Chemistry B*, **2006**, 110, 7238.

[20] Frens, G., "Controlled Nucleation for Regulation of Particle-Size in Monodisperse Gold Suspensions", *Nature-Physical Science*, **1973**, 241, 20.

[21] Liang, H. P.; Wan, L. J.; Bai, C. L.; Jiang, L., "Gold Hollow Nanospheres: Tunable Surface Plasmon Resonance Controlled by Interior-Cavity Sizes", *Journal of Physical Chemistry B*, **2005**, 109, 7795.

[22] Schwartzberg, A. M.; Olson, T. Y.; Talley, C. E.; Zhang, J. Z., "Synthesis, Characterization, and Tunable Optical Properties of Hollow Gold Nanospheres?", *Journal of Physical Chemistry B*, **2006**, 110, 19935.

[23] Shukla, S.; Priscilla, A.; Banerjee, M.; Bhonde, R. R.; Ghatak, J.; Satyam, P. V.; Sastry, M., "Porous Gold Nanospheres by Controlled Transmetalation Reaction: A Novel Material for Application in Cell Imaging", *Chemistry of Materials*, **2005**, 17, 5000.

[24] Perez-Juste, J.; Pastoriza-Santos, I.; Liz-Marzan, L. M.; Mulvaney, P., "Gold Nanorods: Synthesis, Characterization and Applications", *Coordination Chemistry Reviews*, **2005**, 249, 1870.

[25] Murphy, C. J.; Sau, T. K.; Gole, A. M.; Orendorff, C. J.; Gao, J.; Gou, L.; Hunyadi, S. E.; Li, T., "Anisotropic Metal Nanoparticles: Synthesis, Assembly, and Optical Applications", *Journal of Physical Chemistry B*, **2005**, 109, 13857.

[26] Ha, T. H.; Koo, H. J.; Chung, B. H., "Shape-Controlled Syntheses of Gold Nanoprisms and Nanorods Influenced by Specific Adsorption of Halide Ions", *Journal of Physical Chemistry C*, **2006**, 111, 1123.

[27] Ah, C. S.; Yun, Y. J.; Park, H. J.; Kim, W. J.; Ha, D. H.; Yun, W. S., "Size-Controlled Synthesis of Machinable Single Crystalline Gold Nanoplates", *Chemistry of Materials*, **2005**, 17, 5558.

[28] Millstone, J. E.; Park, S.; Shuford, K. L.; Qin, L.; Schatz, G. C.; Mirkin, C. A., "Observation of a Quadrupole Plasmon Mode for a Colloidal Solution of Gold Nanoprisms", *Journal of the American Chemical Society*, **2005**, 127, 5312.

[29] Millstone, J. E.; Metraux, G. S.; Mirkin, C. A., "Controlling the Edge Length of Gold

Nanoprisms Via a Seed-Mediated Approach", *Advanced Functional Materials*, **2006**, 16, 1209.

[30] Kim, F.; Connor, S.; Song, H.; Kuykendall, T.; Yang, P. D., "Platonic Gold Nanocrystals", *Angewandte Chemie-International Edition*, **2004**, 43, 3673.

[31] Li, C. C.; Shuford, K. L.; Chen, M. H.; Lee, E. J.; Cho, S. O., "A Facile Polyol Route to Uniform Gold Octahedra with Tailorable Size and Their Optical Properties", *ACS Nano*, **2008**, 2, 1760.

[32] Seo, D.; Park, J. C.; Song, H., "Polyhedral Gold Nanocrystals with Oh Symmetry: From Octahedra to Cubes", *Journal of the American Chemical Society*, **2006**, 128, 14863.

[33] Chen, J.; McLellan, J. M.; Siekkinen, A.; Xiong, Y.; Li, Z. Y.; Xia, Y., "Facile Synthesis of Gold- Silver Nanocages with Controllable Pores on the Surface", *Journal of the American Chemical Society*, **2006**, 128, 14776.

[34] Skrabalak, S. E.; Chen, J.; Sun, Y.; Lu, X.; Au, L.; Cobley, C. M.; Xia, Y., "Gold Nanocages: Synthesis, Properties, and Applications", *Accounts of Chemical Research*, **2008**, 41, 1587.

[35] Kumar, P. S.; Pastoriza-Santos, I.; Rodriguez-Gonzalez, B.; Garcia de Abajo, F. J.; Liz-Marzan, L. M., "High-Yield Synthesis and Optical Response of Gold Nanostars", *Nanotechnology*, **2008**, 19, 15606.

[36] Qiu, P.; Mao, C.B., " Seed-Mediated Shape Evolution of Gold Nanomaterials: from Spherical Nanoparticles to Polycrystalline Nanochains and Single-Crystalline Nanowires", *Journal of Nanoparticle Research*, **2009**, 11, 885.

[37] Bhargava, S. K.; Booth, J. M.; Agrawal, S.; Coloe, P.; Kar, G., "Gold Nanoparticle Formation During Bromoaurate Reduction by Amino Acids", *Langmuir*, **2005**, 21, 5949.

[38] Basu, N.; Bhattacharya, R.; Mukherjee, P., "Protein-Mediated Autoreduction of Gold Salts to Gold Nanoparticles", *Biomedical Materials*, **2008**, 3, 034105.

[39] Xie, J.; Lee, J. Y.; Wang, D. I. C., "Synthesis of Single-Crystalline Gold Nanoplates in Aqueous Solutions through Biomineralization by Serum Albumin Protein", *Journal of Physical Chemistry C*, **2007**, 28, 10226.

[40] Pastoriza-Santos, I.; Liz-Marzan, L. M., "N,N-Dimethylformamide as a Reaction Medium for Metal Nanoparticle Synthesis", *Advanced Functional Materials*, **2009**, 19, 679.

[41] Ha, T. H.; Koo, H. J.; Chung, B. H., "Shape-Controlled Syntheses of Gold Nanoprisms and Nanorods Influenced by Specific Adsorption of Halide Ions", *Journal of Physical Chemistry C*, **2007**, 111, 1123.

[42] Grzelczak, M.; Perez-Juste, J.; Mulvaney, P.; Liz-Marzan, L. M., "Shape Control in Gold Nanoparticle Synthesis", *Chemical Society Reviews*, **2008**, 37, 1783.

[43] Edwards, P. P.; Thomas, J. M., "Gold in a Metallic Divided State - from Faraday to Present-Day Nanoscience", *Angewandte Chemie-International Edition*, **2007**, 46, 5480.

[44] Sun, Y. G.; Xia, Y. N., "Shape-Controlled Synthesis of Gold and Silver Nanoparticles", *Science*, **2002**, 298, 2176.

[45] Gole, A.; Murphy, C. J., "Seed-Mediated Synthesis of Gold Nanorods: Role of the Size and Nature of the Seed", *Chemistry of Materials*, **2004**, 16, 3633.

[46] Jana, N. R.; Gearheart, L.; Murphy, C. J., "Wet Chemical Synthesis of High Aspect Ratio Cylindrical Gold Nanorods", *Journal of Physical Chemistry B*, **2001**, 105, 4065.

[47] Gou, L.; Murphy, C. J., "Fine-Tuning the Shape of Gold Nanorods", *Chemistry of Materials*, **2005**, 17, 3668.

[48] Sau, T. K.; Murphy, C. J., "Seeded High Yield Synthesis of Short Au Nanorods in Aqueous Solution", *Langmuir*, **2004**, 20, 6414.

[49] Nikoobakht, B.; El-Sayed, M. A., "Preparation and Growth Mechanism of Gold Nanorods (Nrs) Using Seed-Mediated Growth Method", *Chemistry of Materials*, **2003**, 15, 1957.

[50] Hao, F.; Nehl, C. L.; Hafner, J. H.; Nordlander, P., "Plasmon Resonances of a Gold Nanostar", *Nano Letters*, **2007**, 7, 729.

[51] Sanchez-Iglesias, A.; Pastoriza-Santos, I.; Perez-Juste, J.; Rodriguez-Gonzalez, B.; de Abajo, F. J. G.; Liz-Marzan, L. M., "Synthesis and Optical Properties of Gold Nanodecahedra with Size Control", *Advanced Materials*, **2006**, 18, 2529.

[52] Rodriguez-Fernandez, J.; Perez-Juste, J.; de Abajo, F. J. G.; Liz-Marzan, L. M., "Seeded Growth of Submicron Au Colloids with Quadrupole Plasmon Resonance Modes", *Langmuir*, **2006**, 22, 7007.

[53] Carbo-Argibay, E.; Rodriguez-Gonzalez, B.; Pacifico, J.; Pastoriza-Santos, I.; Perez-Juste, J.; Liz-Marzan, L. M., "Chemical Sharpening of Gold Nanorods: The Rod-to-Octahedron Transition", *Angewandte Chemie-International Edition*, **2007**, 46, 8983.

[54] Yin, Y.; Erdonmez, C.; Aloni, S.; Alivisatos, A. P., "Faceting of Nanocrystals During Chemical Transformation: From Solid Silver Spheres to Hollow Gold Octahedra", *Journal of the American Chemical Society*, **2006**, 128, 12671.

[55] Zhang, J. Z., "Biomedical Applications of Shape-Controlled Plasmonic Nanostructures: A Case Study of Hollow Gold Nanospheres for Photothermal Ablation Therapy of Cancer", *The Journal of Physical Chemistry Letters*, **2010**, 1, 686.

[56] Li, Z.; Tao, J.; Lu, X.; Zhu, Y.; Xia, Y., "Facile Synthesis of Ultrathin Au Nanorods by Aging the Aucl (Oleylamine) Complex with Amorphous Fe Nanoparticles in Chloroform", *Nano Letters*, **2008**, 8, 3052.

[57] Yavuz, M. S.; Cheng, Y.; Chen, J.; Cobley, C. M.; Zhang, Q.; Rycenga, M.; Xie, J.; Kim, C.; Song, K. H.; Schwartz, A. G., "Gold Nanocages Covered by Smart Polymers for Controlled Release with near-Infrared Light", *Nature materials*, **2009**, 8, 935.

[58] Link, S.; El-Sayed, M. A., "Optical Properties and Ultrafast Dynamics of Metallic Nanocrystals", *Annual Rreview of Physical Chemistry*, **2003**, 54, 331.

[59] Liu, X.; Atwater, M.; Wang, J.; Huo, Q., "Extinction Coefficient of Gold

Nanoparticles with Different Sizes and Different Capping Ligands", *Colloids and Surfaces B: Biointerfaces*, **2007**, 58, 3.

[60] Yu, Y. Y.; Chang, S. S.; Lee, C. L.; Wang, C. R. C., "Gold Nanorods: Electrochemical Synthesis and Optical Properties", *Journal of Physical Chemistry B*, **1997**, 101, 6661.

[61] Wijaya, A.; Schaffer, S. B.; Pallares, I. G.; Hamad-Schifferli, K., "Selective Release of Multiple DNA Oligonucleotides from Gold Nanorods", *ACS Nano*, **2008**, 3, 80.

[62] Zijlstra, P.; Chon, J. W. M.; Gu, M., "Five-Dimensional Optical Recording Mediated by Surface Plasmons in Gold Nanorods", *Nature*, **2009**, 459, 410.

[63] Shi, W.; Sahoo, Y.; Swihart, M. T.; Prasad, P. N., "Gold Nanoshells on Polystyrene Cores for Control of Surface Plasmon Resonance", *Langmuir*, **2005**, 21, 1610.

[64] Prodan, E.; Nordlander, P.; Halas, N. J., "Electronic Structure and Optical Properties of Gold Nanoshells", *Nano Letters*, **2003**, 3, 1411.

[65] Oldenburg, S. J.; Averitt, R. D.; Westcott, S. L.; Halas, N. J., "Nanoengineering of Optical Resonances", *Chemical Physics Letters*, **1998**, 288, 243.

[66] Oldenburg, S. J.; Jackson, J. B.; Westcott, S. L.; Halas, N. J., "Infrared Extinction Properties of Gold Nanoshells", *Applied Physics Letters*, **1999**, 75, 2897.

[67] Gobin, A. M.; Lee, M. H.; Halas, N. J.; James, W. D.; Drezek, R. A.; West, J. L., "Near-Infrared Resonant Nanoshells for Combined Optical Imaging and Photothermal Cancer Therapy", *Nano Letters*, **2007**, 7, 1929.

[68] Lin, A.; Hirsch, L.; Lee, M. H.; Barton, J.; Halas, N.; West, J.; Drezek, R., "Nanoshell-Enabled Photonics-Based Imaging and Therapy of Cancer", *Technology in Cancer Research & Treatment*, **2004**, 3, 33.

[69] Takahashi, H.; Niidome, T.; Kawano, T.; Yamada, S.; Niidome, Y., "Surface Modification of Gold Nanorods Using Layer-by-Layer Technique for Cellular Uptake", *Journal of Nanoparticle Research*, **2008**, 10, 221.

[70] Sperling, R. A.; Parak, W. J., "Surface Modification, Functionalization and Bioconjugation of Colloidal Inorganic Nanoparticles", *Philosophical Transactions of the Royal Society A: Mathematical, Physical and Engineering Sciences*, **2010**, 368, 1333.

[71] Neouze, M. A.; Schubert, U., "Surface Modification and Functionalization of Metal and Metal Oxide Nanoparticles by Organic Ligands", *Monatshefte Fur Chemie*, **2008**, 139, 183.

[72] Elghanian, R.; Storhoff, J. J.; Mucic, R. C.; Letsinger, R. L.; Mirkin, C. A., "Selective Colorimetric Detection of Polynucleotides Based on the Distance-Dependent Optical Properties of Gold Nanoparticles", *Science*, **1997**, 277, 1078.

[73] Storhoff, J. J.; Elghanian, R.; Mucic, R. C.; Mirkin, C. A.; Letsinger, R. L., "One-Pot Colorimetric Differentiation of Polynucleotides with Single Base Imperfections Using Gold Nanoparticle Probes", *Journal of the American Chemical Society*, **1998**, 120, 1959.

[74] Reynolds Iii, R. A.; Mirkin, C. A.; Letsinger, R. L., "Homogeneous, Nanoparticle-Based Quantitative Colorimetric Detection of Oligonucleotides", *Journal of the American Chemical Society*, **2000**, 122, 3795.

[75] Park, S. J.; Taton, T. A.; Mirkin, C. A., "Array-Based Electrical Detection of DNA with Nanoparticle Probes", *Science*, **2002**, 295, 1503.

[76] Nam, J. M.; Stoeva, S. I.; Mirkin, C. A., "Bio-Bar-Code-Based DNA Detection with Pcr-Like Sensitivity", *Journal of the American Chemical Society*, **2004**, 126, 5932.

[77] Lee, J. S.; Ulmann, P. A.; Han, M. S.; Mirkin, C. A., "A DNA- Gold Nanoparticle-Based Colorimetric Competition Assay for the Detection of Cysteine", *Nano Letters*, **2008**, 8, 529.

[78] Lee, J. S.; Han, M. S.; Mirkin, C. A., "Colorimetric Detection of Mercuric Ion (Hg2+) in Aqueous Media Using DNA Functionalized Gold Nanoparticles", *Angewandte Chemie International Edition*, **2007**, 46, 4093.

[79] Liu, J.; Lu, Y., "A Colorimetric Lead Biosensor Using Dnazyme-Directed Assembly of Gold Nanoparticles", *Journal of the American Chemical Society*, **2003**, 125, 6642.

[80] Xia, F.; Zuo, X. L.; Yang, R. Q.; Xiao, Y.; Kang, D.; Vallee-Belisle, A.; Gong, X.; Yuen, J. D.; Hsu, B. B. Y.; Heeger, A. J.; Plaxco, K. W., "Colorimetric Detection of DNA, Small Molecules, Proteins, and Ions Using Unmodified Gold Nanoparticles and Conjugated Polyelectrolytes", *Proceedings of the National Academy of Sciences of the United States of America*, **2010**, 107, 10837.

[81] Loo, C.; Lowery, A.; Halas, N.; West, J.; Drezek, R., "Immunotargeted Nanoshells for Integrated Cancer Imaging and Therapy", *Nano Letters*, **2005**, 5, 709.

[82] El-Sayed, I. H.; Huang, X.; El-Sayed, M. A., "Selective Laser Photo-Thermal Therapy of Epithelial Carcinoma Using Anti-Egfr Antibody Conjugated Gold Nanoparticles", *Cancer Letters*, **2006**, 239, 129.

[83] Huang, X.; Jain, P. K.; El-Sayed, I. H.; El-Sayed, M. A., "Plasmonic Photothermal Therapy (Pptt) Using Gold Nanoparticles", *Lasers in Medical Science*, **2008**, 23, 217.

[84] Chen, J.; Wang, D.; Xi, J.; Au, L.; Siekkinen, A.; Warsen, A.; Li, Z. Y.; Zhang, H.; Xia, Y.; Li, X., "Immuno Gold Nanocages with Tailored Optical Properties for Targeted Photothermal Destruction of Cancer Cells", *Nano Letters*, **2007**, 7, 1318.

[85] Barhoumi, A.; Huschka, R.; Bardhan, R.; Knight, M. W.; Halas, N. J., "Light-Induced Release of DNA from Plasmon-Resonant Nanoparticles: Towards Light-Controlled Gene Therapy", *Chemical Physics Letters*, **2009**, 482, 171.

[86] Chen, C. C.; Lin, Y. P.; Wang, C. W.; Tzeng, H. C.; Wu, C. H.; Chen, Y. C.; Chen, C. P.; Chen, L. C.; Wu, Y. C., "DNA- Gold Nanorod Conjugates for Remote Control of Localized Gene Expression by near Infrared Irradiation", *Journal of the American Chemical Society*, **2006**, 128, 3709.

[87] Han, G.; You, C. C.; Kim, B.; Turingan, R. S.; Forbes, N. S.; Martin, C. T.; Rotello, V. M., "Light Regulated Release of DNA and Its Delivery to Nuclei by Means of Photolabile Gold Nanoparticles", *Angewandte Chemie*, **2006**, 118, 3237.

[88] Segalman, R. A., "Patterning with Block Copolymer Thin Films", *Materials Science and Engineering: R: Reports*, **2005**, 48, 191.

[89]Haryono, A.; Binder, W. H., "Controlled Arrangement of Nanoparticle Arrays in Block Copolymer Domains", *Small*, **2006**, 2, 600.

[90]Thurn-Albrecht, T.; Steiner, R.; DeRouchey, J.; Stafford, C. M.; Huang, E.; Bal, M.; Tuominen, M.; Hawker, C. J.; Russell, T. P., "Nanoscopic Templates from Oriented Block Copolymer Films", *Advanced Materials*, **2000**, 12, 787.

[91]Chiu, J. J.; Kim, B. J.; Kramer, E. J.; Pine, D. J., "Control of Nanoparticle Location in Block Copolymers", *Journal of the American Chemical Society*, **2005**, 127, 5036.

[92]Sohn, B. H.; Seo, B. H., "Fabrication of the Multilayered Nanostructure of Alternating Polymers and Gold Nanoparticles with Thin Films of Self-Assembling Diblock Copolymers", *Chemistry of Materials*, **2001**, 13, 1752.

[93]Sohn, B. H.; Choi, J. M.; Yoo, S. I.; Yun, S. H.; Zin, W. C.; Jung, J. C.; Kanehara, M.; Hirata, T.; Teranishi, T., "Directed Self-Assembly of Two Kinds of Nanoparticles Utilizing Monolayer Films of Diblock Copolymer Micelles", *Journal of the American Chemical Society*, **2003**, 125, 6368.

[94]Sohn, B. H.; Yoo, S. I.; Seo, B. W.; Yun, S. H.; Park, S. M., "Nanopatterns by Free-Standing Monolayer Films of Diblock Copolymer Micelles with in Situ Core-Corona Inversion", *Journal of the American Chemical Society*, **2001**, 123, 12734.

[95]Tsutsumi, K.; Funaki, Y.; Hirokawa, Y.; Hashimoto, T., "Selective Incorporation of Palladium Nanoparticles into Microphase-Separated Domains of Poly (2-Vinylpyridine)-Block-Polyisoprene", *Langmuir*, **1999**, 15, 5200.

[96]Heddle, J. G., "Protein Cages, Rings and Tubes: Useful Components of Future Nanodevices?", *Nanotechnology, Science and Applications*, **2008**, 1, 67.

[97]McMillan, R. A.; Paavola, C. D.; Howard, J.; Chan, S. L.; Zaluzec, N. J.; Trent, J. D., "Ordered Nanoparticle Arrays Formed on Engineered Chaperonin Protein Templates", *Nature Materials*, **2002**, 1, 247.

[98]Sun, J.; DuFort, C.; Daniel, M. C.; Murali, A.; Chen, C.; Gopinath, K.; Stein, B.; De, M.; Rotello, V. M.; Holzenburg, A., "Core-Controlled Polymorphism in Virus-Like

Particles", *Proceedings of the National Academy of Sciences*, **2007**, 104, 1354.

[99] Douglas, T.; Young, M., "Virus Particles as Templates for Materials Synthesis", *Advanced Materials*, **1999**, 11, 679.

[100] Dixit, S. K.; Goicochea, N. L.; Daniel, M. C.; Murali, A.; Bronstein, L.; De, M.; Stein, B.; Rotello, V. M.; Kao, C. C.; Dragnea, B., "Quantum Dot Encapsulation in Viral Capsids", *Nano Letters*, **2006**, 6, 1993.

[101] Klem, M. T.; Willits, D.; Solis, D. J.; Belcher, A. M.; Young, M.; Douglas, T., "Bio Inspired Synthesis of Protein Encapsulated Copt Nanoparticles", *Advanced Functional Materials*, **2005**, 15, 1489.

[102] Kramer, R. M.; Li, C.; Carter, D. C.; Stone, M. O.; Naik, R. R., "Engineered Protein Cages for Nanomaterial Synthesis", *Journal of the American Chemical Society*, **2004**, 126, 13282.

[103] McMillan, R. A.; Howard, J.; Zaluzec, N. J.; Kagawa, H. K.; Mogul, R.; Li, Y. F.; Paavola, C. D.; Trent, J. D., "A Self-Assembling Protein Template for Constrained Synthesis and Patterning of Nanoparticle Arrays", *Journal of the American Chemical Society*, **2005**, 127, 2800.

[104] Loo, L. N.; Guenther, R. H.; Basnayake, V. R.; Lommel, S. A.; Franzen, S., "Controlled Encapsidation of Gold Nanoparticles by a Viral Protein Shell", *Journal of the American Chemical Society*, **2006**, 128, 4502.

[105] Seeman, N. C., "Nucleic Acid Junctions and Lattices", *Journal of Theoretical Biology*, **1982**, 99, 237.

[106] Aldaye, F. A.; Sleiman, H. F., "Modular Access to Structurally Switchable 3d Discrete DNA Assemblies", *Journal of the American Chemical Society*, **2007**, 129, 13376.

[107] Rothemund, P. W. K., "Folding DNA to Create Nanoscale Shapes and Patterns", *Nature*, **2006**, 440, 297.

[108] He, Y.; Ye, T.; Su, M.; Zhang, C.; Ribbe, A. E.; Jiang, W.; Mao, C., "Hierarchical Self-Assembly of DNA into Symmetric Supramolecular Polyhedra", *Nature*, **2008**, 452, 198.

[109] Lin, C.; Liu, Y.; Yan, H., "Designer DNA Nanoarchitectures?", *Biochemistry*, **2009**, 48, 1663.

[110] Feldkamp, U.; Niemeyer, C. M., "Rational Design of DNA Nanoarchitectures", *Angewandte Chemie International Edition*, **2006**, 45, 1856.

[111] Lin, C.; Liu, Y.; Rinker, S.; Yan, H., "DNA Tile Based Self Assembly: Building Complex Nanoarchitectures", *ChemPhysChem*, **2006**, 7, 1641.

[112] Le, J. D.; Pinto, Y.; Seeman, N. C.; Musier-Forsyth, K.; Taton, T. A.; Kiehl, R. A., "DNA-Templated Self-Assembly of Metallic Nanocomponent Arrays on a Surface", *Nano Letters*, **2004**, 4, 2343.

[113] Zhang, J.; Liu, Y.; Ke, Y.; Yan, H., "Periodic Square-Like Gold Nanoparticle Arrays Templated by Self-Assembled 2d DNA Nanogrids on a Surface", *Nano Letters*, **2006**, 6, 248.

[114] Pal, S.; Sharma, J.; Yan, H.; Liu, Y., "Stable Silver Nanoparticle-DNA Conjugates for Directed Self-Assembly of Core-Satellite Silver-Gold Nanoclusters", *Chemical communications (Cambridge, England)*, **2009**, 6059.

[115] Sharma, J.; Chhabra, R.; Cheng, A.; Brownell, J.; Liu, Y.; Yan, H., "Control of Self-Assembly of DNA Tubules through Integration of Gold Nanoparticles", *Science*, **2009**, 323, 112.

[116] Zheng, J.; Constantinou, P. E.; Micheel, C.; Alivisatos, A. P.; Kiehl, R. A.; Seeman, N. C., "Two-Dimensional Nanoparticle Arrays Show the Organizational Power of Robust DNA Motifs", *Nano Letters*, **2006**, 6, 1502.

[117] Han, L.; Wu, W.; Kirk, F. L.; Luo, J.; Maye, M. M.; Kariuki, N. N.; Lin, Y.; Wang, C.; Zhong, C. J., "A Direct Route toward Assembly of Nanoparticle- Carbon Nanotube Composite Materials", *Langmuir*, **2004**, 20, 6019.

[118] Zhang, M.; Su, L.; Mao, L., "Surfactant Functionalization of Carbon Nanotubes (Cnts) for Layer-by-Layer Assembling of Cnt Multi-Layer Films and Fabrication of Gold Nanoparticle/Cnt Nanohybrid", *Carbon*, **2006**, 44, 276.

[119] Zanella, R.; Basiuk, E. V.; Santiago, P.; Basiuk, V. A.; Mireles, E.; Puente-Lee, I.; Saniger, J. M., "Deposition of Gold Nanoparticles onto Thiol-Functionalized Multiwalled Carbon Nanotubes", *Journal of Physical Chemistry B*, **2005**, 109, 16290.

[120] Correa-Duarte, M. A.; Perez-Juste, J.; Sanchez-Iglesias, A.; Giersig, M.; Liz-Marzan, L. M., "Aligning Au Nanorods by Using Carbon Nanotubes as Templates", *Angewandte Chemie-International Edition*, **2005**, 44, 4375.

[121] Simard, J.; Briggs, C.; Boal, A. K.; Rotello, V. M., "Formation and Ph-Controlled Assembly of Amphiphilic Gold Nanoparticles", *Chemical Communications*, **2000**, 2000, 1943.

[122] Si, S.; Mandal, T. K., "Ph-Controlled Reversible Assembly of Peptide-Functionalized Gold Nanoparticles?", *Langmuir*, **2007**, 23, 190.

[123] Sun, Z.; Ni, W.; Yang, Z.; Kou, X.; Li, L.; Wang, J., "Ph Controlled Reversible Assembly and Disassembly of Gold Nanorods", *Small*, **2008**, 4, 1287.

[124] Dillenback, L. M.; Goodrich, G. P.; Keating, C. D., "Temperature-Programmed Assembly of DNA: Au Nanoparticle Bioconjugates", *Nano Letters*, **2006**, 6, 16.

[125] Kim, J. Y.; Lee, J. S., "Synthesis and Thermally Reversible Assembly of DNA-Gold Nanoparticle Cluster Conjugates", *Nano Letters*, **2009**, 9, 4564.

[126] Nie, Z. H.; Fava, D.; Kumacheva, E.; Zou, S.; Walker, G. C.; Rubinstein, M., "Self-Assembly of Metal-Polymer Analogues of Amphiphilic Triblock Copolymers", *Nature Materials*, **2007**, 6, 609.

[127] Hirsch, L. R.; Stafford, R. J.; Bankson, J. A.; Sershen, S. R.; Rivera, B.; Price, R. E.; Hazle, J. D.; Halas, N. J.; West, J. L., "Nanoshell-Mediated near-Infrared Thermal Therapy of Tumors under Magnetic Resonance Guidance", *Proceedings of the National Academy of Sciences of the United States of America*, **2003**, 100, 13549.

[128] Huang, X. H.; El-Sayed, I. H.; Qian, W.; El-Sayed, M. A., "Cancer Cell Imaging and Photothermal Therapy in the near-Infrared Region by Using Gold Nanorods", *Journal of the American Chemical Society*, **2006**, 128, 2115.

[129] Moskovits, M., "Surface-Enhanced Raman Spectroscopy: A Brief Retrospective", *Journal of Raman Spectroscopy*, **2005**, 36, 485.

[130] Elghanian, R.; Storhoff, J. J.; Mucic, R. C.; Letsinger, R. L.; Mirkin, C. A., "Selective Colorimetric Detection of Polynucleotides Based on the Distance-Dependent Optical Properties of Gold Nanoparticles", *Science*, **1997**, 277, 1078.

[131] Maier, S. A.; Brongersma, M. L.; Kik, P. G.; Meltzer, S.; Requicha, A. A. G.; Atwater, H. A., "Plasmonics - a Route to Nanoscale Optical Devices", *Advanced Materials*, **2001**, 13, 1501.

[132] Schaadt, D. M.; Feng, B.; Yu, E. T., "Enhanced Semiconductor Optical Absorption Via Surface Plasmon Excitation in Metal Nanoparticles", *Applied Physics Letters*, **2005**, 86, 063106.

[133] Chen, S. H.; Wang, Z. L.; Ballato, J.; Foulger, S. H.; Carroll, D. L., "Monopod, Bipod, Tripod, and Tetrapod Gold Nanocrystals", *Journal of the American Chemical Society*, **2003**, 125, 16186.

[134] Hao, E.; Bailey, R. C.; Schatz, G. C.; Hupp, J. T.; Li, S. Y., "Synthesis and Optical Properties Of "Branched" Gold Nanocrystals", *Nano Letters*, **2004**, 4, 327.

[135] Sau, T. K.; Murphy, C. J., "Room Temperature, High-Yield Synthesis of Multiple Shapes of Gold Nanoparticles in Aqueous Solution", *Journal of the American Chemical Society*, **2004**, 126, 8648.

[136] Nehl, C. L.; Liao, H. W.; Hafner, J. H., "Optical Properties of Star-Shaped Gold Nanoparticles", *Nano Letters*, **2006**, 6, 683.

[137] Esenturk, E. N.; Walker, A. R. H., "Surface-Enhanced Raman Scattering Spectroscopy Via Gold Nanostars", *Journal of Raman Spectroscopy*, **2009**, 40, 86.

[138] Song, Y. J.; Yang, Y.; Medforth, C. J.; Pereira, E.; Singh, A. K.; Xu, H. F.; Jiang, Y. B.; Brinker, C. J.; van Swol, F.; Shelnutt, J. A., "Controlled Synthesis of 2-D and 3-D Dendritic Platinum Nanostructures", *Journal of the American Chemical Society*, **2004**, 126, 635.

[139] Song, Y. J.; Jiang, Y. B.; Wang, H. R.; Pena, D. A.; Qiu, Y.; Miller, J. E.; Shelnutt, J. A., "Platinum Nanodendrites", *Nanotechnology*, **2006**, 17, 1300.

[140] Ullah, M. H.; Chung, W. S.; Kim, I.; Ha, C. S., "Ph-Selective Synthesis of Monodisperse Nanoparticles and 3d Dendritic Nanoclusters of Ctab-Stabilized Platinum for Electrocatalytic O-2 Reduction", *Small*, **2006**, 2, 870.

[141] Wang, L.; Yamauchi, Y., "Block Copolymer Mediated Synthesis of Dendritic Platinum Nanoparticles", *Journal of the American Chemical Society*, **2009**, 131, 9152.

[142] Lim, B.; Jiang, M. J.; Camargo, P. H. C.; Cho, E. C.; Tao, J.; Lu, X. M.; Zhu, Y. M.; Xia, Y. A., "Pd-Pt Bimetallic Nanodendrites with High Activity for Oxygen Reduction", *Science*, **2009**, 324, 1302.

[143] Wang, L.; Yamauchi, Y., "Facile Synthesis of Three-Dimensional Dendritic Platinum Nanoelectrocatalyst", *Chemistry of Materials*, **2009**, 21, 3562.

[144] Panda, A. B.; Acharya, S.; Efrima, A., "Ultranarrow Znse Nanorods and Nanowires: Structure, Spectroscopy, and One-Dimensional Properties", *Advanced Materials*, **2005**, 17, 2471.

[145] Acharya, S.; Patla, I.; Kost, J.; Efrima, S.; Golan, Y., "Switchable Assembly of Ultra Narrow Cds Nanowires and Nanorods", *Journal of the American Chemical Society*, **2006**, 128, 9294.

[146] Yu, S. H.; Qian, Y. T. In *Self-Organized Nanoscale Materials*; Adachi;, M., Lockwood., D. J., Eds.; Springer New York: **2006**, p 101.

[147] Wang, D. S.; Hao, C. H.; Zheng, W.; Peng, Q.; Wang, T. H.; Liao, Z. M.; Yu, D. P.; Li, Y. D., "Ultralong Single-Crystalline Ag_2S Nanowires: Promising Candidates for Photoswitches and Room-Temperature Oxygen Sensors", *Advanced Materials*, **2008**, 20,

2628.

[148] Shi, Y.; Li, H.; Chen, L. Q.; Huang, X. J., "Obtaining Ultra-Long Copper Nanowires Via a Hydrothermal Process", *Science and Technology of Advanced Materials*, **2005**, 6, 761.

[149] Jana, N. R.; Gearheart, L.; Murphy, C. J., "Evidence for Seed-Mediated Nucleation in the Chemical Reduction of Gold Salts to Gold Nanoparticles", *Chemistry of Materials*, **2001**, 13, 2313.

[150] Orendorff, C. J.; Sau, T. K.; Murphy, C. J., "Shape-Dependent Plasmon-Resonant Gold Nanoparticles", *Small*, **2006**, 2, 636.

[151] Prodan, E.; Radloff, C.; Halas, N. J.; Nordlander, P., "A Hybridization Model for the Plasmon Response of Complex Nanostructures", *Science*, **2003**, 302, 419.

[152] Xia, Y. N.; Yang, P. D.; Sun, Y. G.; Wu, Y. Y.; Mayers, B.; Gates, B.; Yin, Y. D.; Kim, F.; Yan, Y. Q., "One-Dimensional Nanostructures: Synthesis, Characterization, and Applications", *Advanced Materials*, **2003**, 15, 353.

[153] Maier, S. A.; Kik, P. G.; Atwater, H. A.; Meltzer, S.; Harel, E.; Koel, B. E.; Requicha, A. A. G., "Local Detection of Electromagnetic Energy Transport Below the Diffraction Limit in Metal Nanoparticle Plasmon Waveguides", *Nature Materials*, **2003**, 2, 229.

[154] Law, M.; Sirbuly, D. J.; Johnson, J. C.; Goldberger, J.; Saykally, R. J.; Yang, P. D., "Nanoribbon Waveguides for Subwavelength Photonics Integration", *Science*, **2004**, 305, 1269.

[155] Wei, Q. H.; Su, K. H.; Durant, S.; Zhang, X., "Plasmon Resonance of Finite One-Dimensional Au Nanoparticle Chains", *Nano Letters*, **2004**, 4, 1067.

[156] Lin, S.; Li, M.; Dujardin, E.; Girard, C.; Mann, S., "One-Dimensional Plasmon Coupling by Facile Self-Assembly of Gold Nanoparticles into Branched Chain Networks", *Advanced Materials*, **2005**, 17, 2553.

[157] Hu, J. T.; Odom, T. W.; Lieber, C. M., "Chemistry and Physics in One Dimension: Synthesis and Properties of Nanowires and Nanotubes", *Accounts of Chemical Research*, **1999**, 32, 435.

[158] Huang, Y.; Duan, X. F.; Wei, Q. Q.; Lieber, C. M., "Directed Assembly of One-Dimensional Nanostructures into Functional Networks", *Science*, **2001**, 291, 630.

[159] Gudiksen, M. S.; Lauhon, L. J.; Wang, J.; Smith, D. C.; Lieber, C. M., "Growth of Nanowire Superlattice Structures for Nanoscale Photonics and Electronics", *Nature*, **2002**, 415, 617.

[160] Kovtyukhova, N. I.; Mallouk, T. E., "Nanowires as Building Blocks for Self-Assembling Logic and Memory Circuits", *Chemistry-a European Journal*, **2002**, 8, 4355.

[161] Melosh, N. A.; Boukai, A.; Diana, F.; Gerardot, B.; Badolato, A.; Petroff, P. M.; Heath, J. R., "Ultrahigh-Density Nanowire Lattices and Circuits", *Science*, **2003**, 300, 112.

[162] Zhang, J. L.; Du, J. M.; Han, B. X.; Liu, Z. M.; Jiang, T.; Zhang, Z. F., "Sonochemical Formation of Single-Crystalline Gold Nanobelts", *Angewandte Chemie-International Edition*, **2006**, 45, 1116.

[163] Sun, Y. G.; Mayers, B.; Xia, Y. N., "Transformation of Silver Nanospheres into Nanobelts and Triangular Nanoplates through a Thermal Process", *Nano Letters*, **2003**, 3, 675.

[164] Mohamed, M. B.; Wang, Z. L.; El-Sayed, M. A., "Temperature-Dependent Size-Controlled Nucleation and Growth of Gold Nanoclusters", *Journal of Physical Chemistry A*, **1999**, 103, 10255.

[165] Cho, K. S.; Talapin, D. V.; Gaschler, W.; Murray, C. B., "Designing Pbse Nanowires and Nanorings through Oriented Attachment of Nanoparticles", *Journal of the American Chemical Society*, **2005**, 127, 7140.

[166] Sun, Y. G.; Gates, B.; Mayers, B.; Xia, Y. N., "Crystalline Silver Nanowires by

Soft Solution Processing", *Nano Letters*, **2002**, 2, 165.

[167] Tao, A.; Sinsermsuksakul, P.; Yang, P. D., "Polyhedral Silver Nanocrystals with Distinct Scattering Signatures", *Angewandte Chemie-International Edition*, **2006**, 45, 4597.

[168] Pei, L. H.; Mori, K.; Adachi, M., "Formation Process of Two-Dimensional Networked Gold Nanowires by Citrate Reduction of Aucl4- and the Shape Stabilization", *Langmuir*, **2004**, 20, 7837.

[169] Biggs, S.; Mulvaney, P.; Zukoski, C. F.; Grieser, F., "Study of Anion Adsorption at the Gold-Aqueous Solution Interface by Atomic-Force Microscopy", *Journal of the American Chemical Society*, **1994**, 116, 9150.

[170] Wall, J. F.; Grieser, F.; Zukoski, C. F., "Monitoring Chemical Reactions at the Gold/Solution Interface Using Atomic Force Microscopy", *Journal of the Chemical Society-Faraday Transactions*, **1997**, 93, 4017.

[171] Vasilev, K.; Zhu, T.; Wilms, M.; Gillies, G.; Lieberwirth, I.; Mittler, S.; Knoll, W.; Kreiter, M., "Simple, One-Step Synthesis of Gold Nanowires in Aqueous Solution", *Langmuir*, **2005**, 21, 12399.

[172] Murphy, C. J.; Jana, N. R., "Controlling the Aspect Ratio of Inorganic Nanorods and Nanowires", *Advanced Materials*, **2002**, 14, 80.

[173] Busbee, B. D.; Obare, S. O.; Murphy, C. J., "An Improved Synthesis of High-Aspect-Ratio Gold Nanorods", *Advanced Materials*, **2003**, 15, 414.

[174] Lee, K.-H.; Huang, K.-M.; Tseng, W.-L.; Chiu, T.-C.; Lin, Y.-W.; Chang, H.-T., "Manipulation of the Growth of Gold and Silver Nanomaterials on Glass by Seeding Approach", *Langmuir*, **2007**, 23, 1435

[175] Millstone, J. E.; Park, S.; Shuford, K. L.; Qin, L. D.; Schatz, G. C.; Mirkin, C. A., "Observation of a Quadrupole Plasmon Mode for a Colloidal Solution of Gold Nanoprisms", *Journal of the American Chemical Society*, **2005**, 127, 5312.

[176] Rodrı´guez-Fernandez, J.; Perez-Juste, J.; Abajo, F. J. G. d.; Liz-Marzan, L. M., "Seeded Growth of Submicron Au Colloids with Quadrupole Plasmon Resonance Modes", *Langmuir*, **2006**, 22, 7007.

[177] Zou, X. Q.; Ying, E. B.; Dong, S. J., "Seed-Mediated Synthesis of Branched Gold Nanoparticles with the Assistance of Citrate and Their Surface-Enhanced Raman Scattering Properties", *Nanotechnology*, **2006**, 17, 4758.

[178] Grabar, K. C.; Allison, K. J.; Baker, B. E.; Bright, R. M.; Brown, K. R.; Freeman, R. G.; Fox, A. P.; Keating, C. D.; Musick, M. D.; Natan, M. J., "Two-Dimensional Arrays of Colloidal Gold Particles: A Flexible Approach to Macroscopic Metal Surfaces", *Langmuir*, **1996**, 12, 2353.

[179] Pinta, M. *Modern Methods for Trace Element Analysis*; Ann Arbor Science Publishers, **1978**.

[180] Alvarez, M. M.; Khoury, J. T.; Schaaff, T. G.; Shafigullin, M. N.; Vezmar, I.; Whetten, R. L., "Optical Absorption Spectra of Nanocrystal Gold Molecules", *Journal of Physical Chemistry B*, **1997**, 101, 3706.

[181] Chang, S. S.; Shih, C. W.; Chen, C. D.; Lai, W. C.; Wang, C. R. C., "The Shape Transition of Gold Nanorods", *Langmuir*, **1999**, 15, 701.

[182] Link, S.; El-Sayed, M. A., "Spectral Properties and Relaxation Dynamics of Surface Plasmon Electronic Oscillations in Gold and Silver Nanodots and Nanorods", *Journal of Physical Chemistry B*, **1999**, 103, 8410.

[183] Ung, T.; Liz-Marzan, L. M.; Mulvaney, P., "Optical Properties of Thin Films of Au@Sio2 Particles", *Journal of Physical Chemistry B*, **2001**, 105, 3441.

[184] Brown, K. R.; Natan, M. J., "Hydroxylamine Seeding of Colloidal Au Nanoparticles in Solution and on Surfaces", *Langmuir*, **1998**, 14, 726.

[185] Tang, Z. Y.; Kotov, N. A.; Giersig, M., "Spontaneous Organization of Single Cdte Nanoparticles into Luminescent Nanowires", *Science*, **2002**, 297, 237.

[186] Zhang, H.; Wang, D. Y., "Controlling the Growth of Charged-Nanoparticle Chains through Interparticle Electrostatic Repulsion", *Angewandte Chemie-International Edition*, **2008**, 47, 3984.

[187] Biggs, S.; Chow, M. K.; Zukoski, C. F.; Grieser, F., "The Role of Colloidal Stability in the Formation of Gold Sols", *Journal of Colloid and Interface Science*, **1993**, 160, 511.

[188] Kiely, C. J.; Fink, J.; Brust, M.; Bethell, D.; Schiffrin, D. J., "Spontaneous Ordering of Bimodal Ensembles of Nanoscopic Gold Clusters", *Nature*, **1998**, 396, 444.

[189] Penn, R. L.; Banfield, J. F., "Imperfect Oriented Attachment: Dislocation Generation in Defect-Free Nanocrystals", *Science*, **1998**, 281, 969.

[190] Tsai, M. H.; Chen, S. Y.; Shen, P., "Imperfect Oriented Attachment: Accretion and Defect Generation of Nanosize Rutile Condensates", *Nano Letters*, **2004**, 4, 1197.

[191] Shankar, S. S.; Rai, A.; Ankamwar, B.; Singh, A.; Ahmad, A.; Sastry, M., "Biological Synthesis of Triangular Gold Nanoprisms", *Nature Materials*, **2004**, 3, 482.

[192] Akthakul, A.; Hochbaum, A. I.; Stellacci, F.; Mayes, A. M., "Size Fractionation of Metal Nanoparticles by Membrane Filtration", *Advanced Materials*, **2005**, 17, 532.

[193] Sweeney, S. F.; Woehrle, G. H.; Hutchison, J. E., "Rapid Purification and Size Separation of Gold Nanoparticles Via Diafiltration", *Journal of the American Chemical Society*, **2006**, 128, 3190.

[194] Hanauer, M.; Pierrat, S.; Zins, I.; Lotz, A.; Sonnichsen, C., "Separation of Nanoparticles by Gel Electrophoresis According to Size-and Shape", *Nano Letters*, **2007**, 7, 2881.

[195] Xu, X. Y.; Caswell, K. K.; Tucker, E.; Kabisatpathy, S.; Brodhacker, K. L.; Scrivens, W. A., "Size and Shape Separation of Gold Nanoparticles with Preparative Gel Electrophoresis", *Journal of Chromatography A*, **2007**, 1167, 35.

[196] McLeod, M. C.; Anand, M.; Kitchens, C. L.; Roberts, C. B., "Precise and Rapid

Size Selection and Targeted Deposition of Nanoparticle Populations Using Co2 Gas Expanded Liquids", *Nano Letters*, **2005**, 5, 461.

[197] Chen, G.; Wang, Y.; Tan, L. H.; Yang, M. X.; Tan, L. S.; Chen, Y.; Chen, H. Y., "High-Purity Separation of Gold Nanoparticle Dimers and Trimers", *Journal of the American Chemical Society*, **2009**, 131, 4218.

[198] Sun, X. M.; Tabakman, S. M.; Seo, W. S.; Zhang, L.; Zhang, G. Y.; Sherlock, S.; Bai, L.; Dai, H. J., "Separation of Nanoparticles in a Density Gradient: Feco@C and Gold Nanocrystals", *Angewandte Chemie-International Edition*, **2009**, 48, 939.

[199] Bai, L.; Ma, X. J.; Liu, J. F.; Sun, X. M.; Zhao, D. Y.; Evans, D. G., "Rapid Separation and Purification of Nanoparticles in Organic Density Gradients", *Journal of the American Chemical Society*, **2010**, 132, 2333.

[200] Sadeghi, R.; Zafarani-Moattar, M. T., "Thermodynamics of Aqueous Solutions of Polyvinylpyrrolidone", *Journal of Chemical Thermodynamics*, **2004**, 36, 665.

[201] Davidson, R. L.; Sittig, M. *Water-Soluble Resins*; Reinhold Publishing Corporation, 1962.

[202] LAMB, H. *Hydrodynamics*; 6th ed.; Cambridge University Press, 1975.

[203] Falabella, J. B.; Cho, T. J.; Ripple, D. C.; Hackley, V. A.; Tarlov, M. J., "Characterization of Gold Nanoparticles Modified with Single-Stranded DNA Using Analytical Ultracentrifugation and Dynamic Light Scattering", *Langmuir*, **2010**, 26, 12740.

[204] Qiu, P. H.; Jensen, C.; Charity, N.; Towner, R.; Mao, C. B., " Oil Phase Evaporation-Induced Self-Assembly of Hydrophobic Nanoparticles into Spherical Clusters with Controlled Surface Chemistry in an Oil-in-Water Dispersion and Comparison of Behaviors of Individual and Clustered Iron Oxide Nanoparticles" *Journal of the American Chemical Society*, **2010,** ASAP.

[205] Su, K. H.; Wei, Q. H.; Zhang, X.; Mock, J. J.; Smith, D. R.; Schultz, S., "Interparticle Coupling Effects on Plasmon Resonances of Nanogold Particles", *Nano*

Letters, **2003**, 3, 1087.

[206] Lu, Y.; Yin, Y. D.; Li, Z. Y.; Xia, Y. A., "Synthesis and Self-Assembly of Au@Sio2 Core-Shell Colloids", *Nano Letters*, **2002**, 2, 785.

[207] Krenn, J. R.; Dereux, A.; Weeber, J. C.; Bourillot, E.; Lacroute, Y.; Goudonnet, J. P.; Schider, G.; Gotschy, W.; Leitner, A.; Aussenegg, F. R.; Girard, C., "Squeezing the Optical near-Field Zone by Plasmon Coupling of Metallic Nanoparticles", *Physical Review Letters*, **1999**, 82, 2590.

[208] Huang, X.; El-Sayed, I. H.; Qian, W.; El-Sayed, M. A., "Cancer Cells Assemble and Align Gold Nanorods Conjugated to Antibodies to Produce Highly Enhanced, Sharp, and Polarized Surface Raman Spectra: A Potential Cancer Diagnostic Marker", *Nano Letters*, **2007**, 7, 1591.

[209] Sudeep, P. K.; Joseph, S. T. S.; Thomas, K. G., "Selective Detection of Cysteine and Glutathione Using Gold Nanorods", *Journal of the American Chemical Society*, **2005**, 127, 6516.

[210] Jana, N. R.; Gearheart, L.; Murphy, C. J., "Seed-Mediated Growth Approach for Shape-Controlled Synthesis of Spheroidal and Rod-Like Gold Nanoparticles Using a Surfactant Template", *Advanced Materials*, **2001**, 13, 1389.

[211] Nikoobakht, B.; El-Sayed, M. A., "Preparation and Growth Mechanism of Gold Nanorods (Nrs) Using Seed-Mediated Growth Method", *Chemistry of Materials*, **2003**, 15, 1957.

[212] Yu, Y. Y.; Chang, S. S.; Lee, C. L.; Wang, C. R. C., "Gold Nanorods: Electrochemical Synthesis and Optical Properties", *Journal of Physical Chemistry B*, **1997**, 101, 6661.

[213] van der Zande, B. M. I.; Pages, L.; Hikmet, R. A. M.; van Blaaderen, A., "Optical Properties of Aligned Rod-Shaped Gold Particles Dispersed in Poly(Vinyl Alcohol) Films", *Journal of Physical Chemistry B*, **1999**, 103, 5761.

[214] Hu, X. G.; Cheng, W. L.; Wang, T.; Wang, E. K.; Dong, S. J., "Well-Ordered

End-to-End Linkage of Gold Nanorods", *Nanotechnology*, **2005**, 16, 2164.

[215] Zhang, S. Z.; Kou, X. S.; Yang, Z.; Shi, Q. H.; Stucky, G. D.; Sun, L. D.; Wang, J. F.; Yan, C. H., "Nanonecklaces Assembled from Gold Rods, Spheres, and Bipyramids", *Chemical Communications*, **2007**, 18, 1816.

[216] Pan, B. F.; Ao, L. M.; Gao, F.; Tian, H. Y.; He, R.; Cui, D. X., "End-to-End Self-Assembly and Colorimetric Characterization of Gold Nanorods and Nanospheres Via Oligonucleotide Hybridization", *Nanotechnology*, **2005**, 16, 1776.

[217] Nie, Z.; Fava, D., "Self-Assembly of Metal-Polymer Analogues of Amphiphilic Triblock Copolymers", *Nature Materials*, **2007**, 6, 609.

[218] Caswell, K. K.; Wilson, J. N.; Bunz, U. H. F.; Murphy, C. J., "Preferential End-to-End Assembly of Gold Nanorods by Biotin-Streptavidin Connectors", *Journal of the American Chemical Society*, **2003**, 125, 13914.

[219] Chang, J. Y.; Wu, H. M.; Chen, H.; Ling, Y. C.; Tan, W. H., "Oriented Assembly of Au Nanorods Using Biorecognition System", *Chemical Communications*, **2005**, 1092.

[220] Ikeda, T.; Kamiya, R.; Yamaguchi, S., "Excretion of Flagellin by a Short-Flagella Mutant of Salmonella Typhimurium", *Journal of Bacteriology*, **1983**, 153, 506.

[221] Pastoriza-Santos, I.; Perez-Juste, J.; Liz-Marzan, L. M., "Silica-Coating and Hydrophobation of Ctab-Stabilized Gold Nanorods", *Chemistry of Materials*, **2006**, 18, 2465.

[222] Kerridge, D.; Horne, R. W.; Glauert, A. M., "Structural Components of Flagella from Salmonella Typhimurium", *Journal of Molecular Biology*, **1962**, 4, 227.

[223] Westerlund-Wikstrom, B., "Peptide Display on Bacterial Flagella: Principles and Applications", *International Journal of Medical Microbiology*, **2000**, 290, 223.

[224] Ghosh, S. K.; Pal, T., "Interparticle Coupling Effect on the Surface Plasmon Resonance of Gold Nanoparticles: From Theory to Applications", *Chemical Reviews*,

2007, 107, 4797.

[225] Nie, Z.; Fava, D.; Kumacheva, E.; Zou, S.; Walker, G. C.; Rubinstein, M., "Self-Assembly of Metal-Polymer Analogues of Amphiphilic Triblock Copolymers", *Nature Materials*, **2007**, 6, 609.

[226] Dyck, J., "The Evolution of Feathers", *Zoologica Scripta*, **1985**, 14, 137.

[227] Lei, F. M.; Qu, Y. H.; Gan, Y. L.; Gebauer, A.; Kaiser, M., "The Feather Microstructure of Passerine Sparrows in China", *Journal Fur Ornithologie*, **2002**, 143, 205.

[228] Whitesides, G. M., "The Origins and the Future of Microfluidics", *Nature*, **2006**, 442, 368.

[229] Borenstein, J. T.; Weinberg, E. J.; Orrick, B. K.; Sundback, C.; Kaazempur-Mofrad, M. R.; Vacanti, J. P., "Microfabrication of Three-Dimensional Engineered Scaffolds", *Tissue Engineering*, **2007**, 13, 1837.

[230] Zhang, W. J.; Liu, W.; Cui, L.; Cao, Y. L., "Tissue Engineering of Blood Vessel", *Journal of Cellular and Molecular Medicine*, **2007**, 11, 945.

[231] Lin, Y. M.; Boccaccini, A. R.; Polak, J. M.; Bishop, A. E., "Biocompatibility of Poly-Dl-Lactic Acid (Pdlla) for Lung Tissue Engineering", *Journal of Biomaterials Applications*, **2006**, 21, 109.

[232] Huh, D.; Fujioka, H.; Tung, Y. C.; Futai, N.; Paine, R.; Grotberg, J. B.; Takayama, S., "Acoustically Detectable Cellular-Level Lung Injury Induced by Fluid Mechanical Stresses in Microfluidic Airway Systems", *Proceedings of the National Academy of Sciences of the United States of America*, **2007**, 104, 18886.

[233] Ando, Y.; Zhao, X.; Sugai, T.; Kumar, M., "Growing Carbon Nanotubes", *Materials Today*, **2004**, 7, 22.

[234] Colli, A.; Hofmann, S.; Fasoli, A.; Ferrari, A. C.; Ducati, C.; Dunin-Borkowski, R. E.; Robertson, J., "Synthesis and Optical Properties of Silicon Nanowires Grown by

Different Methods", *Applied Physics a-Materials Science & Processing*, **2006**, 85, 247.

[235] Zhang, H. X.; Ge, J. P.; Wang, J.; Li, Y. D., "Atmospheric Pressure Chemical Vapour Deposition Synthesis of Sulfides, Oxides, Silicides and Metal Nanowires with Metal Chloride Precursors", *Nanotechnology*, **2006**, 17, 253.

[236] Cao, G. Z.; Liu, D. W., "Template-Based Synthesis of Nanorod, Nanowire, and Nanotube Arrays", *Advances in Colloid and Interface Science*, **2008**, 136, 45.

[237] Li, D.; Xia, Y. N., "Electrospinning of Nanofibers: Reinventing the Wheel?", *Advanced Materials*, **2004**, 16, 1151.

[238] Zhao, Y.; Cao, X. Y.; Jiang, L., "Bio-Mimic Multichannel Microtubes by a Facile Method", *Journal of the American Chemical Society*, **2007**, 129, 764.

[239] Li, J.; Papadopoulos, C.; Xu, J., "Nanoelectronics - Growing Y-Junction Carbon Nanotubes", *Nature*, **1999**, 402, 253.

[240] Meng, G. W.; Jung, Y. J.; Cao, A. Y.; Vajtai, R.; Ajayan, P. M., "Controlled Fabrication of Hierarchically Branched Nanopores, Nanotubes, and Nanowires", *Proceedings of the National Academy of Sciences of the United States of America*, **2005**, 102, 7074.

[241] Wei, Z. X.; Zhang, L. J.; Yu, M.; Yang, Y. S.; Wan, M. X., "Self-Assembling Sub-Micrometer-Sized Tube Junctions and Dendrites of Conducting Polymers", *Advanced Materials*, **2003**, 15, 1382.

[242] Wiley, B.; Sun, Y. G.; Mayers, B.; Xia, Y. N., "Shape-Controlled Synthesis of Metal Nanostructures: The Case of Silver", *Chemistry-a European Journal*, **2005**, 11, 454.

[243] Xiong, Y. J.; Xia, Y. N., "Shape-Controlled Synthesis of Metal Nanostructures: The Case of Palladium", *Advanced Materials*, **2007**, 19, 3385.

[244] Xia, Y. N.; Xiong, Y. J.; Lim, B.; Skrabalak, S., E., "Shape-Controlled Synthesis of Metal Nanocrystals: Simple Chemistry Meets Complex Physics?", *Angewandte*

Chemie International Edition, **2009**, 48, 60.

[245] Sun, Y. G.; Mayers, B.; Herricks, T.; Xia, Y. N., "Polyol Synthesis of Uniform Silver Nanowires: A Plausible Growth Mechanism and the Supporting Evidence", *Nano Letters*, **2003**, 3, 955.

[246] Ochoa, N. A.; Pradanos, P.; Palacio, L.; Pagliero, C.; Marchese, J.; Hernandez, A., "Pore Size Distributions Based on Afm Imaging and Retention of Multidisperse Polymer Solutes - Characterisation of Polyethersulfone Uf Membranes with Dopes Containing Different Pvp", *Journal of Membrane Science*, **2001**, 187, 227.

[247] Han, M. J.; Nam, S. T., "Thermodynamic and Rheological Variation in Polysulfone Solution by Pvp and Its Effect in the Preparation of Phase Inversion Membrane", *Journal of Membrane Science*, **2002**, 202, 55.

[248] Kang, J. S.; Kim, K. Y.; Lee, Y. M., "Preparation of Pvp Immobilized Microporous Chlorinated Polyvinyl Chloride Membranes on Fabric and Their Hydraulic Permeation Behavior", *Journal of Membrane Science*, **2003**, 214, 311.

[249] Hayama, M.; Yamamoto, K.; Kohori, F.; Sakai, K., "How Polysulfone Dialysis Membranes Containing Polyvinylpyrrolidone Achieve Excellent Biocompatibility?", *Journal of Membrane Science*, **2004**, 234, 41.

[250] Guven, O.; Eltan, E., "Molecular Association in Aqueous-Solutions of High Molecular-Weight Poly(N-Vinyl-2-Pyrrolidone)", *Makromolekulare Chemie-Macromolecular Chemistry and Physics*, **1981**, 182, 3129.

[251] Guven, O.; Yigit, F., "Hydrophilic and Hydrophobic Interactions in Alcohol-Solutions of High Molecular-Weight Poly(N-Vinyl-2-Pyrrolidone)", *Colloid and Polymer Science*, **1984**, 262, 892.

[252] Sun, T.; King, H. E., "Aggregation Behavior in the Semidilute Poly(N-Vinyl-2-Pyrrolidone)/Water System", *Macromolecules*, **1996**, 29, 3175.

[253] Itakura, M.; Inomata, K.; Nose, T., "Aggregation Behavior of Poly(N,N-Diethylacrylamide) in Aqueous Solution", *Polymer*, **2000**, 41, 8681.

[254] Mao, C.; Solis, D. J.; Reiss, B. D.; Kottmann, S. T.; Sweeney, R. Y.; Hayhurst, A.; Georgiou, G.; Iverson, B.; Belcher, A. M., "Virus-Based Toolkit for the Directed Synthesis of Magnetic and Semiconducting Nanowires", *Science*, **2004**, 303, 213.

[255] Nam, K. T.; Kim, D. W.; Yoo, P. J.; Chiang, C. Y.; Meethong, N.; Hammond, P. T.; Chiang, Y. M.; Belcher, A. M., "Virus-Enabled Synthesis and Assembly of Nanowires for Lithium Ion Battery Electrodes", *Science*, **2006**, 312, 885.

[256] Shenton, W.; Douglas, T.; Young, M.; Stubbs, G.; Mann, S., "Inorganic-Organic Nanotube Composites from Template Mineralization of Tobacco Mosaic Virus", *Advanced Materials*, **1999**, 11, 253.

[257] Niu, Z.; Liu, J.; Lee, L. A.; Bruckman, M. A.; Zhao, D.; Koley, G.; Wang, Q., "Biological Templated Synthesis of Water-Soluble Conductive Polymeric Nanowires", *Nano Letters*, **2007**, 7, 3729.

[258] Wang, F.; Li, D.; Mao, C., "Genetically Modifiable Flagella as Templates for Silica Fibers: From Hybrid Nanotubes to 1d Periodic Nanohole Arrays", *Advanced Functional Materials*, **2008**, 18, 4007.

[259] Caruso, F.; Caruso, R. A.; Mohwald, H., "Nanoengineering of Inorganic and Hybrid Hollow Spheres by Colloidal Templating", *Science*, **1998**, 282, 1111.

[260] Foo, C. W. P.; Patwardhan, S. V.; Belton, D. J.; Kitchel, B.; Anastasiades, D.; Huang, J.; Naik, R. R.; Perry, C. C.; Kaplan, D. L., "Novel Nanocomposites from Spider Silk-Silica Fusion (Chimeric) Proteins", *Proceedings of the National Academy of Sciences of the United States of America*, **2006**, 103, 9428.

[261] Toki, M.; Chow, T. Y.; Ohnaka, T.; Samura, H.; Saegusa, T., "Structure of Poly(Vinylpyrrolidone)-Silica Hybrid", *Polymer Bulletin*, **1992**, 29, 653.

[262] Graf, C.; Vossen, D. L. J.; Imhof, A.; van Blaaderen, A., "A General Method to Coat Colloidal Particles with Silica", *Langmuir*, **2003**, 19, 6693.

[263] Yin, Y. D.; Lu, Y.; Sun, Y. G.; Xia, Y. N., "Silver Nanowires Can Be Directly Coated with Amorphous Silica to Generate Well-Controlled Coaxial Nanocables of

Silver/Silica", *Nano Letters*, **2002**, 2, 427.

[264] Fan, H. Y.; Yang, K.; Boye, D. M.; Sigmon, T.; Malloy, K. J.; Xu, H. F.; Lopez, G. P.; Brinker, C. J., "Self-Assembly of Ordered, Robust, Three-Dimensional Gold Nanocrystal/Silica Arrays", *Science*, **2004**, 304, 567.

[265] Puntes, V. F.; Gorostiza, P.; Aruguete, D. M.; Bastus, N. G.; Alivisatos, A. P., "Collective Behaviour in Two-Dimensional Cobalt Nanoparticle Assemblies Observed by Magnetic Force Microscopy", *Nature Materials*, **2004**, 3, 263.

[266] Le, F.; Brandl, D. W.; Urzhumov, Y. A.; Wang, H.; Kundu, J.; Halas, N. J.; Aizpurua, J.; Nordlander, P., "Metallic Nanoparticle Arrays: A Common Substrate for Both Surface-Enhanced Raman Scattering and Surface-Enhanced Infrared Absorption", *ACS Nano*, **2008**, 2, 707.

[267] Velev, O. D.; Gupta, S., "Materials Fabricated by Micro- and Nanoparticle Assembly - the Challenging Path from Science to Engineering", *Advanced Materials*, **2009**, 21, 1897.

[268] Lin, Y.; Skaff, H.; Emrick, T.; Dinsmore, A. D.; Russell, T. P., "Nanoparticle Assembly and Transport at Liquid-Liquid Interfaces", *Science*, **2003**, 299, 226.

[269] Duan, H. W.; Wang, D. Y.; Kurth, D. G.; Mohwald, H., "Directing Self-Assembly of Nanoparticles at Water/Oil Interfaces", *Angewandte Chemie-International Edition*, **2004**, 43, 5639.

[270] Russell, J. T.; Lin, Y.; Boker, A.; Su, L.; Carl, P.; Zettl, H.; He, J. B.; Sill, K.; Tangirala, R.; Emrick, T.; Littrell, K.; Thiyagarajan, P.; Cookson, D.; Fery, A.; Wang, Q.; Russell, T. P., "Self-Assembly and Cross-Linking of Bionanoparticles at Liquid-Liquid Interfaces", *Angewandte Chemie-International Edition*, **2005**, 44, 2420.

[271] Bigioni, T. P.; Lin, X. M.; Nguyen, T. T.; Corwin, E. I.; Witten, T. A.; Jaeger, H. M., "Kinetically Driven Self Assembly of Highly Ordered Nanoparticle Monolayers", *Nature Materials*, **2006**, 5, 265.

[272] Boal, A. K.; Ilhan, F.; DeRouchey, J. E.; Thurn-Albrecht, T.; Russell, T. P.;

Rotello, V. M., "Self-Assembly of Nanoparticles into Structured Spherical and Network Aggregates", *Nature*, **2000**, 404, 746.

[273] Berret, J. F.; Schonbeck, N.; Gazeau, F.; El Kharrat, D.; Sandre, O.; Vacher, A.; Airiau, M., "Controlled Clustering of Superparamagnetic Nanoparticles Using Block Copolymers: Design of New Contrast Agents for Magnetic Resonance Imaging", *Journal of the American Chemical Society*, **2006**, 128, 1755.

[274] Compton, O. C.; Osterloh, F. E., "Evolution of Size and Shape in the Colloidal Crystallization of Gold Nanoparticles", *Journal of the American Chemical Society*, **2007**, 129, 7793.

[275] Murphy, C. J.; Gole, A. M.; Hunyadi, S. E.; Orendorff, C. J., "One-Dimensional Colloidal Gold and Silver Nanostructures", *Inorganic Chemistry*, **2006**, 45, 7544.

[276] Murphy, C. J.; San, T. K.; Gole, A. M.; Orendorff, C. J.; Gao, J. X.; Gou, L.; Hunyadi, S. E.; Li, T., "Anisotropic Metal Nanoparticles: Synthesis, Assembly, and Optical Applications", *Journal of Physical Chemistry B*, **2005**, 109, 13857.

[277] Cushing, B. L.; Kolesnichenko, V. L.; O'Connor, C. J., "Recent Advances in the Liquid-Phase Syntheses of Inorganic Nanoparticles", *Chemical Reviews*, **2004**, 104, 3893.

[278] Swami, A.; Kumar, A.; Sastry, M., "Formation of Water-Dispersible Gold Nanoparticles Using a Technique Based on Surface-Bound Interdigitated Bilayers", *Langmuir*, **2003**, 19, 1168.

[279] Pazos-Perez, N.; Gao, Y.; Hilgendorff, M.; Irsen, S.; Perez-Juste, J.; Spasova, M.; Farle, M.; Liz-Marzan, L. M.; Giersig, M., "Magnetic-Noble Metal Nanocomposites with Morphology-Dependent Optical Response", *Chemistry of Materials*, **2007**, 19, 4415.

[280] Yan, Q.; Purkayastha, A.; Singh, A. P.; Li, H.; Li, A.; Ramanujan, R. V.; Ramanath, G., "High-Coercivity Fept Nanoparticle Assemblies Embedded in Silica Thin Films", *Nanotechnology*, **2009**, 20.

[281] Fan, H. Y.; Wright, A.; Gabaldon, J.; Rodriguez, A.; Brinker, C. J.; Jiang, Y. B.,

"Three-Dimensionally Ordered Gold Nanocrystal/Silica Superlattice Thin Films Synthesized Via Sol-Gel Self-Assembly", *Advanced Functional Materials*, **2006**, 16, 891.

[282] Kim, J.; Kim, H. S.; Lee, N.; Kim, T.; Kim, H.; Yu, T.; Song, I. C.; Moon, W. K.; Hyeon, T., "Multifunctional Uniform Nanoparticles Composed of a Magnetite Nanocrystal Core and a Mesoporous Silica Shell for Magnetic Resonance and Fluorescence Imaging and for Drug Delivery", *Angewandte Chemie-International Edition*, **2008**, 47, 8438.

[283] Li, W. Y.; Camargo, P. H. C.; Au, L.; Zhang, Q.; Rycenga, M.; Xia, Y. N., "Etching and Dimerization: A Simple and Versatile Route to Dimers of Silver Nanospheres with a Range of Sizes", *Angewandte Chemie-International Edition*, **2010**, 49, 164.

[284] Yan, B.; Thubagere, A.; Premasiri, W. R.; Ziegler, L. D.; Dal Negro, L.; Reinhard, B. M., "Engineered Sers Substrates with Multiscale Signal Enhancement: Nanoplarticle Cluster Arrays", *ACS Nano*, **2009**, 3, 1190.

[285] Alexander, K. D.; Hampton, M. J.; Zhang, S. P.; Dhawan, A.; Xu, H. X.; Lopez, R., "A High-Throughput Method for Controlled Hot-Spot Fabrication in Sers-Active Gold Nanoparticle Dimer Arrays", *Journal of Raman Spectroscopy*, **2009**, 40, 2171.

[286] Chen, G.; Wang, Y.; Yang, M. X.; Xu, J.; Goh, S. J.; Pan, M.; Chen, H. Y., "Measuring Ensemble-Averaged Surface-Enhanced Raman Scattering in the Hotspots of Colloidal Nanoparticle Dimers and Trimers", *Journal of the American Chemical Society*, **2010**, 132, 3644.

[287] Ge, J. P.; Hu, Y. X.; Biasini, M.; Beyermann, W. P.; Yin, Y. D., "Superparamagnetic Magnetite Colloidal Nanocrystal Clusters", *Angewandte Chemie-International Edition*, **2007**, 46, 4342.

[288] Ai, H.; Flask, C.; Weinberg, B.; Shuai, X.; Pagel, M. D.; Farrell, D.; Duerk, J.; Gao, J. M., "Magnetite-Loaded Polymeric Micelles as Ultrasensitive Magnetic-Resonance Probes", *Advanced Materials*, **2005**, 17, 1949.

[289] Kim, J.; Lee, J. E.; Lee, S. H.; Yu, J. H.; Lee, J. H.; Park, T. G.; Hyeon, T., "Designed Fabrication of a Multifunctional Polymer Nanomedical Platform for

Simultaneous Cancer-Targeted Imaging and Magnetically Guided Drug Delivery", *Advanced Materials*, **2008**, 20, 478.

[290] Niu, D. C.; Li, Y. S.; Ma, Z.; Diao, H.; Gu, J. L.; Chen, H. R.; Zhao, W. R.; Ruan, M. L.; Zhang, Y. L.; Shi, J. L., "Preparation of Uniform, Water-Soluble, and Multifunctional Nanocomposites with Tunable Sizes", *Advanced Functional Materials*, **2010**, 20, 773.

[291] Happy, T.; Jun Min, X.; Borys, S.; Xu, L.; John, W., "Synthesis of Peolated Fe_3O_4@SiO_2 Nanoparticles Via Bioinspired Silification for Magnetic Resonance Imaging", *Advanced Functional Materials*, **2010**, 20, 722.

[292] Ditsch, A.; Laibinis, P. E.; Wang, D. I. C.; Hatton, T. A., "Controlled Clustering and Enhanced Stability of Polymer-Coated Magnetic Nanoparticles", *Langmuir*, **2005**, 21, 6006.

[293] Euliss, L. E.; Grancharov, S. G.; O'Brien, S.; Deming, T. J.; Stucky, G. D.; Murray, C. B.; Held, G. A., "Cooperative Assembly of Magnetic Nanoparticles and Block Copolypeptides in Aqueous Media", *Nano Letters*, **2003**, 3, 1489.

[294] Sun, S. H.; Zeng, H.; Robinson, D. B.; Raoux, S.; Rice, P. M.; Wang, S. X.; Li, G. X., "Monodisperse MFe_2O_4 (M = Fe, Co, Mn) Nanoparticles", *Journal of the American Chemical Society*, **2004**, 126, 273.

[295] Joo, J.; Na, H. B.; Yu, T.; Yu, J. H.; Kim, Y. W.; Wu, F. X.; Zhang, J. Z.; Hyeon, T., "Generalized and Facile Synthesis of Semiconducting Metal Sulfide Nanocrystals", *Journal of the American Chemical Society*, **2003**, 125, 11100.

[296] Gorelikov, I.; Matsuura, N., "Single-Step Coating of Mesoporous Silica on Cetyltrimethyl Ammonium Bromide-Capped Nanoparticles", *Nano Letters*, **2008**, 8, 369.

[297] Rosen, M. J. *Surfactants and Interfacialphenomena*; wiley, **2004**.

[298] Alexis, F.; Pridgen, E.; Molnar, L. K.; Farokhzad, O. C., "Factors Affecting the Clearance and Biodistribution of Polymeric Nanoparticles", *Molecular Pharmaceutics*, **2008**, 5, 505.

[299] Caliceti, P.; Veronese, F. M., "Pharmacokinetic and Biodistribution Properties of Poly(Ethylene Glycol)-Protein Conjugates", *Advanced Drug Delivery Reviews*, **2003**, 55, 1261.

[300] Gullotti, E.; Yeo, Y., "Extracellularly Activated Nanocarriers: A New Paradigm of Tumor Targeted Drug Delivery", *Molecular Pharmaceutics*, **2009**, 6, 1041.

[301] Pastoriza-Santos, I.; Perez-Juste, J.; Liz-Marzan, L. M., "Silica-Coating and Hydrophobation of Ctab-Stabilized Gold Nanorods", *Chemistry of Materials*, **2006**, 18, 2465.

[302] Gole, A.; Murphy, C. J., "Polyelectrolyte-Coated Gold Nanorods: Synthesis, Characterization and Immobilization", *Chemistry of Materials*, **2005**, 17, 1325.

[303] Santra, S.; Yang, H.; Dutta, D.; Stanley, J. T.; Holloway, P. H.; Tan, W. H.; Moudgil, B. M.; Mericle, R. A., "Tat Conjugated, Fitc Doped Silica Nanoparticles for Bioimaging Applications", *Chemical Communications*, **2004**, 2810.

[304] Hulchanskyy, T. Y.; Roy, I.; Goswami, L. N.; Chen, Y.; Bergey, E. J.; Pandey, R. K.; Oseroff, A. R.; Prasad, P. N., "Organically Modified Silica Nanoparticles with Covalently Incorporated Photosensitizer for Photodynamic Therapy of Cancer", *Nano Letters*, **2007**, 7, 2835.

[305] Lu, C. W.; Hung, Y.; Hsiao, J. K.; Yao, M.; Chung, T. H.; Lin, Y. S.; Wu, S. H.; Hsu, S. C.; Liu, H. M.; Mou, C. Y.; Yang, C. S.; Huang, D. M.; Chen, Y. C., "Bifunctional Magnetic Silica Nanoparticles for Highly Efficient Human Stem Cell Labeling", *Nano Letters*, **2007**, 7, 149.

[306] Lee, J. E.; Lee, N.; Kim, H.; Kim, J.; Choi, S. H.; Kim, J. H.; Kim, T.; Song, I. C.; Park, S. P.; Moon, W. K.; Hyeon, T., "Uniform Mesoporous Dye-Doped Silica Nanoparticles Decorated with Multiple Magnetite Nanocrystals for Simultaneous Enhanced Magnetic Resonance Imaging, Fluorescence Imaging, and Drug Delivery", *Journal of the American Chemical Society*, **2010**, 132, 552.

[307] Alivisatos, A. P., "Semiconductor Clusters, Nanocrystals, and Quantum Dots", *Science*, **1996**, 271, 933.

[308] Selvan, S. T.; Patra, P. K.; Ang, C. Y.; Ying, J. Y., "Synthesis of Silica-Coated Semiconductor and Magnetic Quantum Dots and Their Use in the Imaging of Live Cells", *Angewandte Chemie-International Edition*, **2007**, 46, 2448.

[309] Yi, D. K.; Selvan, S. T.; Lee, S. S.; Papaefthymiou, G. C.; Kundaliya, D.; Ying, J. Y., "Silica-Coated Nanocomposites of Magnetic Nanoparticles and Quantum Dots", *Journal of the American Chemical Society*, **2005**, 127, 4990.

[310] Qiu, P. H.; Mao, C. B., "Biomimetic Branched Hollow Fibers Templated by Self-Assembled Fibrous Polyvinylpyrrolidone Structures in Aqueous Solution", *ACS Nano*, **2010**, 4, 1573.

[311] Buschow, K. H. J. *Handbook of Magnetic Materials*; Elsevier Science, **2006**; Vol. 16.

[312] Lu, J. J.; Huang, H. L., "Energy Barrier, Coercivity and Blocking Temperature Variation of Fine-Particle Systems", *Chinese Journal of Physics*, **2000**, 38, 81.

[313] Gross, A. F.; Diehl, M. R.; Beverly, K. C.; Richman, E. K.; Tolbert, S. H., "Controlling Magnetic Coupling between Cobalt Nanoparticles through Nanoscale Confinement in Hexagonal Mesoporous Silica", *Journal of Physical Chemistry B*, **2003**, 107, 5475.

[314] Corr, S. A.; Byrne, S. J.; Tekoriute, R.; Meledandri, C. J.; Brougham, D. F.; Lynch, M.; Kerskens, C.; O'Dwyer, L.; Gun'ko, Y. K., "Linear Assemblies of Magnetic Nanoparticles as Mri Contrast Agents", *Journal of the American Chemical Society*, **2008**, 130, 4214.

[315] Sahoo, Y.; Cheon, M.; Wang, S.; Luo, H.; Furlani, E. P.; Prasad, P. N., "Field-Directed Self-Assembly of Magnetic Nanoparticles", *Journal of Physical Chemistry B*, **2004**, 108, 3380.

[316] Lu, Y.; Zhao, Y.; Yu, L.; Dong, L.; Shi, C.; Hu, M. J.; Xu, Y. J.; Wen, L. P.; Yu, S. H., "Hydrophilic Co@Au Yolk/Shell Nanospheres: Synthesis, Assembly, and Application to Gene Delivery", *Advanced Materials*, **2010**, 22, 1407.

[317] Singh, H.; Laibinis, P. E.; Hatton, T. A., "Rigid, Superparamagnetic Chains of Permanently Linked Beads Coated with Magnetic Nanoparticles. Synthesis and Rotational Dynamics under Applied Magnetic Fields", *Langmuir*, **2005**, 21, 11500.

[318] Xia, H. B.; Yi, J. B.; Foo, P. S.; Liu, B. H., "Facile Fabrication of Water-Soluble Magnetic Nanoparticles and Their Spherical Aggregates", *Chemistry of Materials*, **2007**, 19, 4087.

[319] Srivastava, S.; Samanta, B.; Arumugam, P.; Han, G.; Rotello, V. M., "DNA-Mediated Assembly of Iron Platinum (FePt) Nanoparticles", *Journal of Materials Chemistry*, **2007**, 17, 52.

[320] Son, S. J.; Reichel, J.; He, B.; Schuchman, M.; Lee, S. B., "Magnetic Nanotubes for Magnetic-Field-Assisted Bioseparation, Biointeraction, and Drug Delivery", *Journal of the American Chemical Society*, **2005**, 127, 7316.

[321] Dobson, J., "Magnetic Nanoparticles for Drug Delivery", *Drug Development Research*, **2006**, 67, 55.

[322] Arruebo, M.; Fernandez-Pacheco, R.; Ibarra, M. R.; Santamaria, J., "Magnetic Nanoparticles for Drug Delivery", *Nano Today*, **2007**, 2, 22.

[323] McBain, S. C.; Yiu, H. H. P.; Dobson, J., "Magnetic Nanoparticles for Gene and Drug Delivery", *International Journal of Nanomedicine*, **2008**, 3, 169.

[324] Sun, C.; Lee, J. S. H.; Zhang, M. Q., "Magnetic Nanoparticles in MR Imaging and Drug Delivery", *Advanced Drug Delivery Reviews*, **2008**, 60, 1252.